

2011

Assessment of Circumferential Myocardial Function Using Radial Tagged MRI

Yujaung Kim
Cleveland State University

Follow this and additional works at: <https://engagedscholarship.csuohio.edu/etdarchive>



Part of the [Biomedical Engineering and Bioengineering Commons](#)

How does access to this work benefit you? Let us know!

Recommended Citation

Kim, Yujaung, "Assessment of Circumferential Myocardial Function Using Radial Tagged MRI" (2011). *ETD Archive*. 672.
<https://engagedscholarship.csuohio.edu/etdarchive/672>

This Thesis is brought to you for free and open access by EngagedScholarship@CSU. It has been accepted for inclusion in ETD Archive by an authorized administrator of EngagedScholarship@CSU. For more information, please contact library.es@csuohio.edu.

**ASSESSMENT OF CIRCUMFERENTIAL MYOCARDIAL FUNCTION
USING RADIAL TAGGED MRI**

YUJAUNG KIM

Bachelor of Science in Electronic System Engineering

Daegu University

February 2007

Submitted in partial fulfillment of requirements for the degree of

MASTER OF SCIENCE IN BIOMEDICAL ENGINEERING

at the

CLEVELAND STATE UNIVERSITY

December 2011

©COPYRIGHT BY YUJAUNG KIM 2011

This thesis has been approved
For the Department of Chemical and Biomedical Engineering
and the College of Graduate Studies by

Thesis Committee Chairperson, D.Sc. Randolph M. Setser
Department of Chemical and Biomedical Engineering

Date

PhD. Sandra Halliburton
Department of Chemical and Biomedical Engineering

Date

PhD. George Chatzimavroudis
Department of Chemical and Biomedical Engineering

Date

ASSESSMENT OF CIRCUMFERENTIAL MYOCARDIAL FUNCTION USING RADIAL TAGGED MRI

YUJAUNG KIM

ABSTRACT

The extent of myocardial abnormalities is related to cardiac disease. The assessment of myocardial function of the left ventricular (LV) described by the LV myocardial deformation plays an important role to understand the effects of cardiovascular disease and therapeutic interventions on LV motion. Cardiac magnetic resonance imaging (CMR) is widely agreed as the most accurate noninvasive imaging modality for the assessment of left ventricular (LV) function. In addition, myocardial-tagging technique can track the myocardial deformation by labeling specific regions.

Although the grid tagging is popular in cardiac research use, it has not been adopted into routine clinical examination with unreliable data between frames. We hypothesized that a radial-tagging methods has geometric advantages over grid tagging method and it is the most direct way for the circumferential strains.

In this study, a semi-automatic radial tagging analysis tool was developed using MATLAB to measure the circumferential strain and rotation angle. The LV MRI short-axis image series (from end of diastole to end of systole) was used to develop and validate the analysis tool from 9 volunteers. The radial tagging analysis tool computes the strain and rotation angle by automatic calculating the mid-wall myocardium and the LV centroid. The results of radial tagging analysis were

evaluated the accuracy by manual mathematical calculating of 2 volunteers and repeating tool operations 3 times to all volunteers. Also the results were compared with the grid tagging analysis and the manual radial tagging analysis tool. To visualize the differences among tools, the RMS (root-mean-square) value of the strains and rotation angle of all volunteers by the time (% of systole) was used.

The results show that the strains and rotation angles of radial tagging analysis have no significant difference with $P>0.05$ compared to grid tagging analysis, which is conventional use, and the measured values are closer than manual radial tagging analysis. Also the tool is easy to use. We assume that the radial tagging method is the most direct way to measure circumferential strain, however it is need to more study to validate the accuracy between the radial and the grid tagging.

TABLE OF CONTENTS

	Page
COPYRIGHT.....	ii
APPROVAL PAGE.....	iii
ABSTRACT.....	iv
LIST OF TABLES	vii
LIST OF FIGURES	viii
CHAPTER I: INTRODUCTION AND SPECIFIC AIMS.....	1
CHAPTER II: BACKGROUND AND MOTIVATION	6
CHAPTER III: METHODS	27
CHAPTER IV: RESULTS	45
CHAPTER V: DISCUSSION	57
REFERENCES	63
APPENDICES	66
A. Program Algorithms	67
B. The strain and rotation curves for each subject	76
C. Copyright Permission	90

LIST OF TABLES

Table	Page
I. Tissue Relaxation Times at 1.5 T	16
II. Data point's location information	32
III. The local myocardium rotation	33
IV. The assessment of strain and rotation of the local myocardium	34
V. Similarities of strain measurement values	56
VI. Similarities of assessed rotation values	56

LIST OF FIGURES

Figure	Page
1. The Great Vessels and the Layers of the Cardiac Wall	7
2. Diagram of the status of diastole and systole	8
3. Schematic Drawing of LV structure and motion	9
4. LV rotational motion during systole and early diastole	10
5. Three dimensional coordinate system of myocardial strain	11
6. The myocardial strain	12
7. MRI instruments	13
8. Schematic diagrams of M	15
9. The application of an RF pulse	15
10. T1, T2 relaxation	16
11. A schematic of slice selection in MRI	17
12. Slice selection	18
13. The various pulse sequence	19
14. Tag plane generation	20
15. Radial tagging sketch	21
16. Grid tagging sketch	21
17. MR grid tagged images	23
18. Radial tagged LV myocardium plane	25
19. A radial tagging analysis tool	26

20. LV deformation parameters	29
21. Labeled segments	30
22. Captured image of myocardium deformation results	31
23. Strain equation and angle formula	33
24. Initial page of the semi-automatic software	35
25. The loaded MRI radial tagging image	36
26. Manipulating the MRI image	36
27. Demonstrate the myocardium of LV	37
28. The calculated mid-myocardium of LV	38
29. Selecting the tag points	38
30. Tag selected by the signal intensity	39
31. The procedure of 'contour' and 'plot'	40
32. Results of the semi-automated radial tagging tool	41
33. Manual radial tagging analysis tool	44
34. The overall strain average curves throughout the 14 subjects	47
35. The comparisons of the rotation average curves of the 14 subjects	48
36. Strain comparison at 60% of systole	50
37. Strain comparison at 100% of systole	51
38. Radial tagging MRI Images of Sample 11.....	52
39. Radial tagging MRI Images of Sample 13.....	52
40. The comparison of rotation at 60% of systole	53
41. The comparison of rotation at 100% of systole.....	54

42. The average strain values with standard errors	55
43. The average rotation with standard errors	55

CHAPTER I

INTRODUCTION AND SPECIFIC AIMS

1.1 Introduction

Worldwide, heart disease is at the top of the most serious health problems and is the leading cause of death for both men and women. According to World Health Organization, cardiovascular diseases account for nearly one-third of the deaths in the world, almost 32% of all deaths in women and 27% in men in 2004. Ischemic heart disease is the most frequent cause of death among the rest of cardiovascular diseases; 7.2 million people died in the world in 2004 [1].

In 2009, the American Heart Association reported that almost one out of every 2.8 deaths resulted from cardiovascular disease in the United States. Also, 1 in 3 American adults suffer from 1 or more types of cardiovascular diseases, such as high blood pressure, coronary heart disease, stroke, congenital cardiovascular defects, and congestive heart failure. The estimated cost of heart disease for the United States in 2009 was \$475.3 billion, which included health care services, medications and lost productivity [2]. Therefore, it is a significant issue to determine reliable diagnosis

methods and therapies for heart disease.

Any organ's structure and function are inextricably linked to body condition like health and disease. The structure and function of myocardial fibers plays a significant role to determine both the normal and pathological properties of the cardiac muscle cells. During cardiac contraction, left ventricular (LV) torsion can depict subclinical myocardial dysfunction as it is directly linked with the myofibers' orientation [3]. Therefore a study on the assessment of the biomechanical properties of normal and abnormal myocardium is important to understand the effects of cardiovascular disease and therapeutic interventions on ventricular performance. For instance, the extent of anatomic and physiologic abnormalities of the myocardium is related to coronary artery disease (CAD). The myocardium abnormalities can be detected by non-invasive imaging modalities such as echocardiography, single photon emission computed tomography, positron emission tomography (PET), contrast material enhanced multi-detector row computed tomography (CT), or magnetic resonance imaging (MRI). The valuation of global and regional left ventricular (LV) function by estimating the volumetric shape, motion and deformations of the left ventricle (LV) from imaging can depict the coronary artery system [4]. Strain and rotation of the LV are two of the most important determinants of LV function.

Echocardiography is the most popular noninvasive modality for imaging LV function due to the fact that it is a relatively simple procedure with low cost, portability, and widespread availability. However, echocardiography is not the most accurate evaluation method of LV myocardial function with major limitations such as poor images and insufficiency of circumferential motion data in myocardial

contraction. Also, gated single photon emission computed tomography (SPECT) is widely used for the evaluation of LV function in the detection of significant coronary artery disease (CAD), although it has relatively low spatial and temporal resolution [5].

While the echocardiography and the SPECT are popular in cardiac clinical use, cardiac magnetic resonance imaging (CMR) is widely agreed to as the most accurate modality for the LV function. The CMR has the obvious advantages of high spatial and temporal resolution tomographic images of the human body in any arbitrary orientation, and excellent soft tissue contrast. Moreover, CMR imaging has been acquired without using ionizing radiation therefore there is almost no risk to the average patients. The CMR allows explaining the LV motion by labeling specific myocardial regions (tagging) with a rectangular or radial grid. The labeling is superimposed on the heart muscle at end-diastole and it becomes tissue property. The tagging deforms with tissue as the heart contracts and fades with time. Strain and rotation can be measured by tracking these tags manually or semi-automatically [6].

Previous studies based on magnetic tagging using spatial modulation of magnetization (SPAMM) for line and grid tagging have been used in many clinical and translational research studies. Although it is known as a very useful technique in the analysis of heart-wall motion, by providing temporal correspondence of material points within the heart wall, it has not been adopted into routine clinical examination. The SPAMM method uses the parameters for analysis LV motion that are too complex and often produce unreliable data correspondence between frames. Recently, a new myocardial tags method applied in radial orientation using selective

saturation bands has been developed and has clinical advantages over SPAMM methods. This study shows that radial tagging is a more direct way for measuring LV circumferential strain and rotation comparing with grid tagging.

1.2 Aim A To develop and evaluate computer software for measuring myocardial strain and rotation in magnetic resonance (MR) radial tagging imaging.

We hypothesized that computer software that incorporate geometric calculation knowledge in the Cartesian coordinate system could objectively analyze the myocardium circumferential strain and rotation angle with signal intensity characteristics in radial tagging MRI images. Previously, manual computer software was developed for assessment of myocardium strain and rotation of LV with the MRI radial tagging images. Using this software, the myocardial strain and rotation angle were calculated assuming the structure of the LV myocardium is like a circle, and rotates in a steady axis.

The purpose of this current study was to develop an advanced automatic computer tool using parameters, which are adjacent to the morphology of the LV for assessing myocardial strain and rotation angle. The computing circumferential strain and rotation with this tool agreed most closely with manually calculated strain and rotation. The accuracy of these strain and rotation measurement tools will be assessed by comparison with manual measurement of the MRI radial tagging images from two volunteers.

1.3 Aim B To validate the operating radial tagging analysis is a straightforward alternative to grid tagging for measuring strain and rotation of the LV. Also, compared to manual radial tagging analysis, previous radial tagging software, this study may be able to reduce analysis time and result more precisely due to the algorithm is more direct and sensitive with the structure of the LV myocardium.

We hypothesized that the coordinate system of radial tags is well suited to the morphology of the LV and may be preferred for circumferential measurement of myocardial strain and rotation angle. Because the radial tagging analysis calculates the changes of myocardium length and rotation along the LV myocardium in circumferential direction, it is the most direct way to achieve the circumferential strain and rotation of LV myocardium. To validate the radial tagging method, the radial tags analysis is compared with the grid tags analysis (SPAMM), which has been used in many clinical and translational research studies.

CHAPTER II

BACKGROUND AND MOTIVATION

The heart muscle fibers shorten while they contract. Therefore, muscle contraction generates strain in myocardial tissue. An assessment of myocardial strain describes how the heart works.

2.1 The General Heart Overview

2.1.1 Cardiac Anatomy and Function

The heart is a specialized pump that passes blood to the body. It is located between the lungs in the mediastinum and is surrounded by the cavity of pericardium. The pericardium is a strong, double-layered sac around the heart and roots of the great vessels. The heart structure develops along the midline of the thoracic embryologically; however, in adults it is lying obliquely and is angled to the left side of the chest. There are four chambers in the heart - the right atrium, right ventricle, left atrium, and left ventricle. These four chambers consist of a multilayered lining - the endocardium, the myocardium, and the epicardium, as showed in Fig.1.

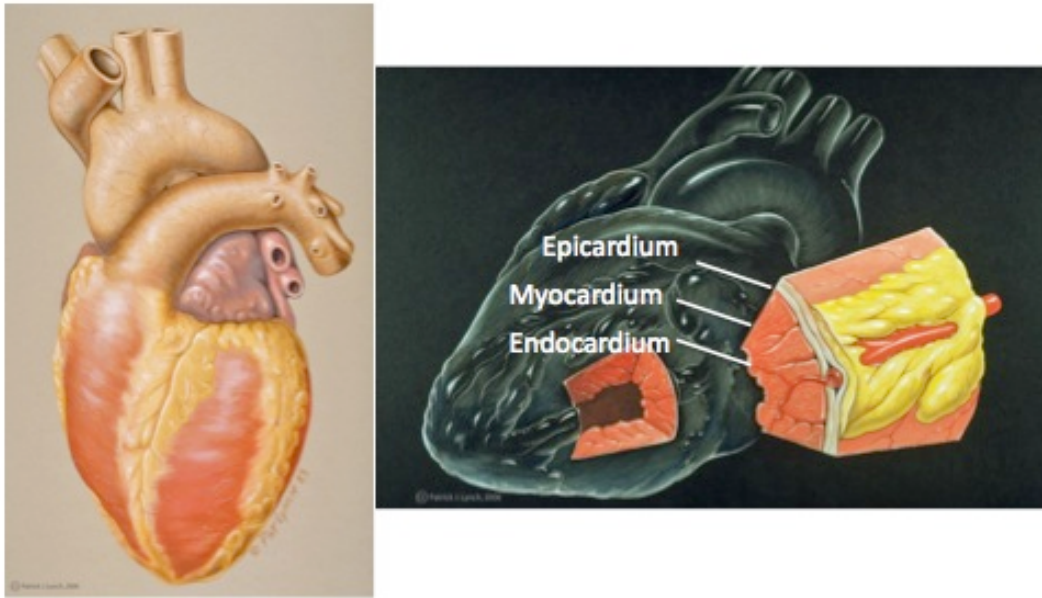


Fig.1 The Heart and Great Vessels (left) and the Layers of the Cardiac Wall (right)

2.1.2 The Cardiovascular System

The heart, the veins, and the blood vessels are the main components of the cardiovascular system. The right atrium receives deoxygenated blood from the body through the superior vena cava and pumps it to the right ventricle. Then the blood passes the lungs via the pulmonary artery to oxygenate the blood. The oxygenated blood from the lungs flows into the left atrium and left ventricle, this cardiac status is called as diastole. Then it pumps out through the aorta to the rest of body cells to provide oxygenated blood, this status called as the systole (Fig. 2). The ventricles work at a relatively high pressure and have thicker walls than the atria that work at much lower pressures [7].

Cardiac ischemia is one of the frequent types of heart disease and may be asymptomatic or may cause chest pain. It is caused when there is insufficient blood flow into the myocardium, or a mismatch of oxygen supply and demand as from an occlusion of a blood vessel. The sign of blood flow deficiency begins from the subendocardium and extends to involve the rest of the myocardial wall. This is followed by diastolic and then systolic dysfunction. These initial events are apparent only when followed by angina. If the process is severe enough, necrosis results.

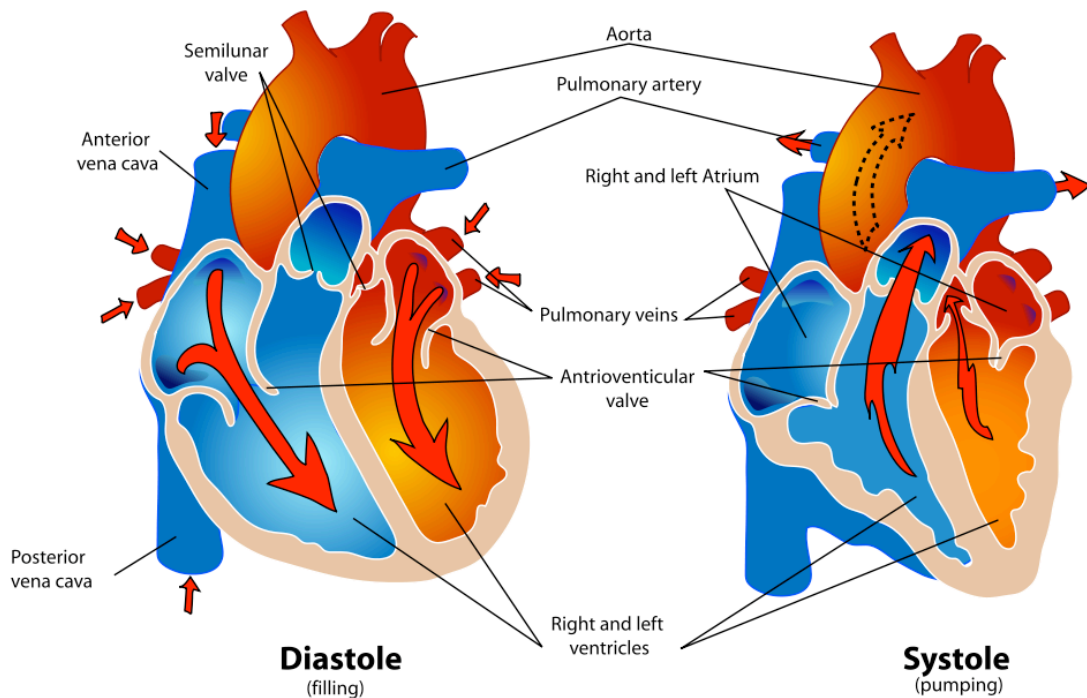


Fig.2 Diagram of the cardiovascular system.

2.2 Strain and Rotation Measurements in the Heart

2.2.1 LV structure and motion

The oblique orientation of the myofiber sheets determines the LV contraction. The myofibers of the endocardial region are right-hand-oblique oriented; the myofibers of the epicardial region are left-handed Fig. 3 [3]. During systole, a wringing motion, which is the isovolumetric contraction of the LV, has been described as a clockwise rotation at the base, and a counterclockwise rotation at the apex. An untwisting motion occurs during isovolumetric relaxation and is directed opposite to the wringing motion, with a counterclockwise rotation at the base, and a clockwise rotation at the apex [6].

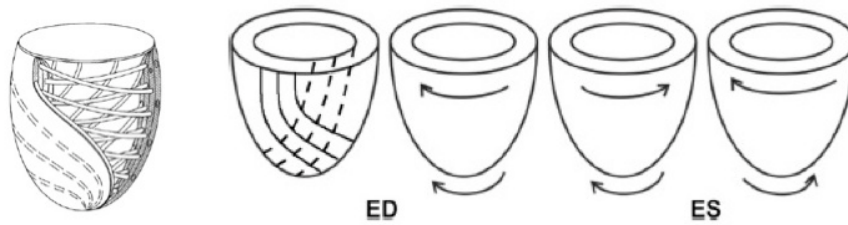


Fig. 3 Schematic Drawing of LV structure and motion. Myofiber directions: solid lines = epicardial region; dashed lines = endocardial region. Untwisting motion: ED = end-diastole; ES = end-systole. Figure used with permission [3]

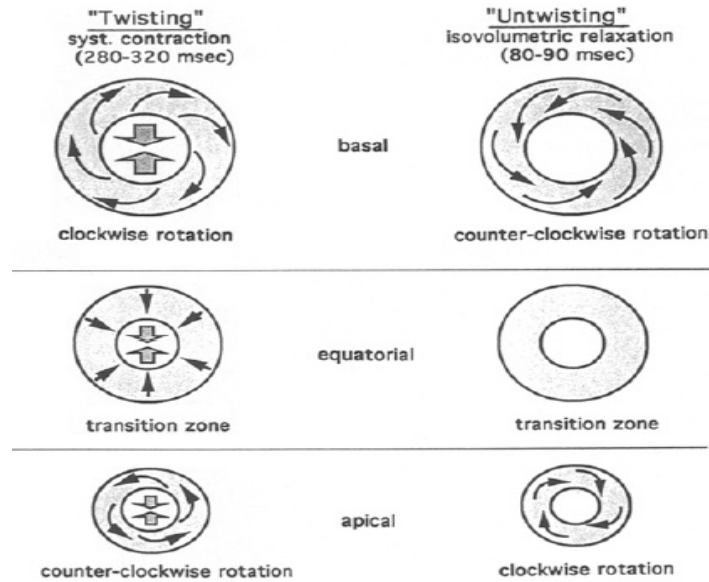


Fig. 4 LV rotational motion during systole (left) and early diastole (right). Figure used with permission [6]

2.2.2 LV structure and function relationship

The mechanical displacement of the myocardium can be detected by the measurement of wall thickening. Myocardial strain relates the assessment of local tissue deformation as an indicator of myocardial contractile function. Usually the deformation of the myocardium is expressed in the radial-circumferential-longitudinal coordinate system, because it is well suited to the cardiac geometry [8]. When the heart contracts, in general, the ventricles become thicker in radial direction, and shorter circumferentially and longitudinally. The radial direction is perpendicular to the epicardial surface, toward the center of the ventricle. Radial strain reflects the local contribution of the myocardium to wall thickening. Circumferential lies in the short-axis plane and is tangent to the heart surface, directed counterclockwise as

viewed from the base. Circumferential strain implies intramural circumferential shortening. The longitudinal is perpendicular to the other two components and parallel to the longitudinal axis of the left ventricle. Longitudinal strain reflects the regional longitudinal shortening from the base to the apex (Fig. 5) [5]. Rotation is a description of the relative angle changes of an object that spins around three coordinate axes. Strain describes fractional element changes in length (in percent) from the resting state (end-diastole) to the state following myocardial contraction (Fig. 6). Strain is characterized not only by the magnitude of the length change, but also by the direction of the change. Negative strain values imply the contraction of the myocardial fibers, and positive values result from the lengthening of the myocardial fibers [9]. Quantitatively, a normal heart has a smoother distribution of strain and stress, than an abnormal heart in the-free wall [10].

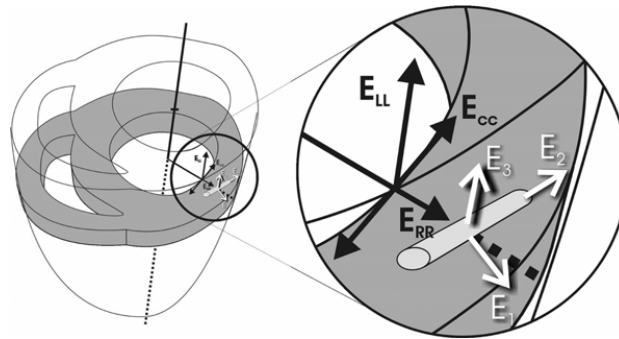


Fig. 5 Three - dimensional coordinate system of myocardial strain. [8]

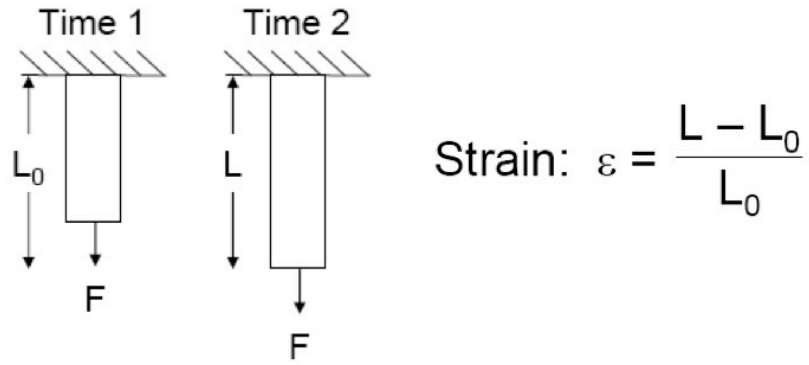


Fig. 6 The myocardial strain.

2.2.3 Strain Measurement Techniques

The heart motion during systole and diastole may be explained by the assessment of LV function like ejection fraction or shortening parameters. Different diagnostic techniques can be used to assess LV function, such as echocardiography, radionuclide angiography, and magnetic resonance imaging or computed tomography. However, a major limitation of these technologies for assessing cardiac function is the uncertainty in the rotational and translational motion measurements of the left ventricle. Recent diagnostic techniques account for cardiac motion only in the radial displacement, but not in the circumferential and longitudinal displacement. Implantation of radiopaque or ultrasound markers has been used in the past for determination of the cardiac motion with three directions. However, these techniques are extremely invasive and cannot be used on a broader range in clinical purposes [6]. The development of myocardial tagging by magnetic resonance (MR) allows determining, noninvasively, all the components of myocardial contraction at once. This MR tagging method can provide a more accurate measurement than assessment of wall thickening (radial displacement) alone [8].

2.3 MRI Image

Magnetic resonance imaging (MRI) is a nonionizing technique with high-resolution tomographic images of the human body in full three-dimensional capabilities and excellent soft-tissue contrast (Fig.7) [19]. MR imaging is based on the absorption and emission of energy in the radiofrequency range of the electromagnetic spectrum. To create images, the MRI utilizes a large magnetic field and radio waves. Any element has an odd number of protons able to be imaged using the magnetic resonance. The human body is primarily composed of water more than 70%, thus, hydrogen is the most abundant element in the body. A hydrogen atom has a single electron spinning about its nucleus, and a charged particle moving in a circular orbit, called spin, possesses a magnetic moment (μ). Each proton produces a small magnetic field, and these small magnetic fields are randomly oriented, in general.

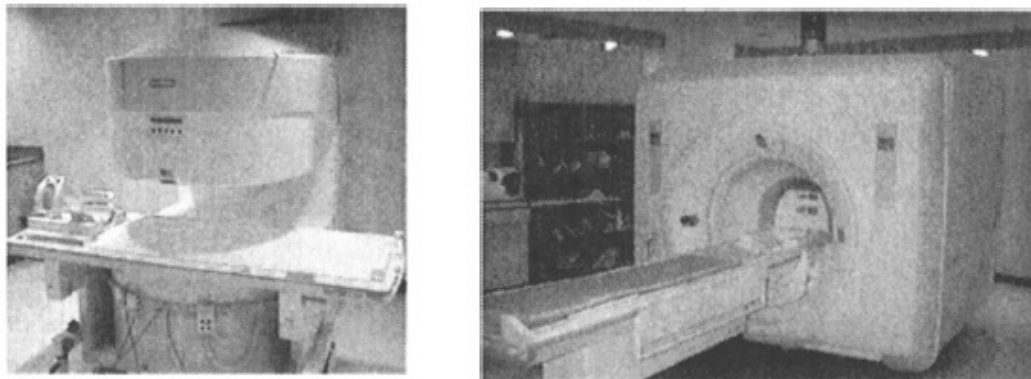


Fig.7 MRI instruments. Left: An open “C-arm” permanent magnet. The magnet has two pole pieces, one above and one below the patient bed, easy access to the patient. Right: A clinical superconducting MRI magnet. Figure used with permission [19]

In the presence of a large magnetic field (B_0), such as a MRI scanner, hydrogen protons will align either parallel or anti-parallel with the direction of the large magnetic field (B_0). All the small proton magnets add up to the equilibrium magnetization (M) and it is much smaller than B_0 . The combination of B_0 and the magnetic moment (μ) of the proton result in the wobbling motion, called precession. This precession takes place at a specific frequency according to the Larmor equation:

$$\omega = \gamma B_0$$

The Larmor frequency of precession (ω) depends on the element and the magnetic field strength (B_0). γ is a constant called the gyromagnetic ratio, for hydrogen, γ is 42.58 MHz/Tesla.

Higher precession frequency results from higher magnetic field strength. The magnetic moment (μ) of each proton can be presented to two orthogonal components, which are longitudinal magnetization (M_z) and transverse magnetization (M_{xy}). The net magnetization (M) results from the summation of the longitudinal components from the parallel and anti-parallel oriented protons. When a mass of protons comes together, the transverse component (randomly oriented) cancels out, and only the longitudinal component leaves (Fig.8) [15].

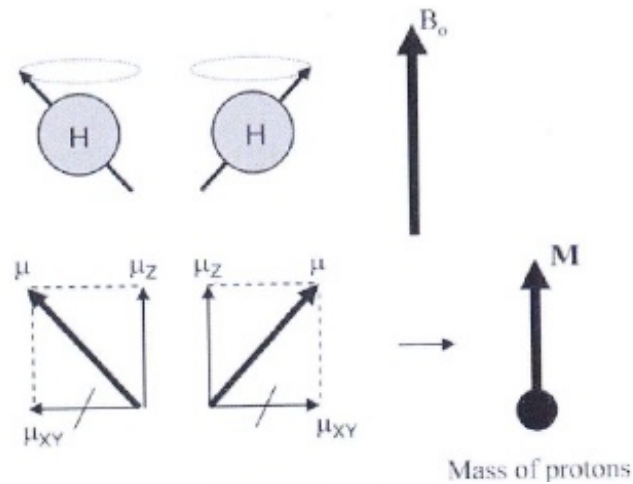


Fig.8 Schematic diagrams of precession of the proton and net magnetization, M

The MRI signal occurs from the interaction between the magnetic field of MRI instrument and hydrogen protons. The signal from the specific tissues and organs has to be acquired for an image construction. To excite the tissues and make them emit a signal, the excitation signal is provided by applying a second external magnetic field (B_1). By applying a radiofrequency (RF) pulse through a second magnetic field (B_1), combined with B_0 , flips the net magnetization from the longitudinal direction Z toward the transverse plane XY . The degree of the flip of M_z into the XY plane is determined by the strength of B_1 and the duration of its application (Fig.9).

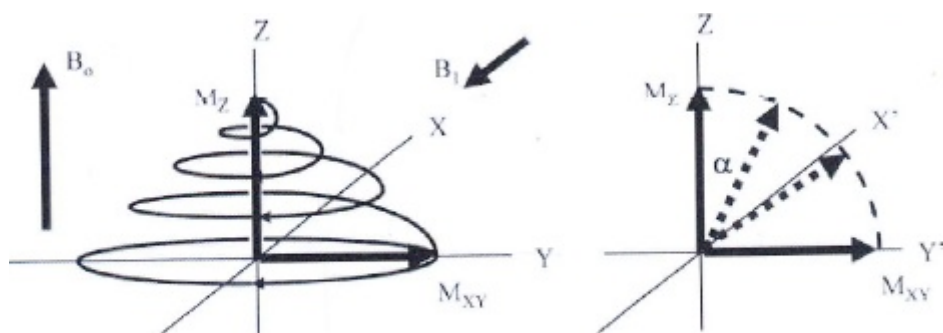


Fig.9 The application of an RF pulse through a second magnetic field B_1

When after the excitation of the protons, the protons would emit the excessive excitation energy to the surroundings. This relaxation of the protons (return of the protons from the excited state to the equilibrium state) result in decay of transverse magnetization (M_{xy}) and a recovery of longitudinal magnetization (M_z). There are two types of relaxation called T1 and T2. Both of them are distinct property of different tissues and provide contrast in magnetic resonance images Table I. T1 is the time for longitudinal magnetization (M_z) and takes 63.2% of the original M_z to recover. T2 is the time for transverse magnetization (M_{xy}) and takes 63.2% of the initial M_{xy} to disappear Fig. 10.

Table I Tissue Relaxation Times at 1.5 T

Tissue	T2 (msec)	T1 (msec)
Adipose	80	260
Liver	42	500
Muscle	45	870
White Matter	90	780
Gray Matter	100	920
Cerebrospinal Fluid	160	2400

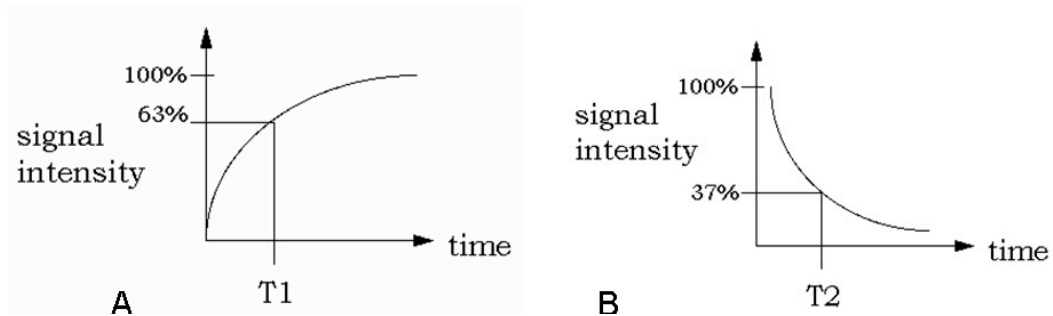


Fig. 10 A: T1 relaxation: Recovery of signal in the M_z direction.

B: T2 relaxation: Decrease in signal in the xy plane.

The sum of the NMR individual signals from protons enables the distinguishing of different tissues, but not spatial locations. A spatial variation on the main static field can be achieved by applying magnetic field gradients during the image procedure. A magnetic field gradient superimposes a weak magnetic field that changes linearly with position on the main static field. The symbols for a magnetic field gradient in the x, y, and z directions are G_x , G_y , and G_z . For spatial localization, the image processing can be divided into three sequences: slice selection, frequency encoding, and phase encoding.

Slice selection is performed using a magnetic field gradient simultaneously with the application of the excitation RF pulse. The region of interest in the image can be localized by using a frequency-selective pulse in the y, the z, or the x directions corresponding to the coronal, axial, or sagittal slice of the image. An oblique slice angle can be accomplished using two of the gradients applied Fig. 11.

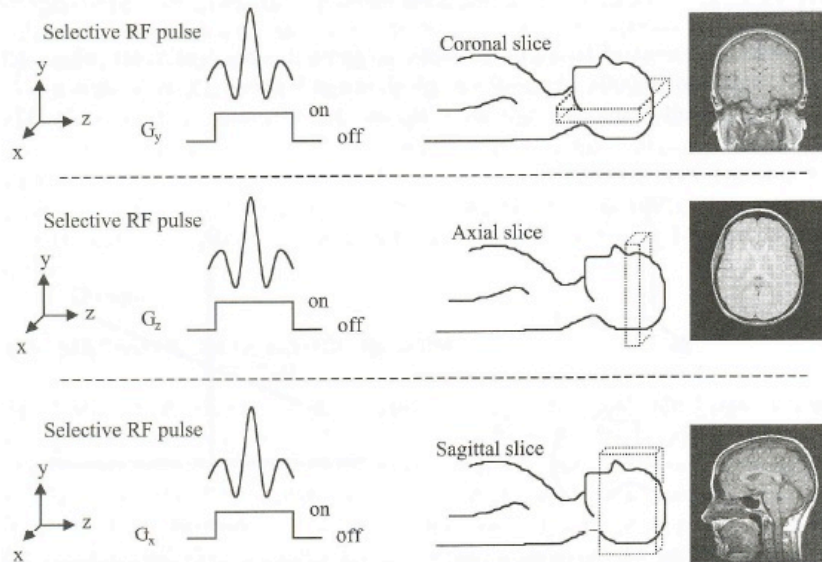


Fig.11 A schematic of slice selection in MRI. Figure used with permission [19]

Frequency encoding gradient is applied with data acquisition in the orthogonal direction of the slice selection gradient. With frequency encoding gradient, the variation in the precessional frequencies across the slice leads to localize image in orthogonal direction with slice selection. For instance, the right arms from the left, in the case of an axial slice Fig. 12.

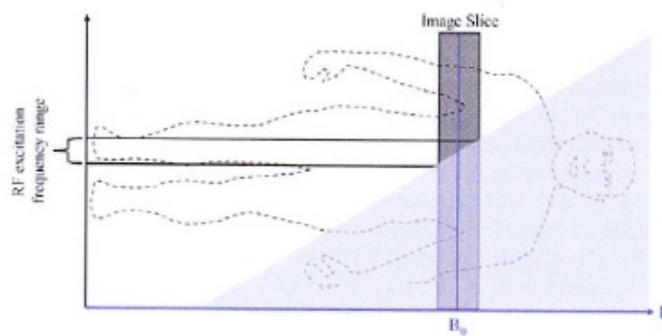


Fig. 12 Slice selection. Figure used with permission [15]

The slice selection and frequency encoding are possible to create a 2D image using frequency differences. To encode proton locations in three orthogonal directions, phase encoding creates phase differences between protons in the third spatial direction. Phase encoding is performed by turning on and off a magnetic field gradient in a specified time interval. The strength and duration of the magnetic field gradient affects the magnitude of the phase difference between the protons.

An MR image is created by repetitive application of the various pulse sequence components such as gradient echo and spin echo. By convention, RF pulse applied first, followed by magnetic field gradients in three orthogonal directions. Lastly, the timing of the resultant MR signal (echo) at the time of data acquisition is shown Fig. 13.

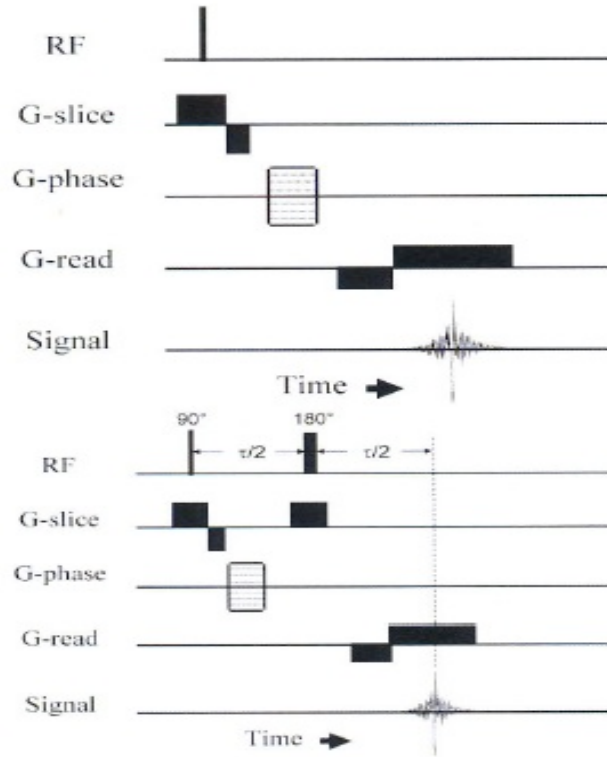


Fig. 13 The various pulse sequence components:
gradient echo (top) and spin echo (bottom).

2.4 Cardiac MRI Image with Tagging Methods (Radial vs. Grid)

Myocardial tagging was first described in 1988 by Zerhouni et al. [11]. Tags are marks of myocardial tissue with radio-frequency (RF) saturation before acquiring images, so that tags appear dark in subsequent magnetic resonance images and differentiate from the rest of the regions (Fig. 14) [9]. The actual protons of tissue in the tagging region have been magnetically altered. These tags move with the underlying tissue. Because tags are perturbations in longitudinal magnetization, tags are transient and are fading exponentially with longitudinal relaxation with constant T_1 [9]. This tagging method is used to label and track specific regions of the

myocardium during contraction. During cardiac motion, tags can be monitored depending on the signal difference (SD) generated between tagged and non-tagged regions [11].

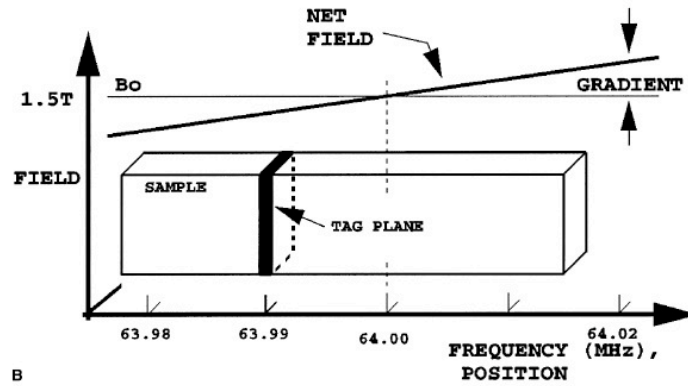


Fig. 14 Tag plane generation. Magnetic field gradient and radiofrequency energy are used to select and invert the magnetization only on the resonant tag plane, where the local field strength causes proton precession to occur at the same frequency as the applied radiofrequency pulse. Figure used with permission [9]

Two myocardial tagging methods of MRI were introduced concurrently. Zerhouni et al. used tags in a radial pattern to track the deformation of the LV myocardium by the tags' intersection with the endocardial and epicardial contours (Fig. 15) [17]. Axel and Dougherty used grid tag planes and their intersection with the lines of the grid to track LV myocardial wall motion (Fig. 16).

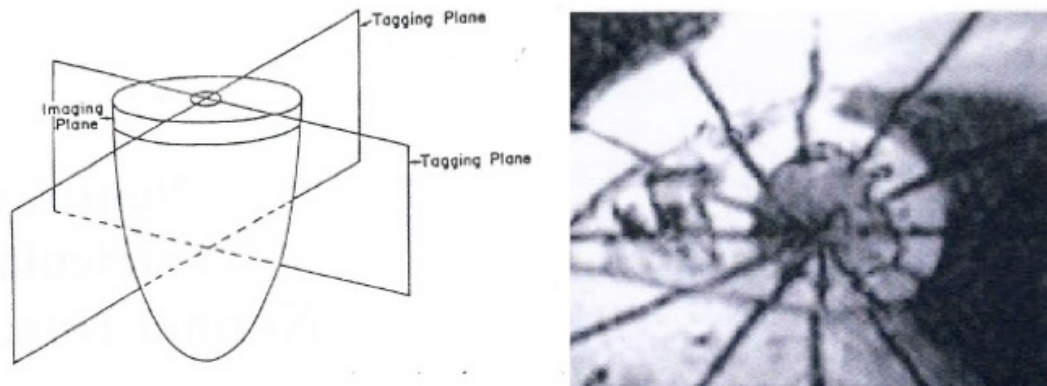


Fig. 15 Radial tagging sketch (left) and imaging plane showed in MRI image (right).
Figure used with permission [17]

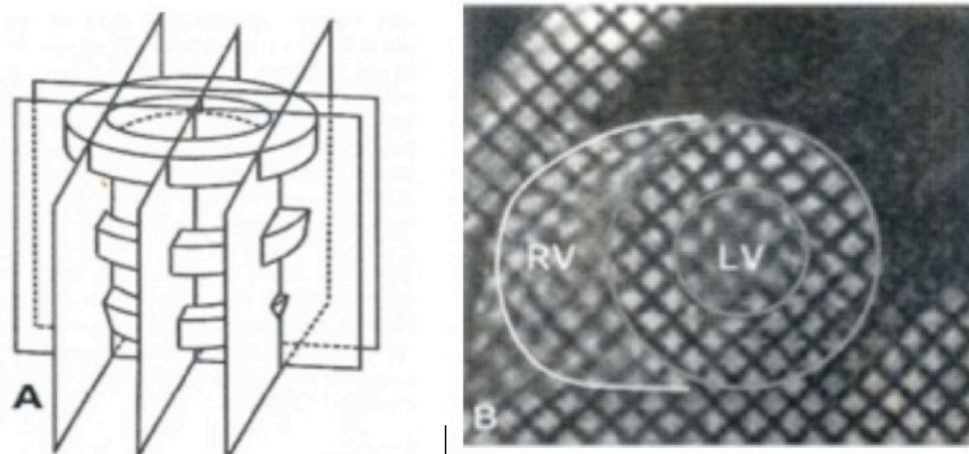


Fig. 16 Grid tagging sketch (left) and showed in imaging plane (right). Figure used with permission [5]

The analysis method used to extract information on myocardial function from the tagged images depends on the clinical purpose for which it is applied. For the visual assessment, tags can be easily observed by the eye. Thus, the tag lines should be as sharp as possible and image quality is significant, whereas temporal resolution and the applicability of semiautomatic postprocessing are less significant. Spatial

modulation of magnetization (SPAMM), a way to generate a tagging pattern, was introduced in 1989 by Axel et al. [13]. A tag is applied twice in 2 orthogonal directions providing a grid pattern. For the image acquisition, a rectangular intensity profile of the tag lines is chosen and presents grid-tagged images. A SPAMM is known as one of the most widely used techniques for visual assessment [5]. However, for quantitative assessment of myocardial deformation, the Harmonic phase (HARP) analysis is currently the most widely used. HARP method provides less user intervention and relatively faster processing time. HARP is used to measure motion directly in the periodic tagging pattern. This traces the spatial phase changes by filtering selected peaks in the k-space frequency of the image [8].

2.4.1 Grid tagging

Before the image acquisition, grid patterns are represented by applying a tag twice in 2 orthogonal plane directions. Then SPAMM grid tagging image data was processed using the HARP software. Therefore, a rectangular intensity profile of the tag lines shows grid-tags on the short-axis plane of the MRI images. With this software, the tagging grid points were tracked from the end diastole to the end systole. A mesh of small triangular elements is connected with a set of tracked tag points (Fig. 17) [18].

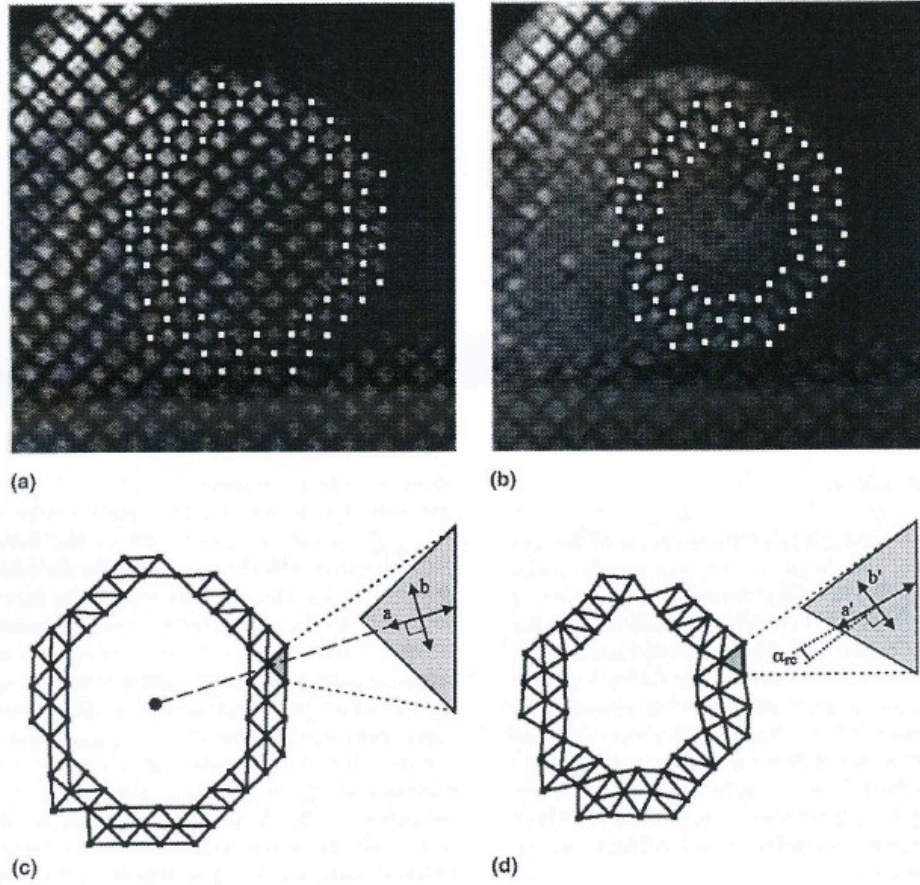


Fig. 17 MR grid tagged images. Measuring the myocardium deformation by tracking triangular elements. Figure used with permission [18]

The enlarged triangle along the myocardial contour presents strains and rotation angles. A single triangle has three parameters: the radial strain ϵ_r (a), circumferential strain ϵ_c (b), and rotation angle α_{rc} (see Figure). The strains correspond to the LV wall thickening or shortening. The rotation angle represents the change in angle between the initially orthogonal line segments a and b . The parameters are used for calculating the strain tensor \mathbf{E} is needed to calculate the strains (1) [14].

$$\begin{aligned}\varepsilon_r &= \sqrt{1 + 2E_{rr}} - 1; & \varepsilon_c &= \sqrt{1 + 2E_{cc}} - 1; \\ \sin \alpha_{rc} &= \frac{2E_{rc}}{(\varepsilon_r + 1)(\varepsilon_c + 1)},\end{aligned}\tag{1}$$

Green's strain tensor \mathbf{E} . E_{rr} and E_{cc} are the diagonal elements of \mathbf{E} , and E_{rc} is the off-diagonal element.

In this study, we used the grid tagging analysis data processed using the HARP software by an experienced observer.

2.4.2 Manual radial tagging

The different states of magnetization between the tagged regions and non-tagged regions persist for a time, and are mainly dependent on longitudinal relaxation time (T1). During that time, a magnetic resonance image acquired orthogonally to the tagging plane will demonstrate the signal intensity difference between the tagged and nontagged region. In radial tagging images, the six tag planes intersected the myocardium and it segments the myocardium in 12 regions (Fig. 18). These 12 segments on the myocardium of each short-axis image are imaged from the end diastole to the end systole. A tag point is defined as the point where a tag crosses the epicardium or endocardium. The centroid is calculated by the selected epicardial and endocardial points. The lengths of the lines connecting each adjacent tag points are used to calculate the strain; the angles are defined as the slopes of the lines connected between each tag point and the centroid. To present and compare the value of strain and angle with different measurement methods, the value are calculated at the mid-wall (red dashed line in Fig.18) between the epicardium and the endocardium from

the tag points.

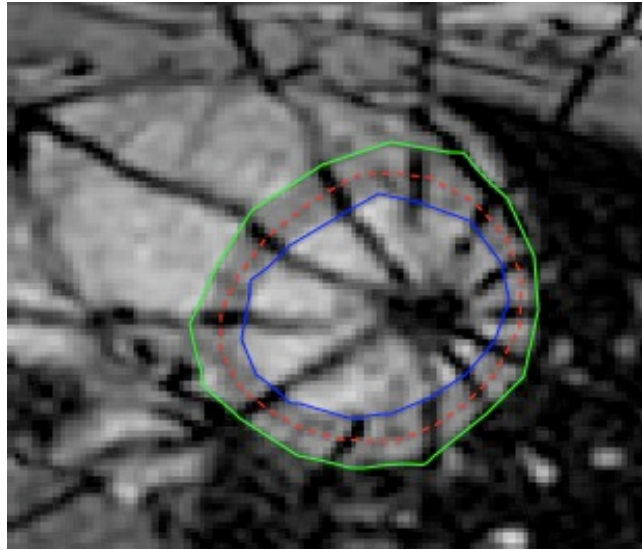


Fig. 18 LV Myocardium segmented 12 regions by radial tagged plane. Green line presents epicardium; blue line is endocardium and red-dashed line is mid-wall.

Previously, a manual radial tagging analysis software was developed to measure the circumferential strain and rotation angle of the LV myocardium. In this tool, loading a series of MRI dicom images and designating the number of radial tag lines to generate points that can be modified along the endo- and epi myocardium. After user selects the centroid, the endocardium points, and the epicardium points manually, the contour of endocardium and epicardium are showing based on circle from the centroid. The centers of these endocardial and epicardial tag points are visually estimated. At the each image frame, user adjusts the every displaced endocardial and epicardial tag points. This tool returns the value of length and angle of 12 segments at each image frame as the result. With this results, the strain is calculated mathematically using the Microsoft excel. The manual radial tagging analysis software has shown in Fig. 19. This software developed from previous study

called the manual radial analysis in this paper. Advanced software for the radial tagging MRI images analysis has been developed and this would be mentioned as the semi-automatic radial tagging analysis tool in this paper.

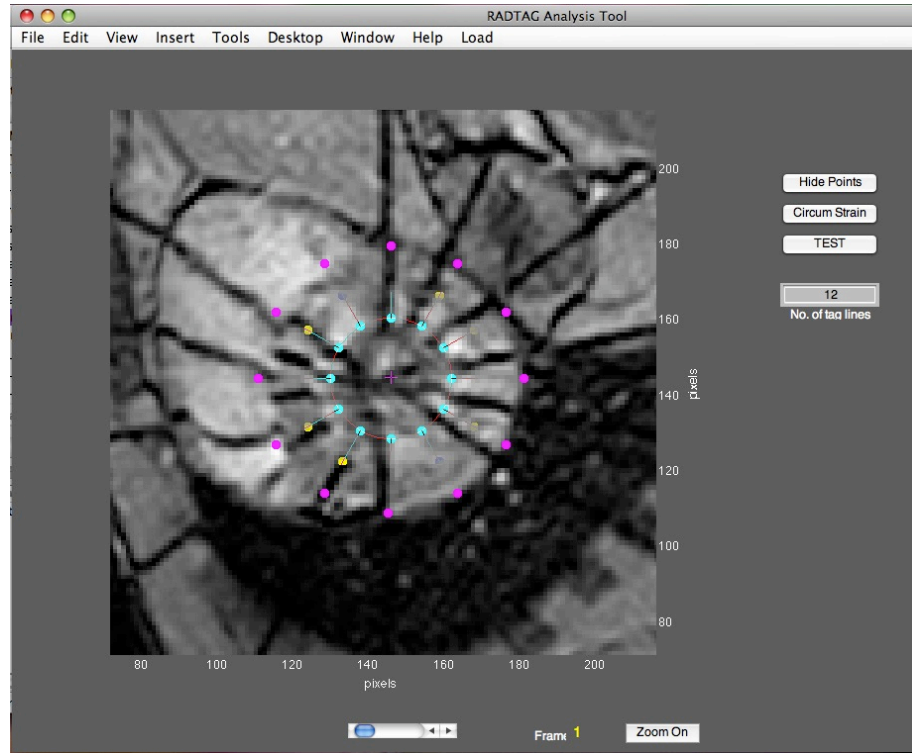


Fig. 19 A radial tagging analysis tool implemented manually.

CHAPTER III

METHODS

3.1 Study protocol

The LV motion can be estimated tag using segmentation methods. The radial and grid tagging analysis software in this study rely on segmentation-based methods. MRI radial tagging image series from 9 volunteers were used to develop computer analysis software and validate this system. One image series of the volunteers was used to develop a semi-automatic analysis system to measure the strain and rotation angle of the myocardium in the left ventricle. To verify the accuracy of the developed computer system, two volunteers' result data from the developed analysis program were compared with the mathematically calculated data performed manually. Ultimately, for the validation of the radial tagging analysis, the measurement of strain and rotation angle from 7 volunteers, was compared with the grid tagging analysis and previous radial tagging study. Images were acquired using a Philips 1.5T MRI scanner at the Cleveland Clinic Main campus in Cleveland, Ohio.

Radial and grid tagging were performed using a cardiac triggered TFE sequence with FOV 320-304 mm², TE 1.8ms, TR 4ms, breath hold 15 sec. Grid tags were applied with 7 mm spacing thickness. Radial tags were spaced by 30 degrees.

Each volunteer has two MRI image series in the different level planes of the LV (apex and mid-wall) and each image series (apex and mid-wall) has 14-20 image frames. Therefore, we have 14 subjects to compare the results among different tools. Images were acquired from the end diastole to the end systole. The number of image frames on each volunteer is different because everyone has different cardiac cycles.

To compare the semi-automatic radial tagging analysis to the grid tagging analysis and the previous manual radial tagging analysis study, the same MRI original Images from all volunteers were analyzed by their own software and the results data used in this study.

3.2 Deformation measurement

The LV myocardium fibers are arranged in a complex architecture: in the mid-wall, the fibers are circumferential; however, subepicardial and subendocardial fibers are almost longitudinally directed. This fiber structure correlates to complex cardiac contraction patterns. Myocardial deformations comprise radial thickening, circumferential shortening, torsion, and longitudinal shortening. In this study, we measured the circumferential strain and rotation angle in short-axis MR images. To measure myocardial deformations, the Radial-Circumferential-Longitudinal (RCL) coordinate system was used as a reference coordinate system. The coordinate data of a myocardial point during the cardiac cycle were used to measure tag

displacement. Specifically, the deformation can be defined from the initial position to the displacement.

$$\mathbf{x}' = \mathbf{x} + \mathbf{u}(\mathbf{x}) := \mathbf{f}(\mathbf{x})$$

Denoting by \mathbf{x} and \mathbf{x}' its position at times t and t' ($t' > t$) respectively, and \mathbf{u} is the displacement and \mathbf{f} is referred to as the deformation.

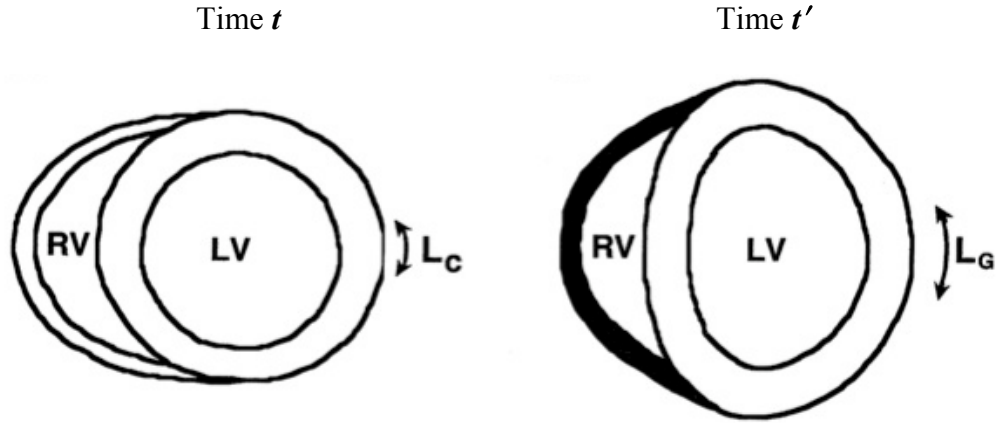


Fig. 20 The LV deformation parameters, strains and rotation angle, are calculated with coordinate values at time t and t' .

To demonstrate the measurement, accuracy of the semi-automated radial tagging method, we compared the data value of developed program with geometric calculation in manual. To confirm the correctness of the developed Matlab program, we show the difference between the results data of Matlab program and mathematical calculation data performed by Excel (Microsoft office). To simplify the process, we used 6 images in one image series instead of 15-20 images.

We plotted the same MRI image series used for semi-automated radial analysis software on the MATLAB figure. Then segments were drawn between the 12 tags and labeled across with the mid-myocardium (between endo- and epi-cardium). Fig. 21 indicates the required points for measuring myocardium

deformation. The blue line defines the myocardium location, which is the center between the epicardium and endocardium. The points of contact of the blue line with the tagging were traced in each image in the series. In this study, myocardium deformation is explained by myocardium strain (length changes) and rotations. First, the semi-automated radial tagging software divided the myocardium contour (blue line) into 12 segments according to red marked numbers on Fig. 21. The length of myocardium contour (blue line) was calculated and the length of each of the partial 12 segments of the first image can be used as a reference value.

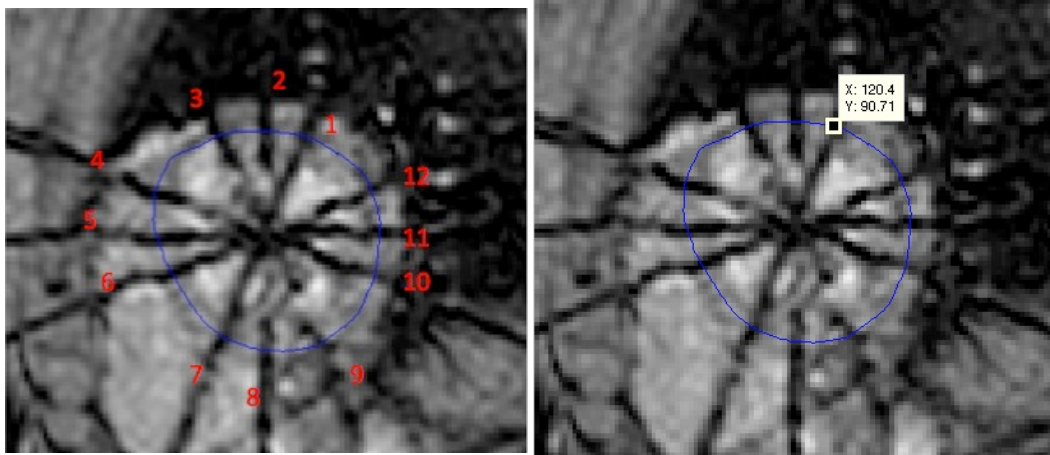


Fig. 21 Labeling the segments along the mid-myocardium (blue line) and extracting x-y coordinates subjects connecting points mid-myocardium and tags.

One image series has 15 - 20 images: the length of all 12 segments location in each image had been compared with the reference value of the first image. This describes how the myocardium had been deformed by time locally and we acquired the specific values (range and rotation rate) as a result (Fig. 22).

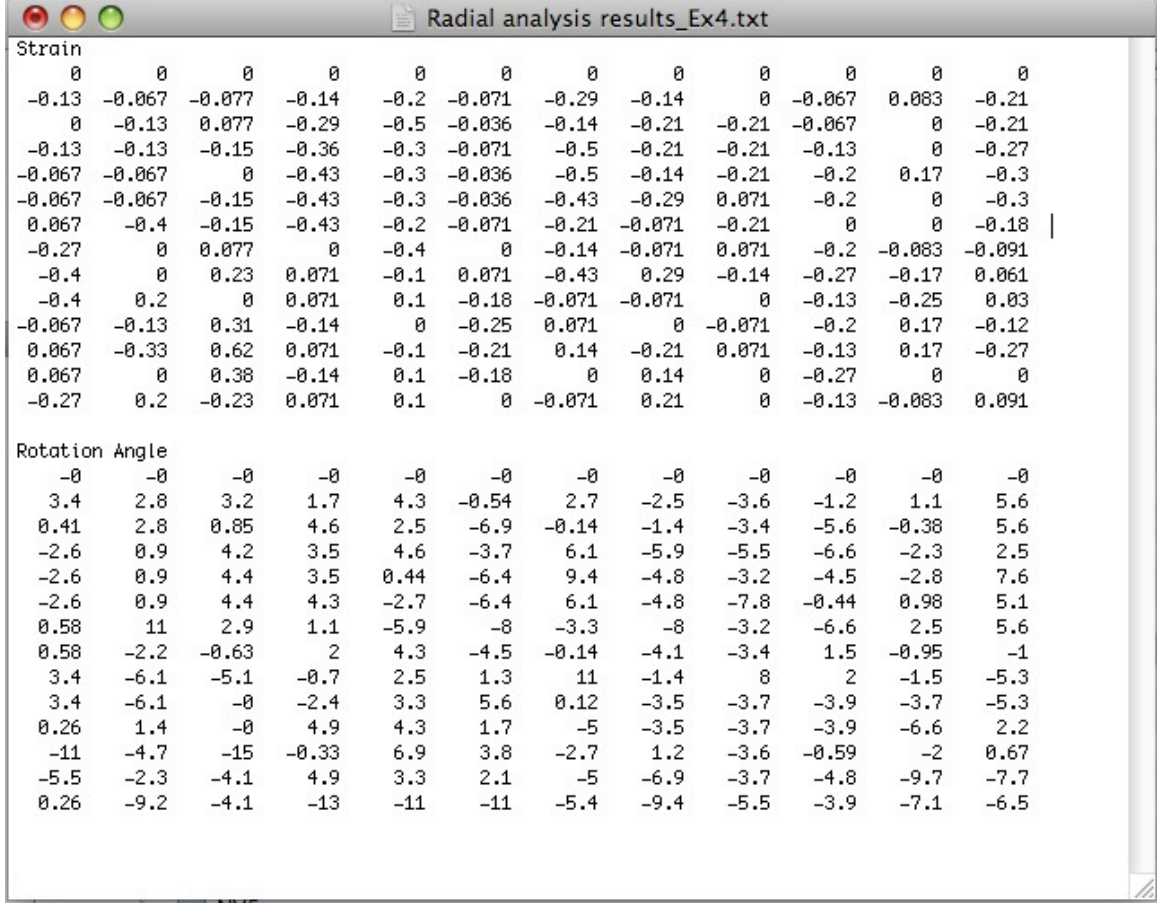


Fig. 22 Captured image of myocardium deformation results from MATLAB.

Column is each image number 1-6, row is partial tag segment divided by 12.

To calculate strain and angle rate manually, we simply extracted 12 location data points between mid-myocardium and tags from image (Fig. 21 right). Table I shows determined data from each image. L values of Table I are the distance in pixels between adjacent subjects. Given the two points (x_1, y_1) and (x_2, y_2) , the distance between these points is given by the formula:

$$d = \sqrt{(x_2 - x_1)^2 + (y_2 - y_1)^2}.$$

Once analyzing the all images showed in Table II, the angles of the region between tags (segments) were calculated. Fig. 23 on right shows the equation to find the angle. The arctangent function command is 'atan2 (x, y)' in Excel. The segmentation angles (radians) are derived by abstracting the coordinates from tags to the center of LV: the resulting angle is in radian from the center of LV. The values in Table II indicate the location data of each of the 12 points and the length between points. Table III indicates the region information, pie-shaped segmentations were listed with their curve length (pixel) and angle (radian).

Table II Data point's location information; crossing between the tags and the mid-myocardium line. L is length value in pixel of segmented myocardium contour, X and Y is x-y coordinate value of image

Seg.	Image 1				Image 2				Image 3				Image 4				Image 5				Image 6			
	X	Y	L		X	Y	L		X	Y	L		X	Y	L		X	Y	L		X	Y	L	
1	138	107	11		138	109	9		140	111	10		138	109	8		138	113	9		145	108	9	
2	127	106	10		129	108	10		130	111	9		130	109	10		129	111	8		136	106	6	
3	117	109	14		119	111	11		121	111	11		121	113	8		121	113	13		130	107	16	
4	110	121	8		113	120	9		114	119	9		115	119	10		112	122	8		116	114	10	
5	108	129	9		111	129	10		111	128	13		112	129	10		110	130	9		111	123	13	
6	110	138	16		111	139	13		113	141	10		113	139	10		110	139	14		109	136	17	
7	120	150	9		120	148	10		121	147	8		120	146	10		119	150	10		117	151	10	
8	129	152	11		130	151	9		129	148	7		130	149	9		129	153	11		127	152	10	
9	140	151	18		139	150	16		136	148	16		139	147	13		139	148	15		137	149	16	
10	152	137	9		149	138	6		148	138	133		148	138	8		149	137	12		150	140	12	
11	152	128	11		151	132	11		15	131	135		151	131	10		150	125	9		152	128	8	
12	151	117	16		150	121	17		150	124	16		151	121	18		146	117	9		152	120	14	

=SQRT((AK15-AK4)^2 +(AL15-AL4)^2)

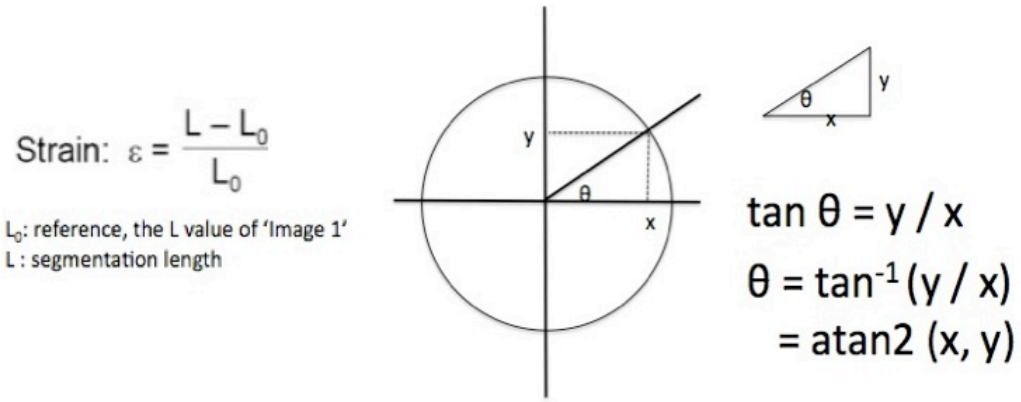


Fig. 23 Strain equation and angle(θ) formula with x-y coordinates.

Table III The local myocardium rotation. The rotation angle (radian) from LV center calculated from Table II data

Partial segment angle (radian)						
	Img 1	Img 2	Img 3	Img 4	Img 5	Img 6
Seg.1	0.52	0.43	0.52	0.43	0.42	0.37
Seg.2	0.40	0.49	0.41	0.41	0.36	0.42
Seg.3	0.61	0.54	0.62	0.53	0.69	0.42
Seg.4	0.43	0.44	0.49	0.57	0.47	0.47
Seg.5	0.38	0.50	0.56	0.55	0.41	0.44
Seg.6	0.74	0.63	0.50	0.52	0.60	0.78
Seg.7	0.40	0.39	0.51	0.51	0.41	0.44
Seg.8	0.43	0.38	0.32	0.37	0.56	0.40
Seg.9	0.80	0.79	0.81	0.78	0.71	0.91
Seg.10	0.39	0.34	0.33	0.37	0.60	0.44
Seg.11	0.46	0.45	0.36	0.39	0.49	0.46
Seg.12	0.72	0.88	0.85	0.85	0.56	0.73

The strain is defined as in Fig. 23, and rotation angles of the segments are simply found by abstracting reference angle (Table IV). Considering the length and angle of the first image on the series as a reference value, the values of following

images (2-6) showed the strain and difference range with the reference. The negative and positive value of angle indicates the deformation directions: a positive value corresponds with counter-clockwise deformation and a negative value indicates clockwise direction.

Table IV The assessment of strain and rotation of the local myocardium. Strain is myocardium deformation range and angle rate is rotation. Values are the difference between each image, segments and the reference image (first, initial time image). Negative value of angle rate means clockwise rotation.

	Strain						Angle rate					
	IMG	Img2	Img3	Img4	Img5	Img6	Img 1	Img 2	Img 3	Img 4	Img 5	Img 6
Seg.1	0	0	0	0	0	0	0.00	-0.09	0.00	-0.09	-0.10	-0.15
Seg.2	0	0	0	0	0	0	0.00	0.09	0.01	0.01	-0.04	0.01
Seg.3	0	0	0	0	0	0	0.00	-0.07	0.01	-0.08	0.08	-0.20
Seg.4	0	0	0	1	0	0	0.00	0.02	0.06	0.15	0.04	0.05
Seg.5	0	0	0	0	0	0	0.00	0.13	0.18	0.17	0.04	0.06
Seg.6	0	0	0	0	0	0	0.00	-0.12	-0.24	-0.23	-0.14	0.04
Seg.7	0	0	0	0	0	0	0.00	-0.01	0.11	0.10	0.00	0.04
Seg.8	0	0	0	0	0	0	0.00	-0.04	-0.10	-0.06	0.13	-0.03
Seg.9	0	0	0	0	0	0	0.00	0.00	0.01	-0.01	-0.09	0.12
Seg.10	0	0	0	0	0	0	0.00	-0.05	-0.06	-0.03	0.20	0.05
Seg.11	0	0	0	0	0	0	0.00	0.00	-0.10	-0.07	0.03	0.01
Seg.12	0	0	0	0	0	0	0.00	0.16	0.13	0.13	-0.16	0.01

3.3 Semi-automatic Radial tagging analysis tool

Software algorithm development

We assume that the MRI radial tagging is the most direct method for acquiring the circumferential strains and rotation angle because the calculated values are geometrically closest with the circumferential strains. To advance the radial tagging analysis tool for assessing the circumferential strain and rotation angle, the mid-myocardium (between the epicardium and the endocardium) and the LV centroid are calculated automatically. The epicardium and the endocardium are manually

delineated, and then the tag-ventricle boundary intersections are automatically designated. There are epicardial and endocardial contours on each image.

Fig. 24 is the initial screen of the semi-automatic radial tagging analysis tool running the 'Show_Images.m' (m-file) in the MATLAB program. All the MATLAB program code files were attached in APPENDIX-A. To operate this semi-automatic radial tagging analysis tool, the first step is loading MRI image series and showing on the screen using the 'Image Load' button in the panel (highlighted with blue in Fig. 25). Using the zoom button, the image can be better to differentiate between the myocardium of LV (Fig 26).

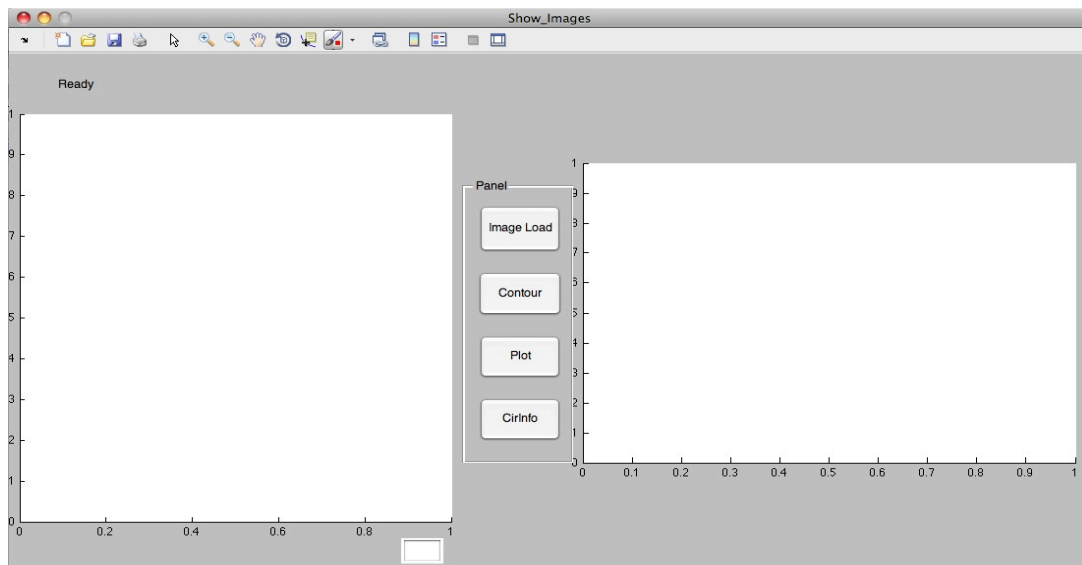


Fig. 24 The start-up screen of the semi-automatic radial analysis software.

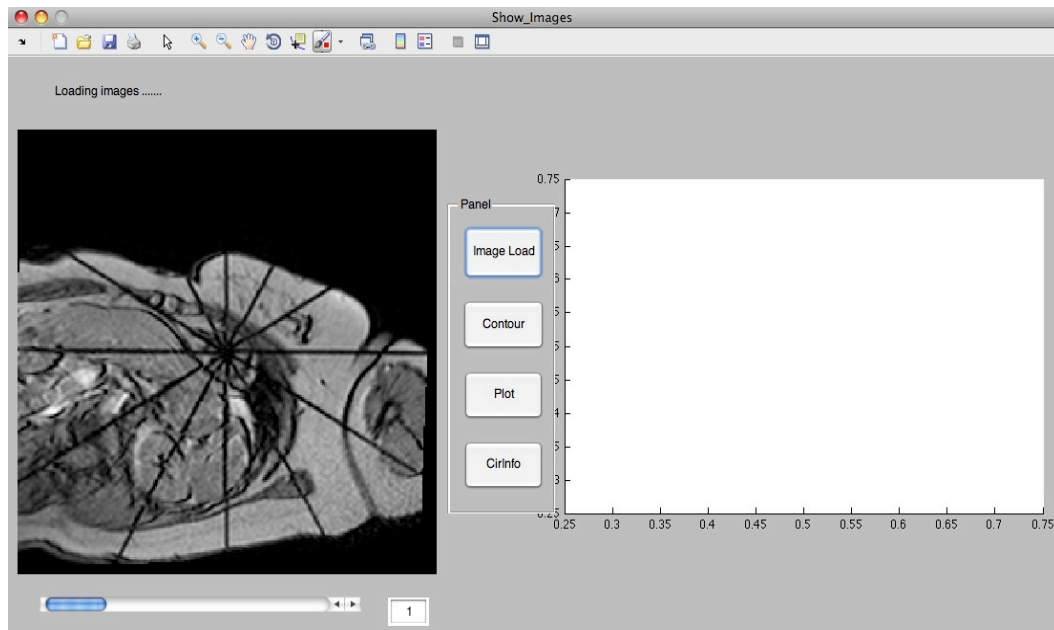


Fig. 25 The loaded MRI radial tagging image series showed in the tool.

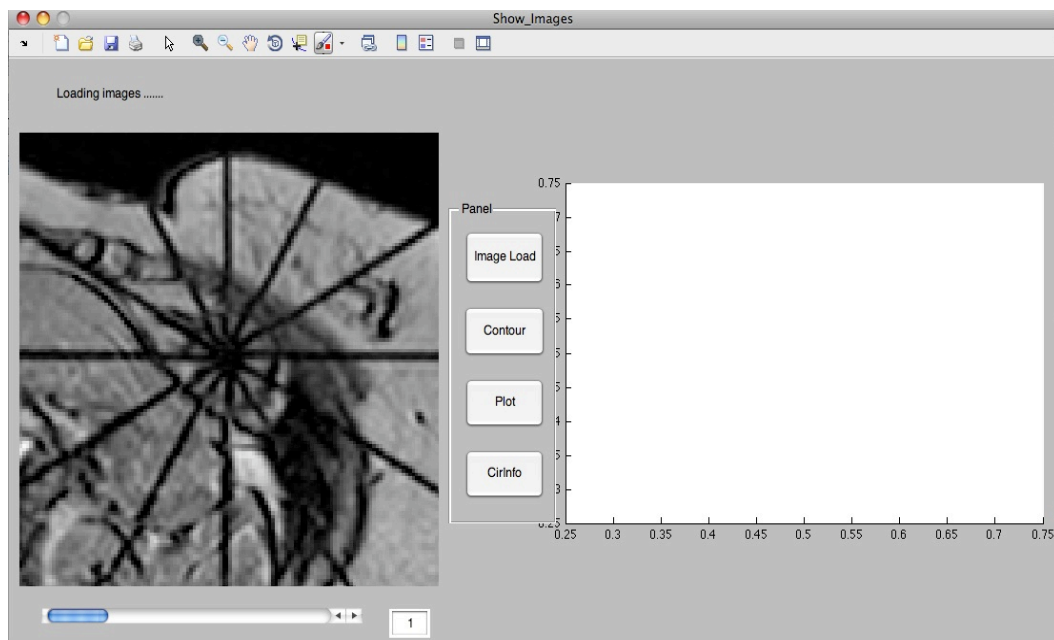
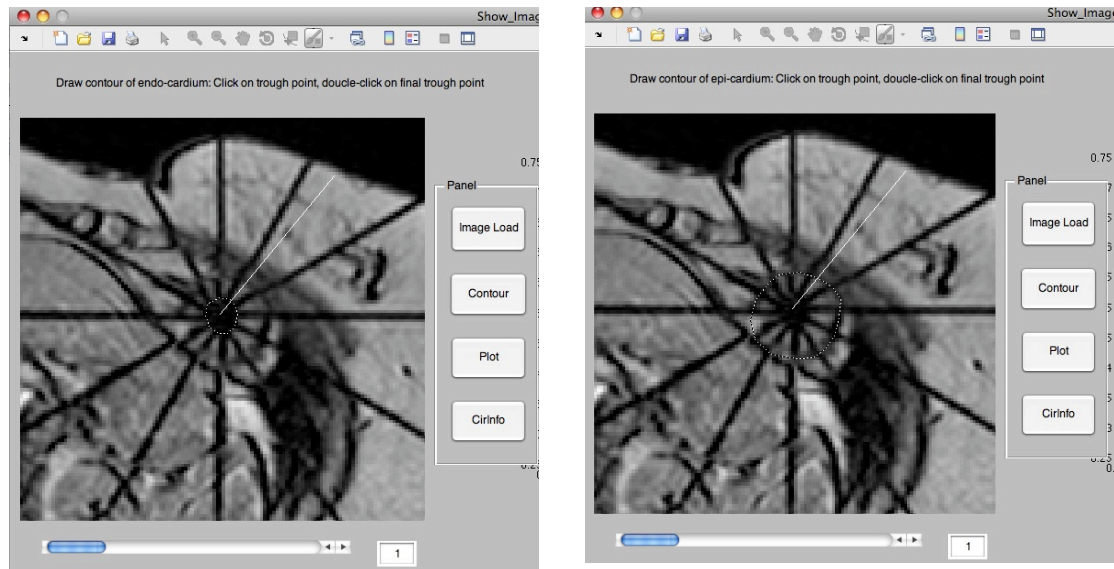


Fig. 26 Manipulating the MRI image for better demonstrating the LV

Second step is clicking the ‘Contour’ button; the user draws manually the endo- and epi-myocardium contours as the instruction in tool screen (Fig 27). The LV myocardium line has been defined as the median line between the endo- and epicardium and it was automatically calculated in the system. Also considering the epicardial and endocardial contour lines separately, the centroid of LV was automatically calculated to measure the rotation angle. The automatically calculated median line of the LV myocardium was shown in Fig. 28 (red contour).



A. Drawing the Endo-cardium line

B. Drawing the Epi-cardium line

Fig. 27 Demonstrate the myocardium of LV: contouring the endo- and epi-cardium

The calculated mid-myocardium contour (red contour in Fig. 25) is represented separately on the right of tool screen (Fig. 28 on right) by clicking the ‘Plot’ button. This is the third step and the plotted graph is represented along pixel length (vertical) verse image signal intensity (horizontal).

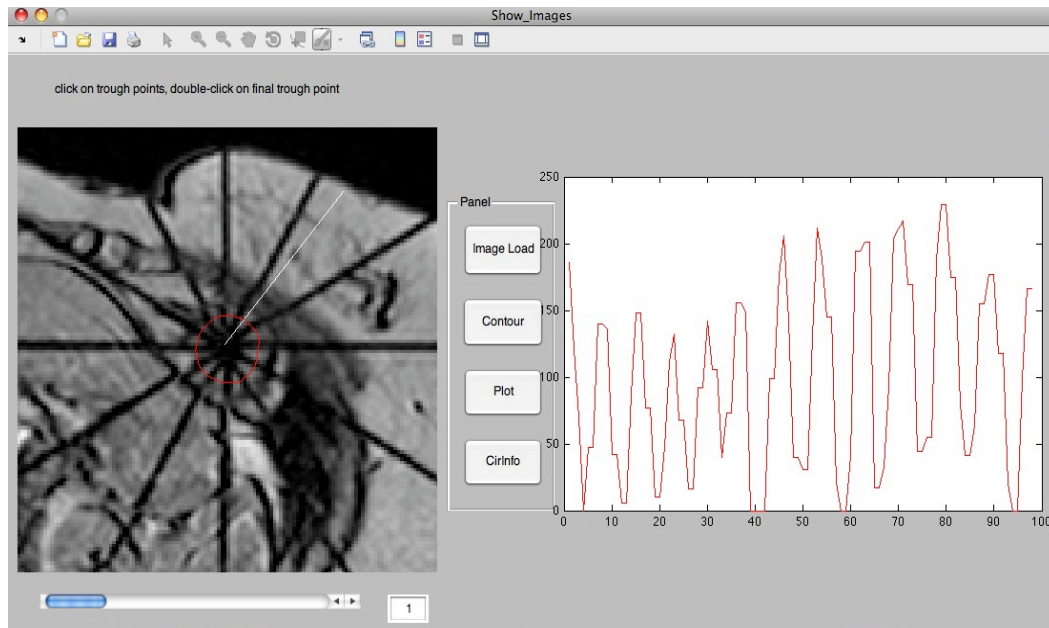


Fig 28 Step3: The calculated mid-myocardium of LV represented along the length and signal intensity.

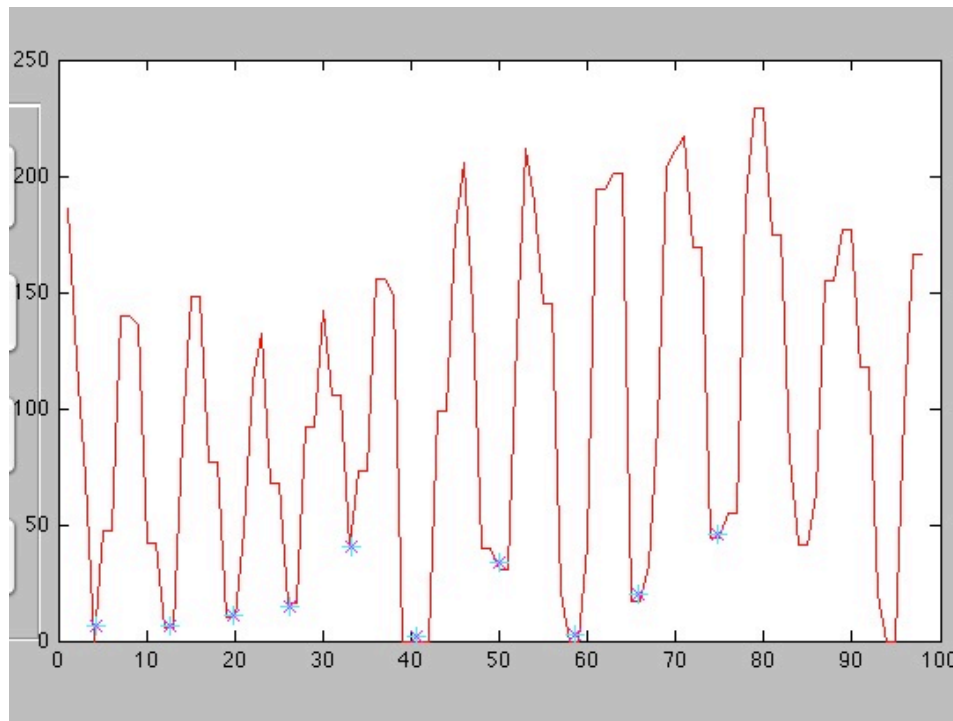


Fig. 29 Selecting the tag points by user on the representing the mid-myocardium contour.

On the representing graph of mid-myocardium contour, 12 tag points are selected manually by user clicks (Fig. 29). The graph indicates the mid-myocardium contour image signal intensity and since tags appear black in the image, the lowest intensity points are considering as tag points. The selected tag points can be shown in the MRI image and user can check if the selected points are in all correct location (Fig. 30). To reset the tag points, user can select new tag points with re-running 'Plot'. Step second and third are repeated until the last image frame. During the repetition, the reference mid-myocardium of the first image frame is shown as white dotted line on the image and the selected tag points from previous image frame shown as circles on the graph (Fig. 31).

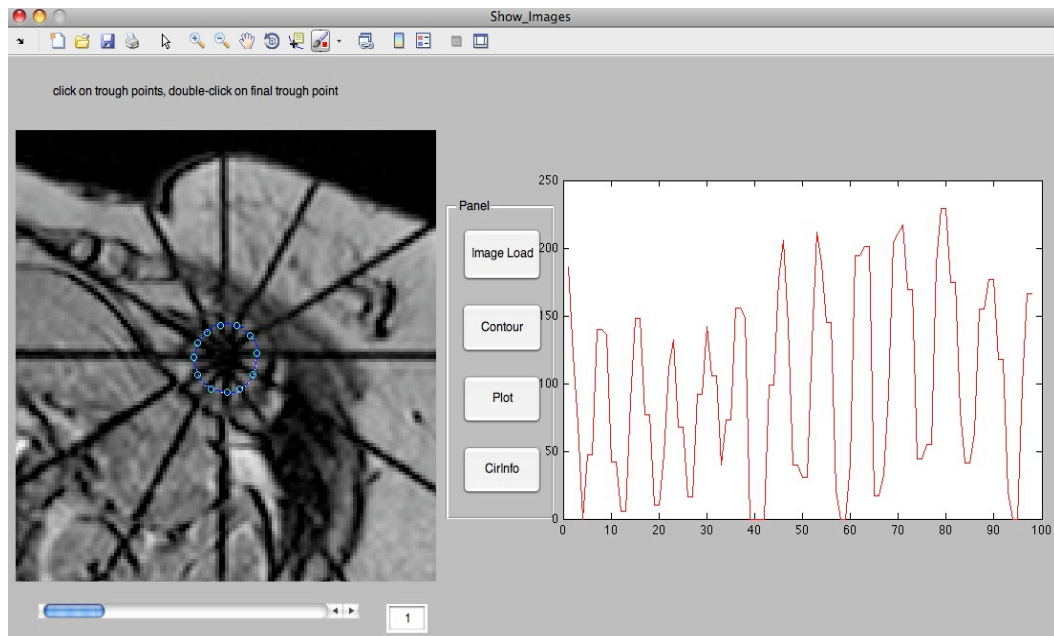


Fig. 30 Selected tag points from signal intensity graph visualized in MRI image.

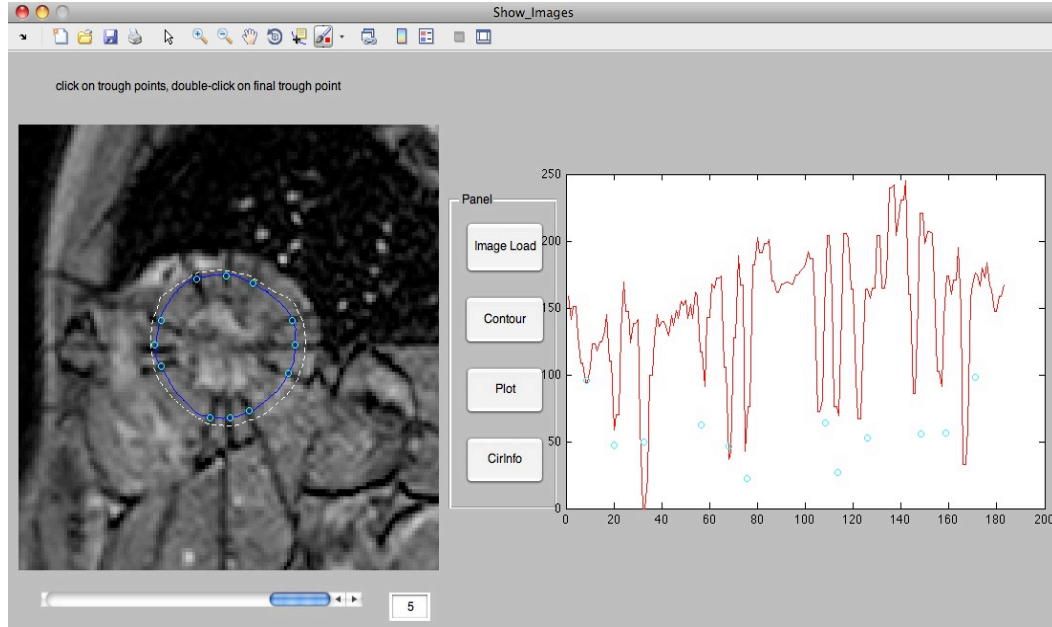


Fig. 31 Repeated ‘contour’ and ‘plot’ through all frames.

After identifying all the tags on mid-myocardium contour through all the image frames, the x-y coordinate location data of 12 tag points are saved. With this data, strain and rotation angle can be calculated mathematically. Strains are length differences between tags with reference image (first MRI image in the series). Rotation angle refers the angle of a tag from the LV centroid in degree. The circumferential strain and the rotation calculation is operated with detected local information. The results are written in a ‘.txt’ file with ‘CirInfo’ button in the GUI (Fig. 32).

Radial analysis results_ex1.txt											
Strain	0	0	0	0	0	0	0	0	0	0	0
	0.067	0.067	-0.077	0.1	-0.17	-0.091	0.18	-0.12	0	0.071	0.23
	0	0	0.077	0	-0.25	0	0.18	-0.12	0	0	0.067
	0	-0.067	0	0	-0.42	0.03	0	-0.18	0	0.071	0.077
	0	-0.13	0	-0.4	-0.25	0.03	0	-0.12	-0.071	0	0.077
	0.067	-0.067	-0.077	-0.2	-0.42	0	-0.091	-0.29	0.14	0.071	-0.077
	-0.067	-0.067	-0.15	-0.4	-0.42	0.03	0	-0.18	-0.071	-0.21	0
	-0.067	-0.067	0	0	-0.17	0.03	0.27	-0.12	0	-0.071	-0.077
	-0.13	-0.067	0.077	0.1	-0.25	-0.03	0.45	-0.18	0.071	-0.071	-0.31
	-0.2	-0.067	0.15	0.1	-0.25	0	0.18	-0.18	0.21	-0.14	-0.077
	-0.13	0.067	-0.077	0.2	-0.17	0.03	-0.091	-0.059	0.43	-0.5	0
	-0.2	0.067	-0.077	-0.1	0	-0.03	0.091	0.12	-0.071	-0.071	0.23
	-0.27	0.2	0	0.1	-0.25	-0.12	-0.091	0.29	0.14	-0.21	0.077
	-0.33	0.13	0	0	-0.33	0	-0.45	0.41	0.071	0.14	-0.23
Rotation Angle	-0	-0	-0	-0	-0	-0	-0	-0	-0	-0	-0
	0.19	4.2	5.2	2.4	2.9	-0.75	-4.6	-3.4	-4.6	-3.5	-2.5
	-2	0.27	0.61	-0.92	-2.1	-8.8	-4.8	-1.8	-6.3	-4.2	-3.9
	-4.6	-2.9	-4.1	-4.2	-3.9	-12	-7.7	-8.6	-12	-9.5	-6.3
	-7.4	-1.6	-2.4	-4.9	3.5e+02	-18	-11	-7.9	-10	-9.5	-6.3
	-7.6	-1.6	2.1	-0.92	-4.2	-15	-7.7	-8.6	-14	-8.5	-6.3
	-1.7	2	5.9	4.2	-4.2	-11	-7.5	-5.1	-4	-2.3	-6.7
	0.4	-0.67	1.3	-0.44	-2.1	-6.5	-7.3	0.21	-2.2	0.98	-1.9
	-0	-0.87	-1.4	-0.44	0.44	-4.2	-7.1	0.58	-2.9	1.5	-0
	-0.18	-3.9	-5.1	-1.9	-0	-5.4	-6.7	-4.2	-8.1	-1	-5.4
	-0	-2.9	-0	-2.4	-0	-3.3	-2.3	-6.4	-4.8	7	-5.4
	2.3	-1.9	-0	-2.4	-4.9	-3.3	-6.5	-7	-3.2	-3.5	-3
	-0	-4.9	-1.9	-2.4	-0	-5.4	-13	-16	-6.5	-0.5	-5.4
	2.6	-4.9	1.3	-0	-0	-8.6	-8.6	-18	-6.5	-2.3	1

Fig. 32 The result screen shot of the semi-automated radial tagging analysis tool
(volunteer NV1 of mid-region of LV).

3.4 Repeatability

To evaluate the reliability of the developed semi-automated radial tagging analysis tool, the analysis operation was repeated three times for each of the volunteers (NV1 - NV7) and also for the mid and apex region of LV MRI image series.

3.5 Analysis

We compare the myocardial strain and rotation angle values measured by different tools. Both grid and radial tagging had been applied before acquiring images to all volunteers. Therefore, there are two MRI images that are grid tagging MRI image and radial tagging MRI image. Grid tagging images were analyzed using HARP software. Radial tagging images were analyzed using two different types of software, manual custom MATLAB software (previous study) and semi-automatic custom MATLAB software.

The average values of the strain and the rotation differences in the segmented regions by tags during the image series had been used to compare with the different analysis tools. The analysis data of the radial tagging analysis tool at the mid and apex region of LV for seven volunteers are sorted in the Excel (Microsoft program).

With radial tagging analysis tool, we get results as strains and rotation angle on each 12 segments of all volunteers by time. Using Excel, we calculated average strain of the LV myocardium through 12 segments (divided by radial tags) by time. Each volunteer has different time echo during acquiring MRI image, it means we need to normalize data to compare with other tools. Therefore, we convert the time line of MRI image (ms) to percent of systole. At the 100% of systole, the LV is contracted and the myocardium is minimized.

For the grid tagging tool, this study did not process HARP performance; rather, we simply used the result data of HARP from a previous study. The results of the grid tagging analysis tool are from seven volunteers' (NV1 - NV7) measurements

for circumferential strain and rotation at the mid and apex region of LV using HARP. Time is the interval between image frames in millisecond, and time interval can be different the using different TE (echo time) in each volunteer or each image acquisition method. Since the frame number has different time domain, we need to normalize the strain and rotation by time domain to compare between volunteers and methods. The measurement values acquired at the 60% and 100% of systole respectively had been compared with the radial tagging tools.

The manual radial tagging analysis tool was already developed and had been used for the previous study [16]. To measure the myocardium deformation, the radial tagging MRI images of all seven volunteers had been used both in manual software and semi-automated software. For the manual radial tagging tool, all points crossing endocardium with tagging and epicardium with tagging were visually adjusted at each frame. When the updating tagging points was completed until the last frame, the length of segments and the rotation differences had been shown by 'Circum Strain' button on GUI (Fig. 33). The measured length information from the MATLAB tool was used to calculate the strain. All the return values from the MATLAB lists on the Microsoft Excel then calculated the strain. The average strain and rotation of 12 segments during the whole frame is the final data for comparing with the grid tagging and the semi-automated radial tagging data. The results show the analysis data of the manual radial tagging tool at the both mid and apex region of LV for seven volunteers. Time is the interval between image frames in milliseconds. This time information would be normalized to compare with the grid and the semi-automated radial tagging analysis tools.

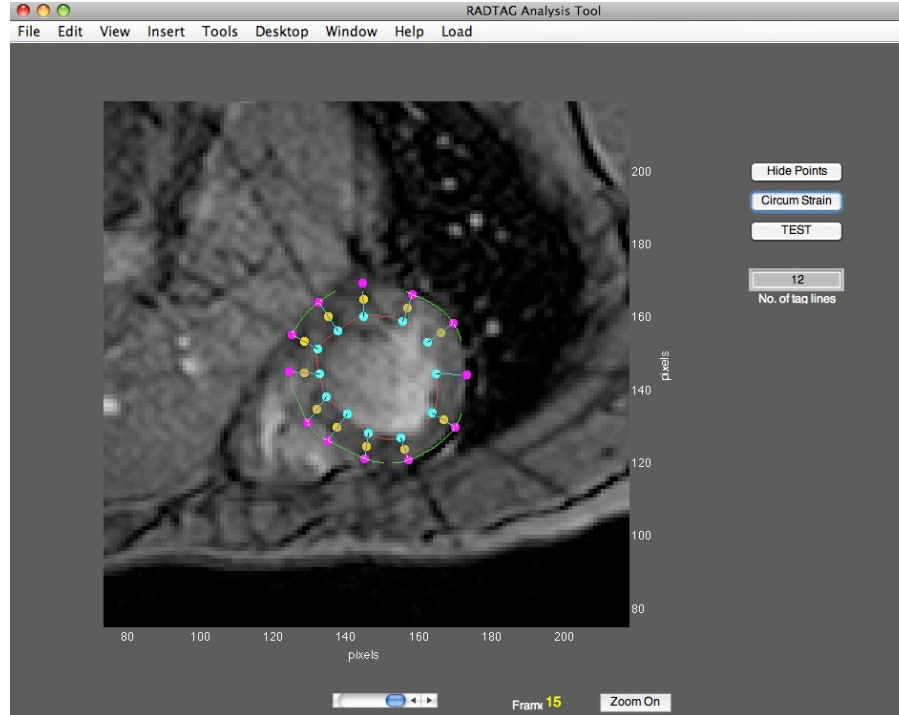


Fig. 33 Image capture of Manual radial tagging analysis tool.

Performed a MATLAB file 'HarpMain.m'.

CHAPTER IV

RESULTS

To compare the measured circumferential strain and rotation differences among the different tools, those data were normalized as time from the end of diastole to 120% of systole due to the different TE (time echo) during the MRI image scan procedure. Tags in MRI images fade as time passes; therefore, we compared values until the time 120% of systole. The following graphs present the strain and rotation angle measurement values of three measurement tools. ‘Grid’ is performed by ‘HARP’ software for the grid tagging. ‘Manual-radial’ represents the manual radial tagging tool developed for the previous study. ‘SemiAutomated-radial’ represents the semi-automatic radial tagging analysis tool developed for this study. The following graphs showed the overall patterns of the strain and rotation measurements performed by different tools during the time between at the 20% and the 120% of systole. These curves were averaged the LV myocardium deformation assessment values throughout the all subjects. The strain and rotation curves of the individual subjects are attached in the appendix B, and this allows comparing the myocardium deformation each

measurement among three different methods. Fig. 34 shows the overall strain curve averaged of the mean value with errors, it indicates the three different tools have similar patterns of the strain measurement. From the beginning of systole to 60% of systole, the strain values are very similar to all the analysis methods. While the grid tagging analysis tool showed the difference value between 60% and 100% of systole, the patterns were close to each other. Similarly, Fig. 35 shows the comparison of the assessed rotation data from three different tools. There are relatively certain differences of measurement of rotation between the grid tagging method and the manual-radial method. The rotation assessment values by the semi-automated method are slightly variable between the values of the grid tagging and the manual-radial tagging analysis tools. While the mean average curves provide the general patterns of the LV myocardium deformation nicely, the errors of the average curves of strain and rotations are considerable and it may refer the low reliability. Therefore, to interpret the differences of measurement values among three different tools, the Root Mean Square (RMS) value with high reliability instead of using the simple mean value would be discussed later in this chapter.

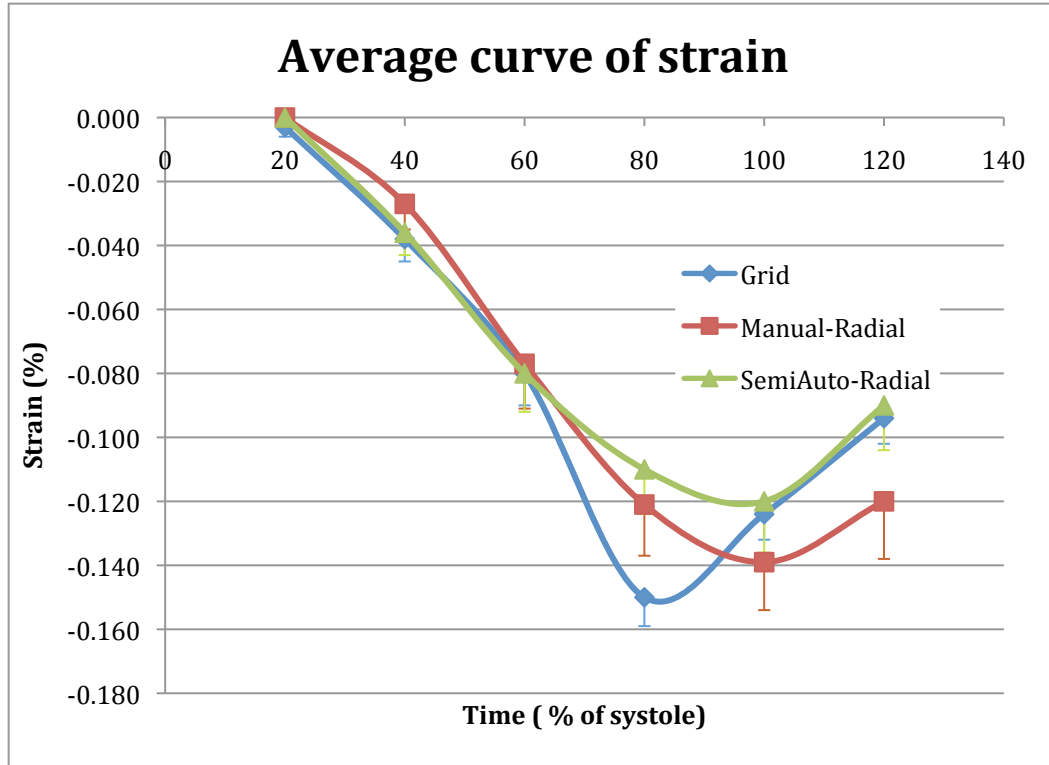


Fig. 34 The overall strain average curves throughout the 14 subjects. The different tools represent the averaged strain value with errors of 14 subjects from the time at the 20% of systole to 120% of systole.

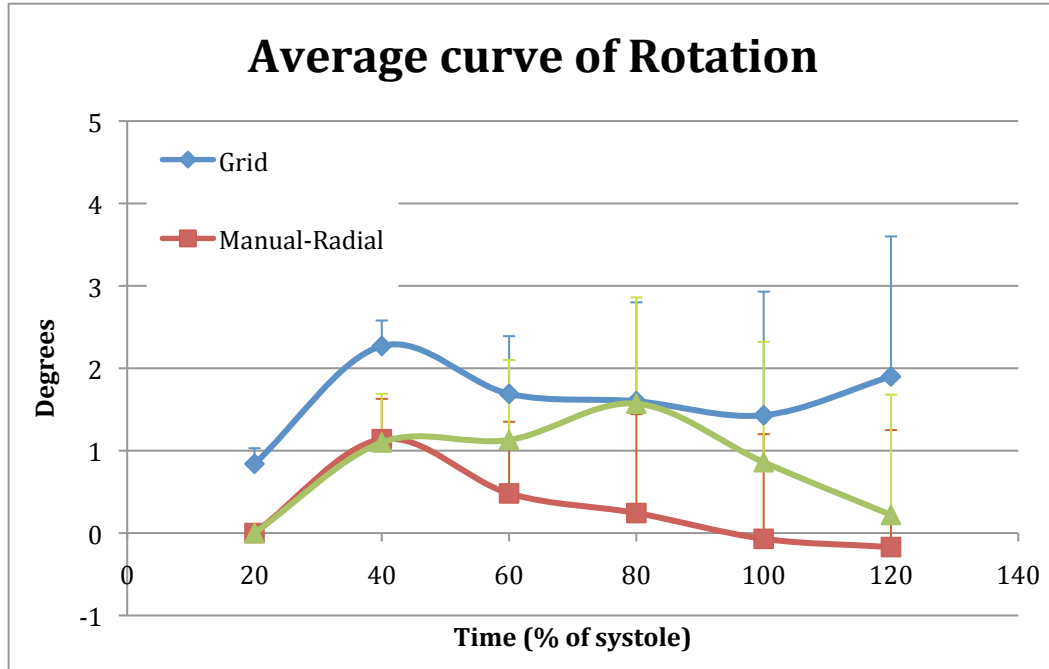


Fig. 35 The comparisons of the rotation average curves of the 14 subjects. The averaged rotation values with errors are represented between the time at the 20% of systole and 120% of systole.

The assessment data of the myocardium strain and rotation angle by the three different tools were enumerated at the time of 60% of systole and 100% of systole. The analyzed subject from the seven volunteers and the each individual has two sets of MRI images, which were acquired at the apex level of LV and the mid-wall level of LV. The acquired strain data indicates the myocardium length difference between the initial image frame and each time domain. The rotation angle value, like the strain, represents the rotations at the point of time comparing with the initial MRI image frame. Since the LV MRI short-axis image series were acquired from end of diastole to end of systole, the bigger value of the strain and rotations were expected as time went on. In this study, the results values at 60% of systole and 100% of systole

had been selected to compare the different analysis tools. If the comparison time point is too early, the myocardium motion changes from the 1st image frame (reference image) are small and it is not effective to compare the differences among different tools. In addition, if the long time point has been chosen, it is probably inadequate due to the tags are transient and fading with time. Therefore, we chose the time at 60% of systole is enough to see the value differences among tools and at 100% of systole the image is clear enough to detect the myocardium regions. The Fig. 36 shows the strain values of every subject at the 60% of systole. The strain values are negative explaining that the shortage of the myocardium length during systole. As the heart contracts, the volume of the LV has been reduced and they myocardium shortened. The Fig. 37, comparing with the Fig. 36, at the 100% of systole shows the higher absolute value of strain. We can assume that the absolute value of strain would be maximized at the 100% of systole. The general pattern of strain through all subjects of 60% and 100% of systole are similar, except the strain result of semi-automated radial for subject 11 represented a noticeable difference with other tools. In addition, the strain value of manual radial tool for subject 13 had a relatively big gap with other tools. The MRI image of both subject 11 and 13 were acquired at apex-level of LV, and in this images, the contour of myocardium was small and hard to differentiate the tagging lines. Fig. 38 and 39 are the LV MRI radial tagging images of the subject 11 and 13, respectively. The MRI images were arranged by time, the Frame 1 is the initial MRI image (a reference image for strain and rotation) acquired at the end of diastole. Time goes on, the tags are fading. Fig. 38 is the apex-level of LV MRI image series; therefore the LV myocardium contour

is relatively smaller than the mid-level of LV image. After time at frame 5, it is hard to tell the LV myocardium contour and select the tag points along the mid-myocardium contour with vision. In Fig. 39, the LV myocardium contour and the tags were apparent at the image frame 1 to 3. While the tags are detected with vision at the frame 5, it is hard to detect the LV myocardium boundary. There are potential risks of errors to use the strain and rotation assessment tools with those low image qualities. Therefore, it would be the reason for the relatively different values of strain and rotation measurement during the tool operations. Even using the same radial tagging MRI image had been used to manual and semi-automated tool, different operators performed tools and there were possibilities to use different criteria for determination of tagging lines which may lead to errors in the measurement value between the manual-radial tagging method and the semi-automated tagging method.

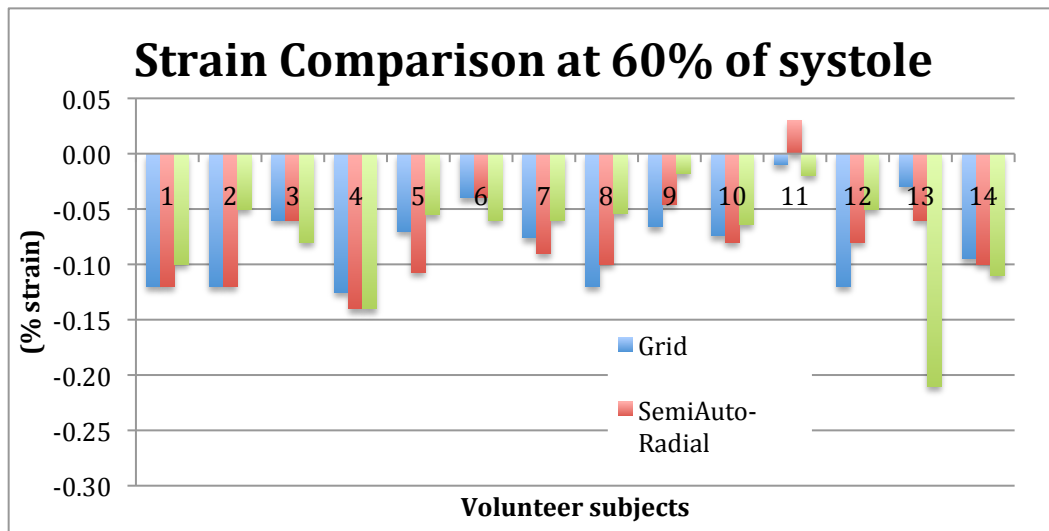


Fig. 36 The comparison graph among different analysis tools. The strain values were acquired at 60% of systole, presented by volunteer subjects at the apex level and the mid-wall level of LV.

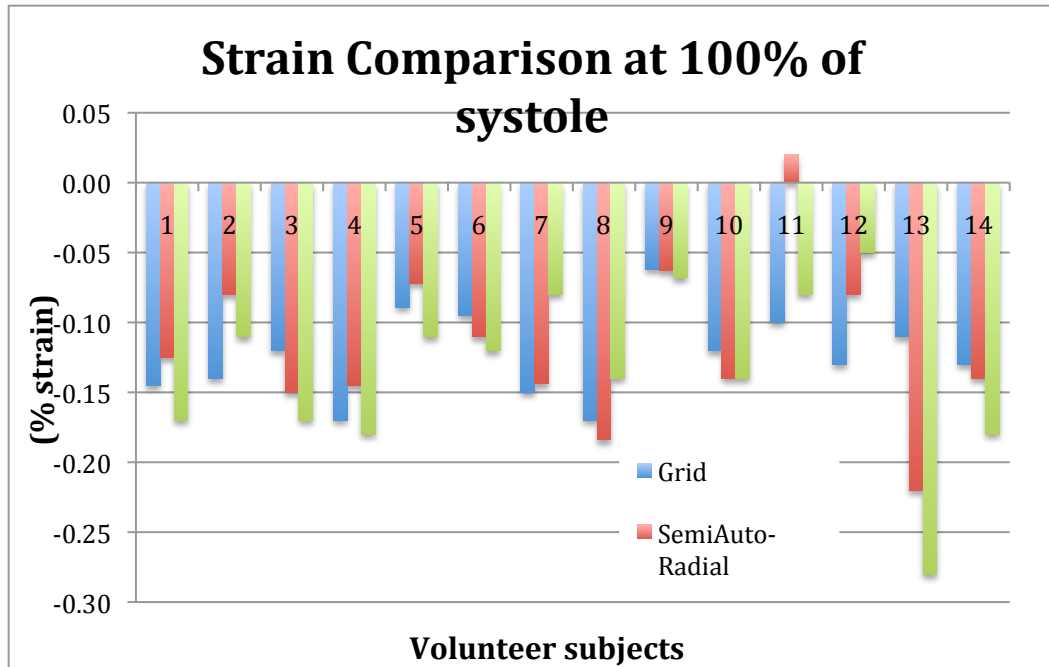


Fig. 37 The comparison graph among different analysis tools. The strain values were acquired at 100% of systole, presented by volunteer subjects at the apex level and the mid-wall level of LV.

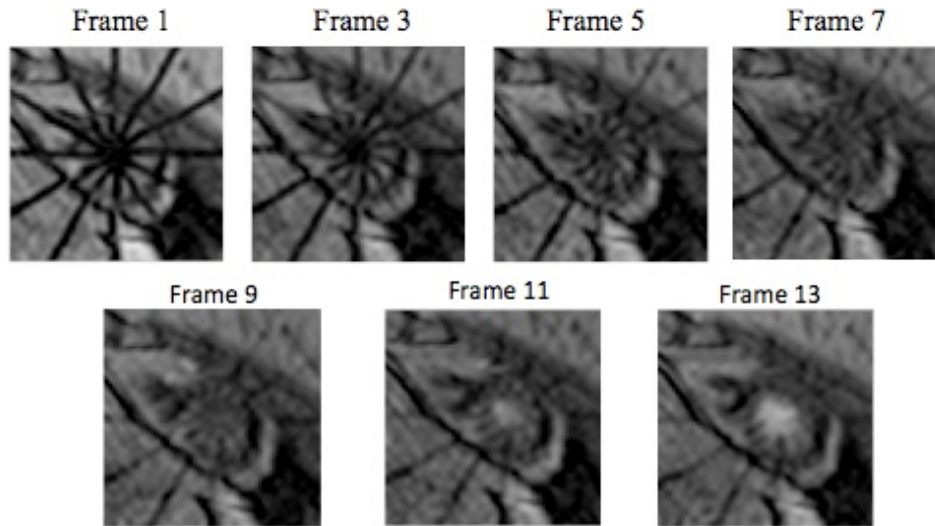


Fig. 38 Radial tagging MRI Images of Subject 11. Frame 1 is the initial frame the image acquired the time at the end of diastole. Visually, only the time at frame 1 and 3 can be differentiate the tags and myocardium contours of LV.

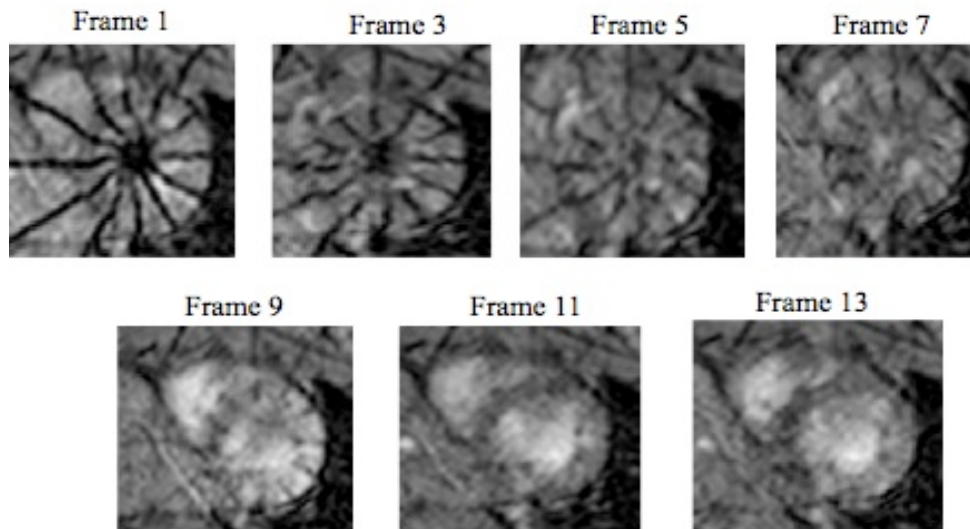


Fig. 39 Radial tagging MRI Images of Subject 13. Frame 1(initial frame of image acquasition) is clear to recognize the myocardium contours and tags. Visually, only the time at frame 1 and 3 can be differentiate the tags and myocardium contours of LV.

The rotation comparison values of the individual subjects had been shown in Fig. 40 at the time 60% of systole and Fig. 41 at 100% of systole. At the 60% of systole, the rotation values were relatively small and it is inappropriate to compare the rotation measurements among different tools. At the 100% of systole, almost each subjects had similar values among three different tools and the differences were not enough to affect the average value. Again, the subject 11 showed dramatically different patterns than other subjects, because the image quality was not clear to differentiate tagging lines and possibly some tagging lines were mis-selected to calculate the rotation. The subjects were individually compared among the different tools by showing the strain and rotation curves (attached in the appendix B).

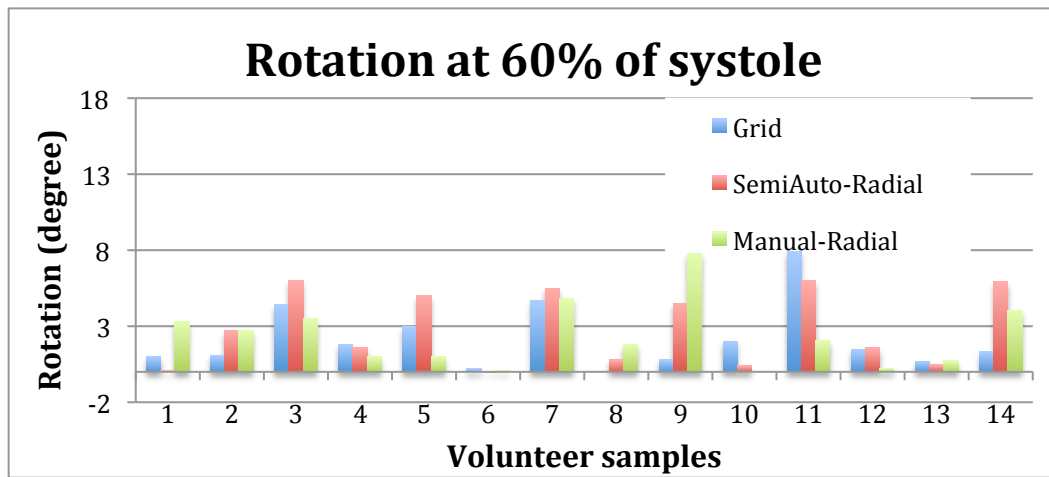


Fig. 40 The comparison the rotation angle among different analysis tools. The presented values were the rotations between at 60% of systole and the 1st image frame (reference image).

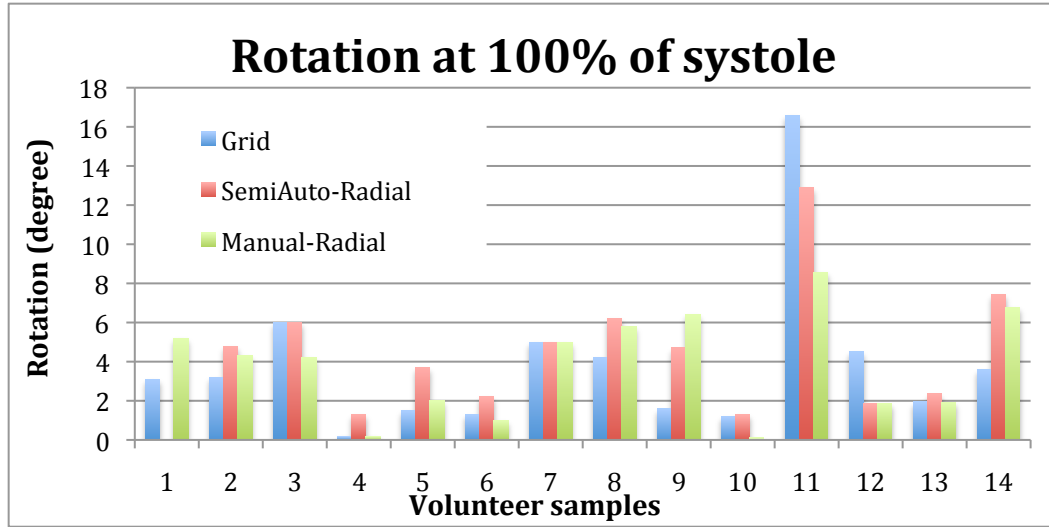


Fig. 41 The comparison the rotation angle among different analysis tools. The presented values were the rotations between at 100% of systole and the 1st image frame (reference image).

To simplify the comparison among different tools we used the quadratic mean (RMS, root mean square) since the varieties were positive and negative. Fig. 42 and Fig. 43 simply show the differences among the three different tools for assessing the myocardium strain and rotation angles. The grid tagging method of strain measurement had standard error 0.010 at 60% and 0.008 at 100% of systole. The semi-automated radial method showed standard error of strain 0.012 and 0.016, at 60% and 100% of systole respectively. The average strain value of manual radial tool had standard error 0.014 and 0.015, at 60% and 100% of systole respectively.

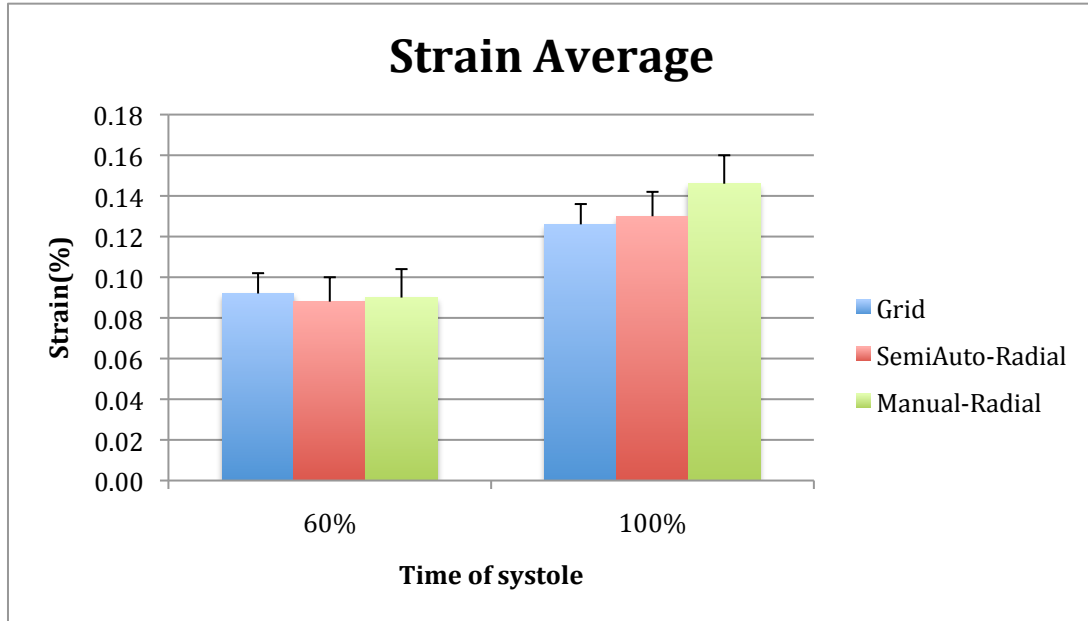


Fig. 42 The comparison of average strain values with standard errors. The graph include the standard error indicated that the averaged strain values were not significantly different each other at each different time (60% and 100% of systole).

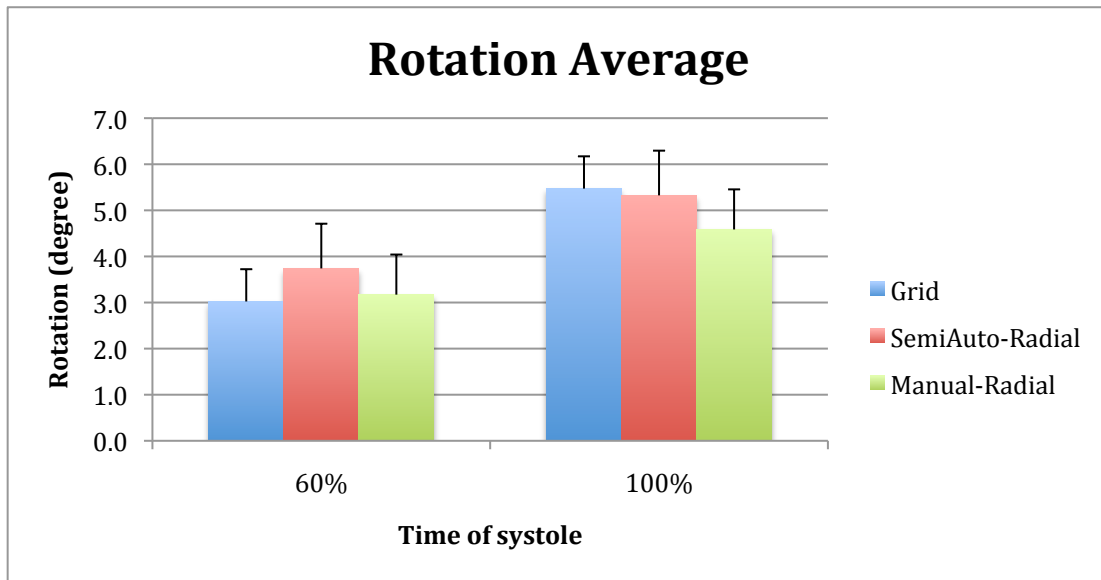


Fig. 43 The average rotation with standard errors. While the average rotation at 100% of systole represented little differences among three tools, the rotation values at 60% of systole were relatively unstable than 100% of systole.

Table V and Table VI show the calculated P-value between tools at the 6 different time intervals to interpret the value differences of the strain and rotation angle among tools.

Table V. Similarities of strain measurement values by comparing tools during the image acquisition. All p-values in this table are bigger than 0.05 meaning there are no significant differences among tools. Therefore, all three tools are acceptable to calculate the strain values.

Time % of systole	T-test of the Strain		
	SemiAuto-Radial to Grid	SemiAuto-Radial to Manual-Radial	Grid to Manual-Radial
20	0.309	0.336	0.270
40	0.730	0.422	0.388
60	0.881	0.840	0.818
80	0.617	0.391	0.343
100	0.844	0.130	0.315
120	0.710	0.106	0.168

Table VI. Similarities of assessed rotation values by comparing each tools during the image acquisition. Between grid and radial tools at 20% of systole showed significant differences of the measured rotation ($P < 0.05$). After 20% of systole, other rotation values of different tools are similar and acceptable to measure the rotation.

Time % of systole	T-test of the rotation angle		
	SemiAuto-Radial to Grid	SemiAuto-Radial to Manual-Radial	Grid to Manual-Radial
20	0.001	0.336	0.001
40	0.102	0.721	0.028
60	0.542	0.218	0.138
80	0.974	0.066	0.202
100	0.518	0.175	0.150
120	0.163	0.312	0.050

CHAPTER V

DISCUSSION

The use of myocardial tagging by magnetic resonance is a noninvasive method for measuring three-dimensional motion and deformation in the human heart. Myocardial tagging is performed on normal MR images by a localized presaturation of magnetization in specific regions in the myocardium. Replacement of these tags during cardiac contraction can track an exact mapping of the spatial heart wall motion [6].

Strain components that are based on a high density of tag data, such as circumferential and longitudinal shortening, or parameters that are combinations of multiple strain components, have the highest measurement precision and the tightest normal ranges. The pattern of three-dimensional motion and strain in the heart is important clinically, because it reflects the basic mechanical function of the myocardium at both local and global levels. Localized abnormalities can be detected and quantified if the pattern of deformation in a given heart is compared to the normal

range for that region, because normal motion and strain in the left ventricle is spatially heterogeneous. [9].

Accurate quantification and timing of regional myocardial function allows early identification of dysfunction, and therefore becomes increasingly important for clinical risk assessment, patient management, and evaluation of therapeutic efficacy. Cardiovascular magnetic resonance imaging with tissue tagging provides highly reproducible data on myocardial function, not only in longitudinal and radial directions, but also in the circumferential direction. Because of the development of faster imaging protocols, improved temporal resolution, less time-consuming postprocessing procedures, and the potential of quantifying myocardial deformation in 3 dimensions at any point in the heart, this technique may serve as an alternative for tissue Doppler echocardiography and is now ready for more widespread clinical use.

A study on the classification of the biomechanical properties of normal and abnormal myocardium is important to understand the effects of cardiovascular disease and therapeutic interventions on ventricular performance. Specifically, the myocardial function of the left ventricular (LV) can explain the LV deformation during cardiac contraction. Cardiac MRI image is widely agreed as the most accurate noninvasive imaging modality for the LV function assessment. In addition, myocardial-tagging method can track the myocardial deformation. A grid pattern tagging technique is conventionally used in clinical and research studies. However, the grid tagging has not been adopted into routine clinical examination. The

parameters of the grid tags make it difficult to calculate LV motion and often result in unreliable data correspondence between frames. Therefore, we assumed that a radial orientation myocardial tagging method has geometric advantages for assessing the circumferential strains and rotation parameters over grid tagging method. In addition, the radial tagging method is more effective than the grid method to examine the local area along the LV myocardium. While the radial tagging method assesses through the overall LV myocardium proportionally, the grid tagging method could miss some local data points of LV myocardium.

In this study, radial tagging analysis software had been developed using the MATLAB to measure the myocardium deformation of the LV. A previous study developed the manual radial tagging analysis software [16]. In this study, we took an advanced approach that the analysis tool system could detect tags semi-automatically and use to calculate the LV myocardium deformation. The semi-automatic detection of tags means the analysis tool finds the LV myocardium contour automatically and plots the signal intensity graph. After then, the system operator selects the tag points, which are shown in low intensity value (tag line is indicated as black line in the MRI image, the black has almost zero intensity value). This semi-automatic way to select the tags could be upgraded to make it automatic; the signal intensity threshold would be able to the extensive work for the future.

To evaluate the accuracy of the data from the developed semi-automatic radial tagging analysis tool, a total of nine volunteers' LV MRI short-axis image series (from end of diastole to end of systole) have been used. The computed values of the myocardium strain and angle with the developed tool had been confirmed by

mathematically calculating through the application of x-y coordinates on images from two volunteers' image series. The other seven volunteers' LV MRI image series had been used to measure the circumferential strain and rotation angle in different analysis tools, which are grid tagging, manual radial tagging and semi-automatic radial tagging. During the MRI procedure, the grid tagging and the radial tagging had different TEs (time echo).

In addition, we compare the strain and the rotation angle among three different tools in this study (grid tagging, manual radial tagging, and semi-automated radial tagging), we normalized the time domain in milliseconds to % of systole. Because the imposed tags fade with time, we simplified the time from the end of diastole to 120% of systole of heart cycle. The measurement values of grid tagging tool are the average deformation values of global myocardium regions, whereas the radial tagging showed the 12 local regions of myocardium in MRI image plane. Therefore, we averaged the strains and the rotation angles of 12 segments in each time. To see the measurement differences of the strains and the rotation angles by the grid tagging analysis tool, semi-automated radial tagging analysis tool, and manual radial tagging analysis tool, the 14 data sets of 7 volunteers (each volunteer has apex and mid-level image data set) had been used (Fig. 35 and Fig. 37). Each of 14 subjects was averaged with the root mean square (RMS) values at the time 20, 40, 60, 80, 100, and 120% of systole; those values represented each analysis tool and were compared.

Fig. 36 and Fig. 37 indicate the calculated average values of the strain measurement from three tools by time at 60% and 100% of systole. Fig. 40 and Fig.

41 are the same procedure for the rotation angle. The measurement values of the rotation angle from 14 subjects (each 7 volunteers has two levels of LV MRI image) were compared with the average value by the time. We can see the rotation angle movement differences among tools at the time 60% and 100% of systole (Fig. 40 and Fig. 41). The big different individual values of strain and rotation were represented at subject 11 and 13 due to the lack of image resolution to distinct the radial tagging lines. However, Fig. 42 and Fig. 43 revealed that those individual differences of subject 11 and 13 affected on average slightly by a relatively small amount of standard errors.

To demonstrate the reliability of the radial tagging tool, the t-test has been used. From the overall measurement data from 14 image sets, p-value has been calculated between grid and semi-automated radial, grid and manual radial, semi-automated radial and manual radial respectively at each time on 20, 40, 60, 80, 100, and 120 % of systole (Table V and Table VI). If p-value from this t-test is smaller than 0.05, we consider that these are significantly different. Table V and VI show that in this study, there is no significant difference between the grid tagging measurement and the radial tagging measurement with P-value > 0.05 except the rotation angle value on the time 20% of systole. At the 20% of systole, the measurement values of radial tagging analysis tools are too small showed as zero. This means the radial tagging analysis tools are not appropriate at the time of early systole (20% of systole). Except 20% of systole, all the values were not showing significant differences among tools.

Similarities of assessed rotation values from each tool were compared during the image acquisition. Between grid and radial tools at 20% of systole showed significant differences of the measured rotation ($P < 0.05$). After 20% of systole, other rotation values of different tools are similar and acceptable to measure the rotation.

In conclusion, this study developed a new analysis method to analyze myocardium deformation by measuring the strains and the rotation angles and validate the accuracy of this tool by comparing it with grid tagging analysis technique, which is conventionally used in clinical and research studies. The results showed no significant differences compared to the grid tagging analysis method with $P > 0.05$. During the whole MRI image acquisition time for measuring the strain and after 20% of systole for measuring the rotation, all myocardium analysis tools used in this study are acceptable. Therefore, we conclude that the developed semi-automated radial tagging analysis tool is a reliable method to measure the myocardial deformation. To compare the effectiveness among different tools for calculating the strain and rotation of the LV myocardium, more data is required and a gold standard value to compare different methods is needed.

REFERENCES

- [1] World Health Organization 2008. The global burden of disease: 2004 update. WHO Library Cataloguing-in Publication Data. ISBN 978 92 4 156371 0.

- [2] Donald Lloyd-Jones, Robert Adams, Mercedes Carnethon, Giovanni De Simone, T. Bruce Ferguson, Katherine Flegal, Earl Ford, Karen Furie, Alan Go, Kurt Greenlund, Nancy Haase, Susan Hailpern, Michael Ho, Virginia Howard, Brett Kissela, Steven Kittner, Daniel Lackland, Lynda Lisabeth, Ariane Marelli, Mary McDermott, James Meigs, Dariush Mozaffarian, Graham Nichol, Christopher O'Donnell, Veronique Roger, Wayne Rosamond, Ralph Sacco, Paul Sorlie, Randell Stafford, Julia Steinberger, Thomas Thom, Sylvia Wasserthiel-Smoller, Nathan Wong, Judith Wylie-Rosett, Yuling Hong and American Heart Association Statistics Committee and Stroke Statistics Subcommittee. Heart Disease and Stroke Statistics 2009 Update. A Report From the American Heart Association Statistics Committee and Stroke Statistics Subcommittee. *Circulation* DOI: 10.1161 / CIRCULATIONAHA. 108. 191261

- [3] Iris K. Russel, Marco J. W. Gotte, Jean G. Bronzwaer, Paul Knnapen, Walter J. Paulus, Albert C. van Rossum. Left Ventricular Torsion: An Expanding Role in the Analysis of Myocardial Dysfunction. *JACC: Cardiovascular Imaging* 2009;2:648-55.

- [4] Lipton MJ, Bogaert J, Boxt LM, Reba RC. Imaging of ischemic heart disease. *Eur Radiol* 2002;12:1061-1080.

- [5] Marco J.W. Gotte, Tjeerd Germans, Iris K. Russel, Jaco J. M. Zwanenburg, J. Tim Marcus, Albert C. van Rossum, Dirk J. van Beldhuisen, FACC. Myocardial Strain and Torsion Quantified by Cardiovascular Magnetic Resonance Tissue Tagging. *Journal of the Americal College of Cardiology* 2006;48:2002-11.

- [6] C. Matter, E. Nagel, M. Stuber, P. Boesiger, O. M. Hess. Assessment of systolic and diastolic LV function by MR myocardial tagging. *Basic Res Cardiol* 1996;91:2:23-28.

- [7] Kenneth P. Moses, John C. Banks, Pedro B. Nava, Darrell Petersen. Atlas of Clinical Gross Anatomy. Elsevier Mosby. 2005 ISBN: 0323037445.
- [8] Castillo E, Lima J A.C., Bluernke D A. Regional myocardial function: advances in MR imaging and analysis. *Radiographics* 2003;23:S127-S140.
- [9] Christopher C. Moore, Elliot R. McVeigh, Elias A. Zerhouni. Quantitative Tagged Magnetic Resonance Imaging of the Normal Human Left Ventricle. *Topics in Magnetic Resonance Imaging*. 2000;11(6):359-371.
- [10] Zhenhua Hu, Dimitris Metaxas, Leon Axel. In vivo strain and stress estimation of the heart left and right ventricles from MRI images. *Medical Image Analysis* 2003;7:435-444.
- [11] Zerhouni EA, Parish DM, Rogers WJ. Human heart: Tagging with MR imaging - A method for noninvasive assessment of myocardial motion. *Radiology* 1988;169:59-63.
- [12] Christine H. Lorenz, John S. Pastorek, Jeffrey M. Bundy. Delineation of Normal Human Left Ventricular Twist Throughout Systole by Tagged Cine Magnetic Resonance Imaging. *Journal of Cardiovascular Magnetic Resonance* 2000;2(2):97-108.
- [13] Axel L, Dougherty L. MR imaging of motion with spatial modulation of magnetization. *Radiology* 1989;91:94-7.
- [14] Joost P.A. Kuijer, J. Tim Marcus, Marco J.W. Gotte, Albert C. van Rossum, Herman J. Ader & Robert M. Heethaar. Variance components of two-dimensional strain parameters in the left-ventricular heart wall obtained by magnetic resonance tagging. *The International Journal of Cardiovascular Imaging* 2001;17:49-60.
- [15] Setser RM, Chatzimavroudis GP. "Magnetic Resonance Imaging Physical Principles and Instrumentation." *Noninvasive Cardiovascular Imaging: A Multimodality Approach*. Ed. Mario Garcia. Lippincott Williams & Wilkins, 2009.
- [16] Kotys MS, Zhou X, Setser RM, Flamm SD. Radial tagging for assessment of circumferential myocardial function. Presented at the 18th Scientific Meeting of the International Society of Magnetic Resonance in Medicine, 2010.
- [17] Maurice B. Buchalter, MB, MRCPI, James L. Weiss, MD, Walter J. Rogers, BS, Elias A. Zerhouni, MD, Myron L. Weisfeldt, MD, Rafael Beyar, MD, DSc, and Edward P. Shapiro, MD. Noninvasive Quantification of Left Ventricular Rotational Deformation in Normal Humans Using Magnetic Resonance Imaging Myocardial Tagging. *Circulation* 1990;81:1236-1244.

[18] Marco J.W Gotte, Albert C van Rossum, Jos W. R Twisk, Joost P.A Kuijer, J. Tim Marcus, Cees A Visser. Quantification of regional contractile function after infarction: strain analysis superior to wall thickening analysis in discriminating infarct from remote myocardium. Journal of the American College of Cardiology 2001;37(3):808-817.

[19] Andrew Webb. Introduction to Biomedical Imaging. New Jersey: John Wiley & Sons, Inc. 2003

APPENDICES

A. Program Algorithms

The following algorithms are written in Matlab 7.7 version, in order to measure the LV myocardium circumferential strain and rotation angles

Graphical User Interface: 'Show_Images.m'

```
function varargout = Show_Images(varargin)
% SHOW_IMAGES M-file for Show_Images.fig
%   SHOW_IMAGES, by itself, creates a new SHOW_IMAGES or raises the
%   existing
%   singleton*.

%   H = SHOW_IMAGES returns the handle to a new SHOW_IMAGES or the
%   handle %   to the existing singleton*.
%   SHOW_IMAGES('CALLBACK',hObject,eventData,handles,...) calls the local
%   function named CALLBACK in SHOW_IMAGES.M with the given input
%   arguments.
%   SHOW_IMAGES('Property','Value',...) creates a new SHOW_IMAGES or
%   raises
%   the existing singleton*. Starting from the left, property value pairs are
%   applied to the GUI before Show_Images_OpeningFcn gets called. An
%   unrecognized property name or invalid value makes property application
%   stop. All inputs are passed to Show_Images_OpeningFcn via varargin.
%   *See GUI Options on GUIDE's Tools menu. Choose "GUI allows only one
%   instance to run (singleton)".
%

% Edit the above text to modify the response to help Show_Images
% Last Modified by GUIDE v2.5 08-Jul-2011 23:39:36
% Begin initialization code - DO NOT EDIT
gui_Singleton = 1;
gui_State = struct('gui_Name',    mfilename, ...
                  'gui_Singleton', gui_Singleton, ...
                  'gui_OpeningFcn', @Show_Images_OpeningFcn, ...
                  'gui_OutputFcn', @Show_Images_OutputFcn, ...
                  'gui_LayoutFcn', [], ...
                  'gui_Callback', []);
if nargin && ischar(varargin{1})
    gui_State.gui_Callback = str2func(varargin{1});
end

if nargout
    [varargout{1:nargout}] = gui_mainfcn(gui_State, varargin{:});
else
    gui_mainfcn(gui_State, varargin{:});
end
```

```

end
% End initialization code - DO NOT EDIT

% --- Executes just before Show_Images is made visible.
function Show_Images_OpeningFcn(hObject, eventdata, handles, varargin)

% This function has no output args, see OutputFcn.
% hObject    handle to figure
% eventdata  reserved - to be defined in a future version of MATLAB
% handles    structure with handles and user data (see GUIDATA)
% varargin   command line arguments to Show_Images (see VARARGIN)

% Choose default command line output for Show_Images
handles.output = hObject;

% Update handles structure
guidata(hObject, handles);
set(hObject,'toolbar','figure');

% UIWAIT makes Show_Images wait for user response (see UIRESUME)
% uiwait(handles.figure1);

% --- Outputs from this function are returned to the command line.
function varargout = Show_Images_OutputFcn(hObject, eventdata, handles)
% varargout  cell array for returning output args (see VARARGOUT);
% hObject    handle to figure
% eventdata  reserved - to be defined in a future version of MATLAB
% handles    structure with handles and user data (see GUIDATA)

% Get default command line output from handles structure
varargout{1} = handles.output;

% --- Executes on slider movement.
function slider1_Callback(hObject, eventdata, handles)
% hObject    handle to slider1 (see GCBO)
% eventdata  reserved - to be defined in a future version of MATLAB
% handles    structure with handles and user data (see GUIDATA)

frame = get(hObject,'Value');
set(hObject,'Value',frame);
set(handles.Frame,'String',num2str(frame));

%axes(handles.axes1);
SliderControl(hObject,handles);

% Hints: get(hObject,'Value') returns position of slider

```

```

%    get(hObject,'Min') and get(hObject,'Max') to determine range of slider

% --- Executes during object creation, after setting all properties.
function slider1_CreateFcn(hObject, eventdata, handles)
% hObject    handle to slider1 (see GCBO)
% eventdata  reserved - to be defined in a future version of MATLAB
% handles    empty - handles not created until after all CreateFcns called

% Hint: slider controls usually have a light gray background.
if isequal(get(hObject,'BackgroundColor'), get(0,'defaultUicontrolBackgroundColor'))
    set(hObject,'BackgroundColor',[.9 .9 .9]);
end
% imagenames = dir('IM_*');
% frameMax = length(imagenames);

% set(handles.slider1, 'Value',1);
% set(handles.slider1, 'Min', 1,'Max', frameMax,'SliderStep',[1/(frameMax-1) 0.3]);

% --- Executes on button press in ImgLoad_button.
function ImgLoad_button_Callback(hObject, eventdata, handles)
% hObject    handle to ImgLoad_button (see GCBO)
% eventdata  reserved - to be defined in a future version of MATLAB
% handles    structure with handles and user data (see GUIDATA)

ImagesLoad(hObject,handles);
guidata(hObject,handles);

function Frame_Callback(hObject, eventdata, handles)
% hObject    handle to Frame (see GCBO)
% eventdata  reserved - to be defined in a future version of MATLAB
% handles    structure with handles and user data (see GUIDATA)

% Hints: get(hObject,'String') returns contents of Frame as text
%    str2double(get(hObject,'String')) returns contents of Frame as a double

% --- Executes during object creation, after setting all properties.
function Frame_CreateFcn(hObject, eventdata, handles)
% hObject    handle to Frame (see GCBO)
% eventdata  reserved - to be defined in a future version of MATLAB
% handles    empty - handles not created until after all CreateFcns called

% Hint: edit controls usually have a white background on Windows.
%    See ISPC and COMPUTER.
if ispc && isequal(get(hObject,'BackgroundColor'),
get(0,'defaultUicontrolBackgroundColor'))

```

```

    set(hObject,'BackgroundColor','white');
end

% --- Executes on button press in contour_button.
function contour_button_Callback(hObject, eventdata, handles)
global mid_x1 mid_y1 mid_I1 mid_table initial_midx initial_midy
% hObject    handle to contour_button (see GCBO)
% eventdata  reserved - to be defined in a future version of MATLAB
% handles    structure with handles and user data (see GUIDATA)
axes(handles.axes1);
frame = get(handles.slider1,'Value');
set(handles.slider1,'Value',frame);
set(handles.Frame,'String',num2str(frame));

% To read DICOM images
imagenames = dir('IM_*');
filenames = imagenames(frame).name;
%info = dicominfo(filenames);
test = dicomread(filenames);

hold on
% Guide line (center point of LV): updated at each volunteer
x=[128 164];
y=[128 84];

plot(handles.axes1,x,y,'w-');
hold off
set(handles.StatusDisp,'string','Draw contour of endo-cardium: Click on trough point,
double-click on final trough point');
drawnow

[endo_x1,endo_y1,endo_I1]=improfile(100);

hold on
set(handles.StatusDisp,'string','Draw contour of epi-cardium: Click on trough point,
double-click on final trough point');

[epi_x1,epi_y1,epi_I1]=improfile(100);
hold off

% calculate and plot intensity values of mid-wall myocardium contour
% creating mid-wall myocardium contour coordinate value array
pre_mid_x1=(endo_x1 + epi_x1)/2;
pre_mid_y1=(endo_y1 + epi_y1)/2;

[mid_x1,mid_y1,mid_I1]=improfile(test,pre_mid_x1,pre_mid_y1);

```

```

mid_table = [mid_x1,mid_y1,mid_I1];

hold on
if frame == 1
    initial_midx = mid_x1;
    initial_midy = mid_y1;
end
hold off

line(mid_x1, mid_y1,'color','r','Parent',handles.axes1);

%PlotGraph(hObject,handles)
PlotGraph (hObject,handles)
guidata(hObject,handles);

% --- Executes on button press in Plot_button.
function Plot_button_Callback(hObject, eventdata, handles)
% hObject    handle to Plot_button (see GCBO)
% eventdata  reserved - to be defined in a future version of MATLAB
% handles    structure with handles and user data (see GUIDATA)
%plot a graph
PlotGraph(hObject,handles)

% --- Executes on button press in CirInfo_button.
function CirInfo_button_Callback(hObject, eventdata, handles)
% handles    structure with handles and user data (see GUIDATA)
write_file(hObject,handles)
close all;

```

Loading a set of Images: 'ImagesLoad.m'

```

function ImagesLoad(hObject,handles)

imagenames = dir('IM_*');
frameMax = length(imagenames);

if isempty(imagenames)
    set(handles.StatusDisp,'tag_freq_analysis: No Out
files found');
    return;
end

set(handles.StatusDisp,'string','Loading images

```

```

.....');
drawnow

set(handles.slider1, 'Value',1);
set(handles.slider1, 'Min', 1, 'Max',
frameMax, 'SliderStep',[1/(frameMax-1) 0.3]);

framenum = get(handles.slider1, 'value');
set(handles.Frame, 'string', num2str(framenum));

filenames = imagenames(framenum).name;
info = dicominfo(filenames);
test = dicomread(info);

handles.himage=imshow(test,[], 'Parent', handles.axes1);
zoom(2);
%axes(handles.axes1);
guidata(hObject, handles);

end

```

Plot the mid-wall of myocardium intensity: 'PlotGraph.m'

```

function PlotGraph(hObject,handles)
global seg_length tag_angle mid_table p1 p2 initial_midx
initial_midy

frame = get(handles.slider1, 'Value');
imagenames = dir('IM_*');
filenames = imagenames(frame).name;
test = dicomread(filenames);

%get new Intensity values
[mid_x1,mid_y1,mid_I1]=improfile(test,mid_table(:,1),mid_
table(:,2));
mid_table = [mid_x1,mid_y1,mid_I1];

axes(handles.axes2);

% plot the intensity value of mid-cardium contour
% x-axis unit: pixel
plot(handles.axes2, mid_table(:,3), 'r-');

hold on
if frame > 1
plot(handles.axes2, p1,p2, 'co');

```

```

end

hold off

set(handles.StatusDisp,'string','click on trough points,
double-click on final trough point');

[p1, p2] = getpts;
sort_p1 = sort(int16(p1),1,'ascend');
AA1 = [sort_p1 mid_table(sort_p1,:)];

% Calculate the length of segments
% (between tagged points on mid-contour line)
% e.g) 1st segment = between 1st and 2nd point clicked by
user on the graph

% N1: mid-contour's length (pixel)
N1 = length(mid_table( : ,1));

L = diff(sort_p1);
L(length(sort_p1),1) = sort_p1(1) + (N1 -
sort_p1(length(sort_p1)));
seg_length{frame} = double(L);

% calculate the center point of heart
center = mean(mid_table(:,1));
center(2) = mean(mid_table(:,2));
theta = atan2 (double(AA1(:,3)- center(2)),
double(AA1(:,2)-center(1)));

tag_angle{frame} = double(theta)*180/pi; %angle: degree

%Showing clicked tag points to MRI Image
axes(handles.axes1);
handles.himage=imshow(test,[],'Parent',handles.axes1);
zoom(2);

%Showing initial mid-conour (at time 1, 1st image)
line(initial_midx,
initial_midy,'parent',handles.axes1,'color','w','LineStyle
e','--');

hold on
%Drawing mid-contour
line(mid_table(:,1),
mid_table(:,2),'Parent',handles.axes1);
plot(handles.axes1,AA1(:,2), AA1(:,3),'co');
hold off

```

Showed the previous selected data: 'SliderControl.m'

```
function SliderControl(hObject,handles)
global mid_x1 mid_y1 mid_I1 mid_table initial_midx
initial_midy

imagenames = dir('IM_*');
framenum = str2double(get(handles.Frame,'string'));

%Loading Image
filenames = imagenames(framenum).name;
info = dicominfo(filenames);
test = dicomread(info);
handles.himage=imshow(test,[],'Parent',handles.axes1);

axes(handles.axes1); zoom (2);

if isempty(mid_table)
    set(handles.StatusDisp,'string','No data to
calculate');
    return;
end

%Showing initial mid-contour (at time 1, 1st image)
line(initial_midx,
initial_midy,'parent',handles.axes1,'color','w','LineStyle
e','--');

hold on
%Drawing mid-contour
line(mid_table(:,1),
mid_table(:,2),'Parent',handles.axes1);
hold off

guidata(hObject, handles);
```

Write results in a file: 'write_file.m'

```
function write_file(hObject,handles)
global seg_length tag_angle

imagenames = dir('IM_*');
total_frames = length(imagenames);

fid = fopen('Radial analysis results.txt' ,'w');

fprintf(fid, 'Strain \n');
```

```

for jj=1:total_frames
    CirC = seg_length{jj} - seg_length{1};
    Strain = CirC ./ seg_length{1};
    % ave_strain = mean(Strain);
    fprintf(fid, '%6.2g \t', Strain);
    fprintf(fid, '\n');
end

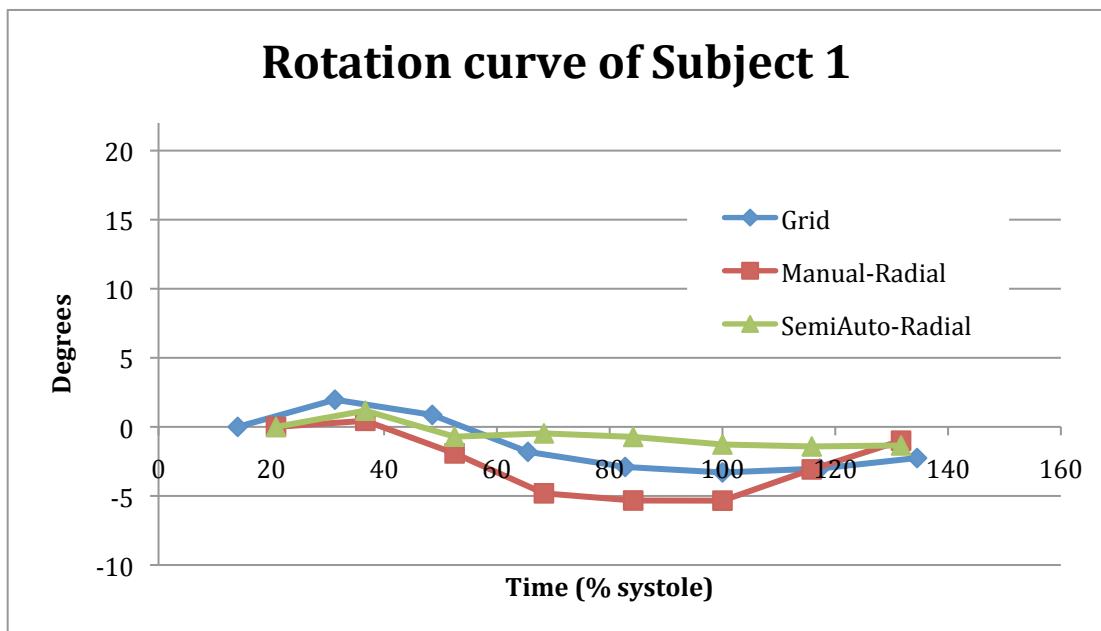
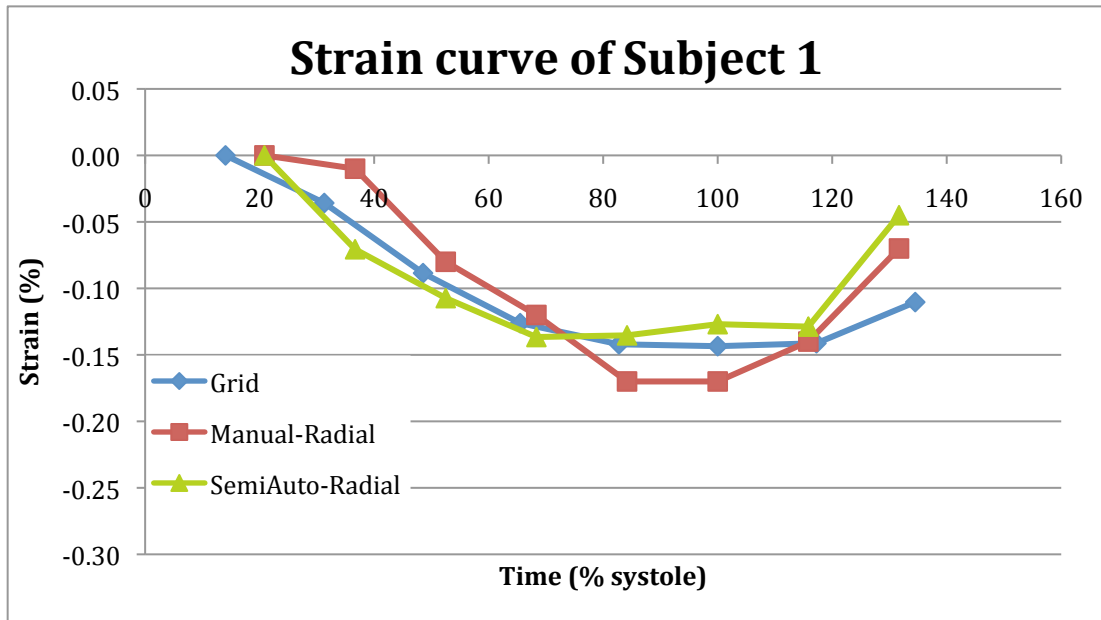
fprintf(fid, '\n');
fprintf(fid, '\n');
fprintf(fid, 'Rotation Angle \n');

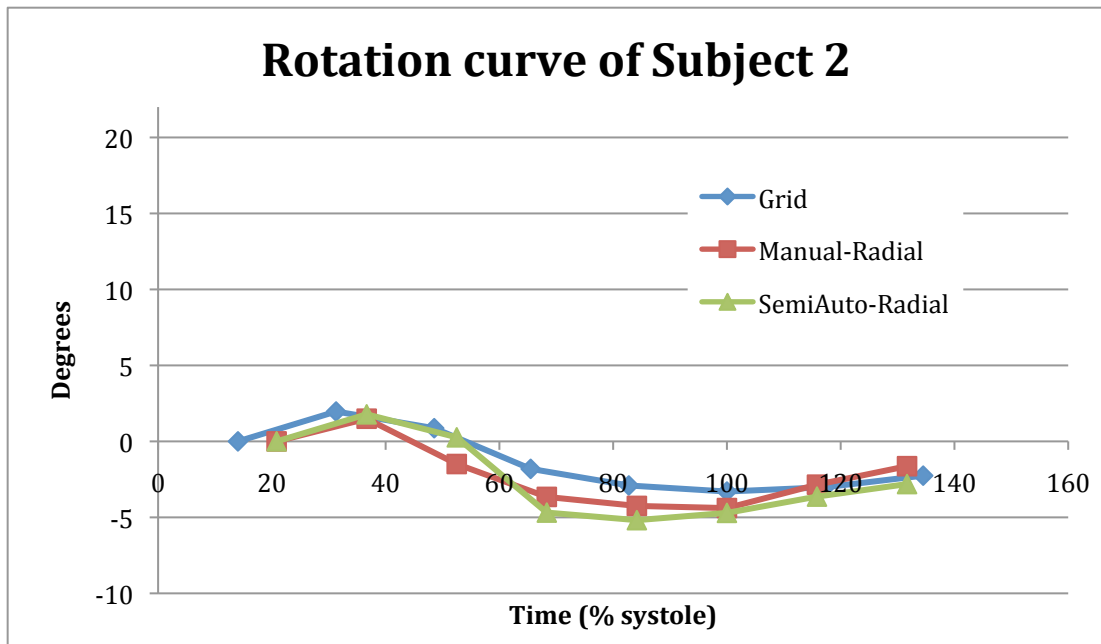
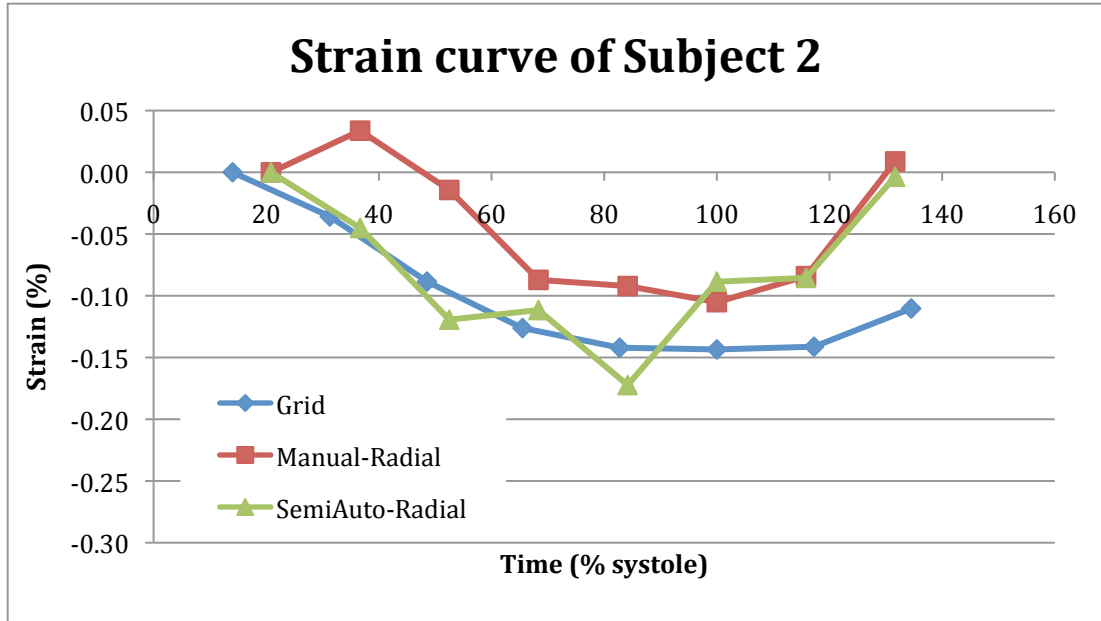
for jj=1:total_frames
    Angle = tag_angle{jj} - tag_angle{1};
    fprintf(fid, '%6.2g \t', -Angle);
    fprintf(fid, '\n');
end

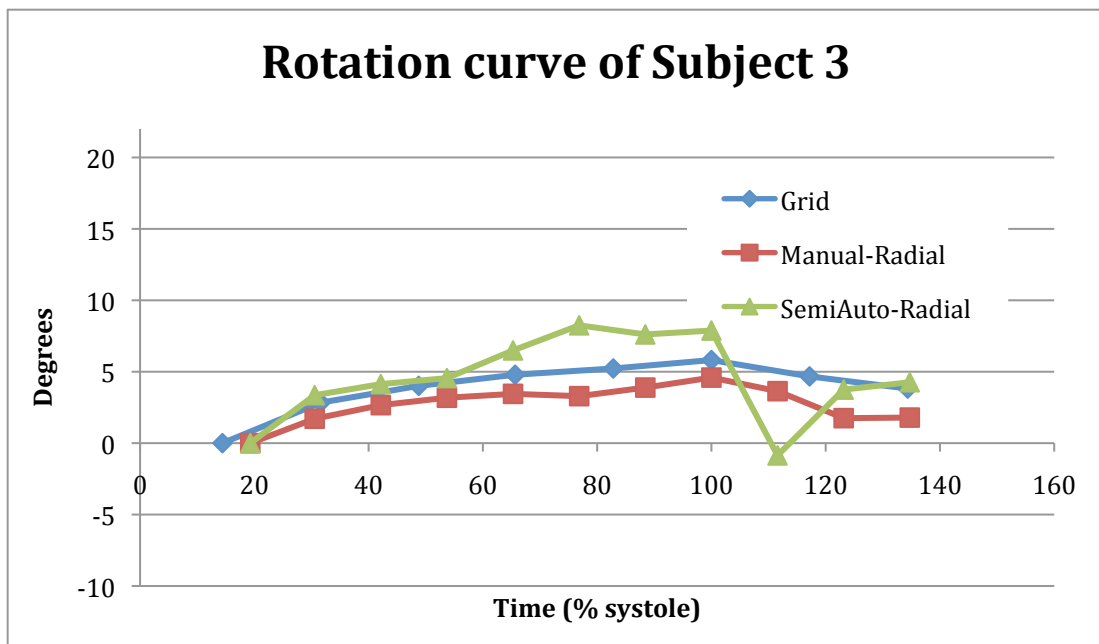
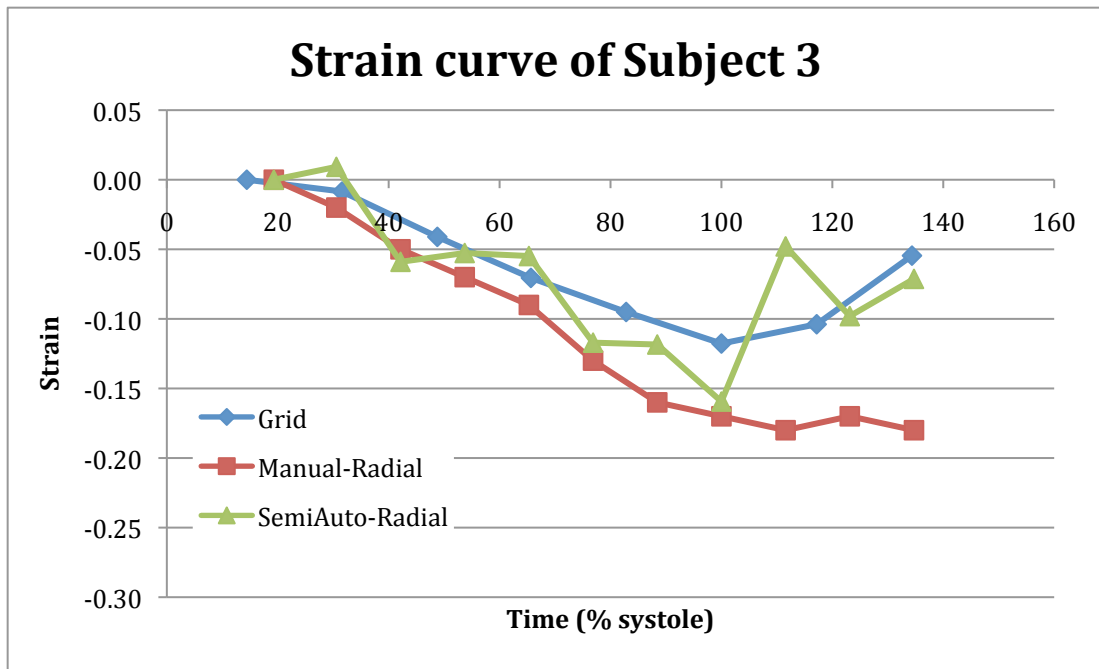
fclose(fid);

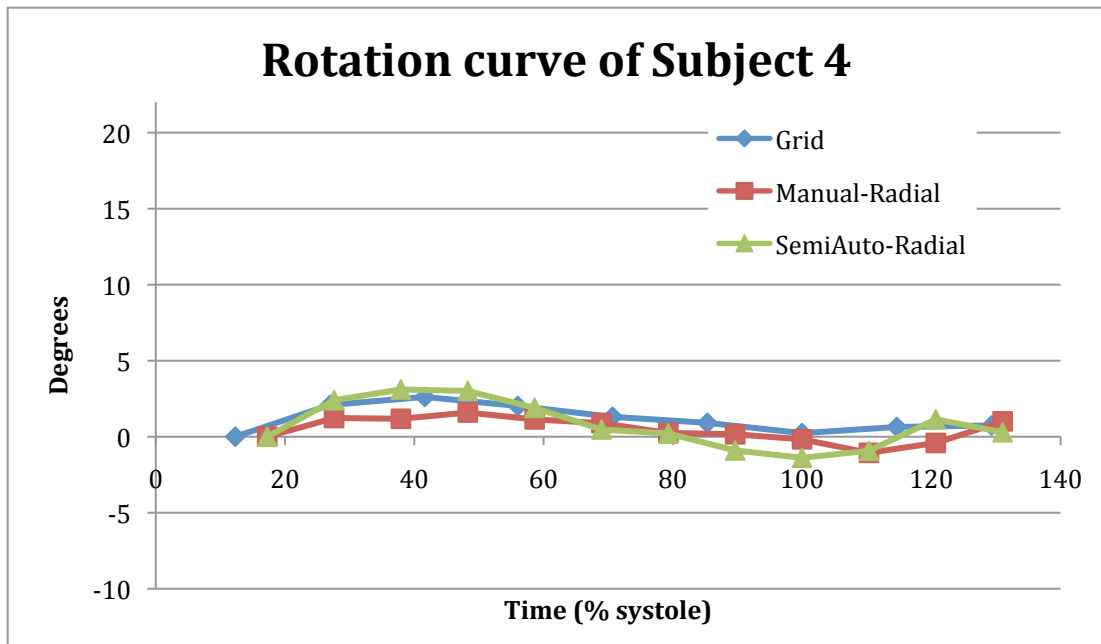
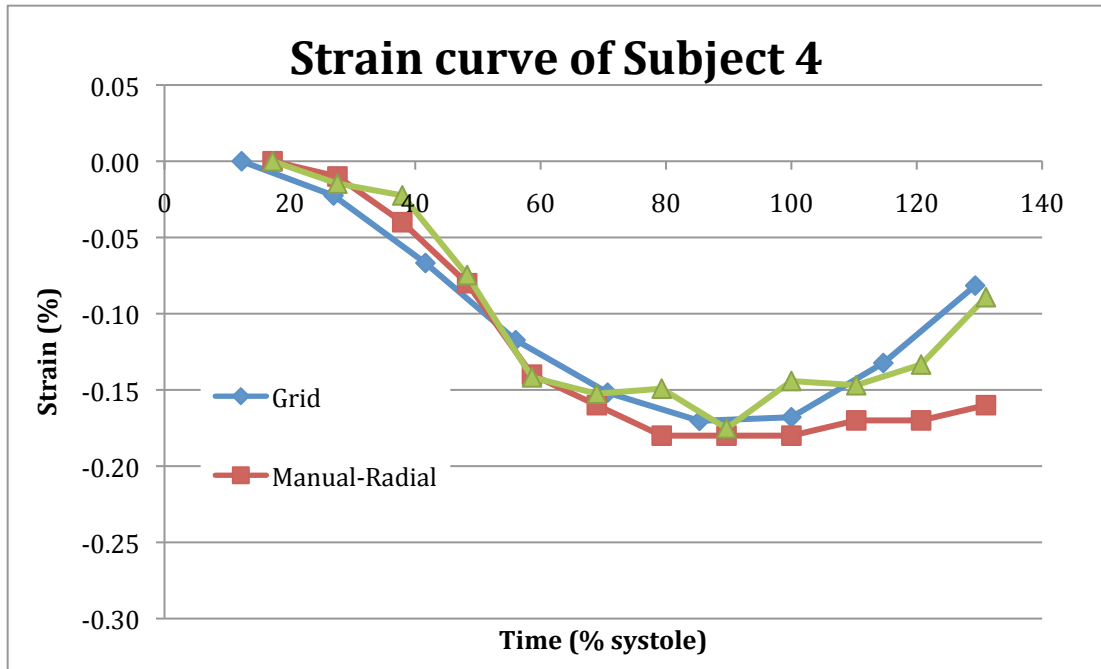
```

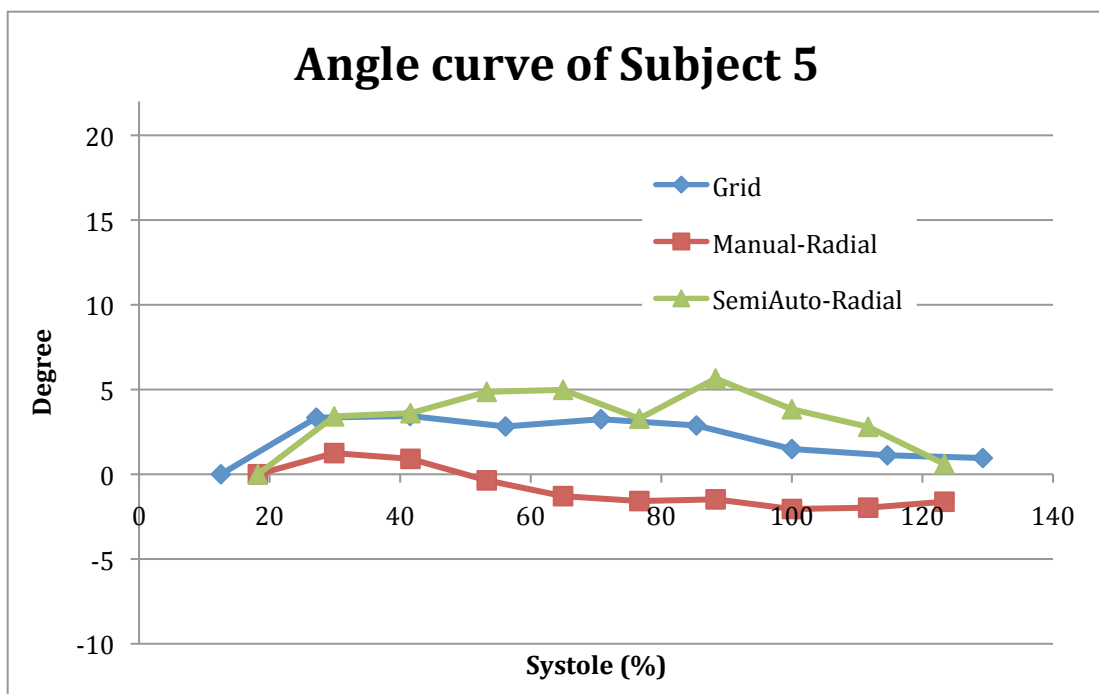
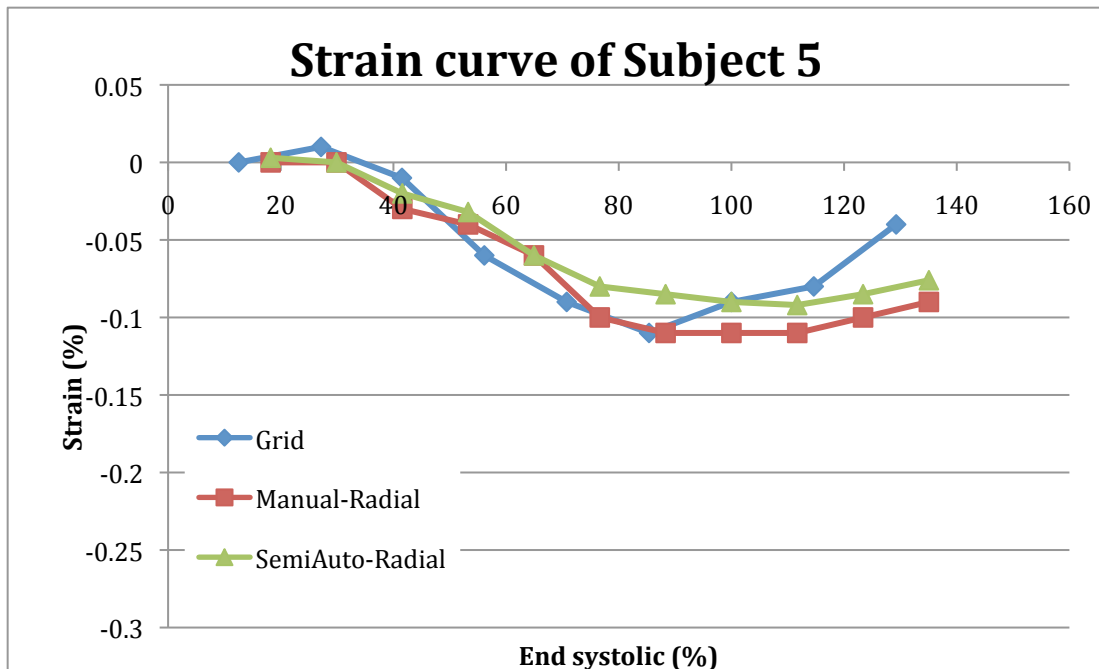
B. The strain and rotation curves for each subject

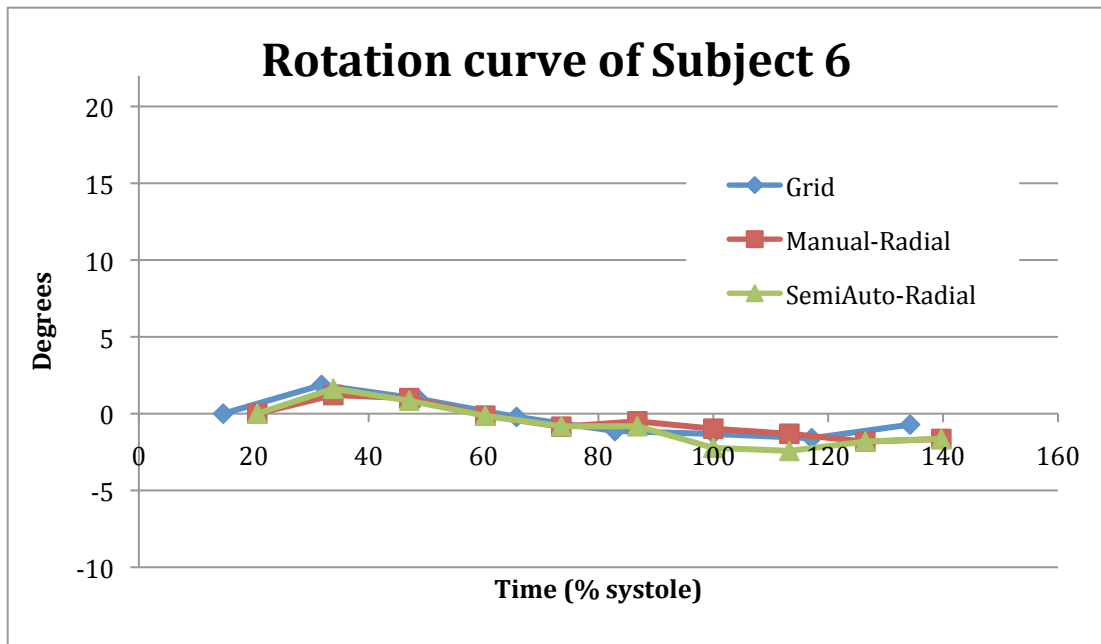
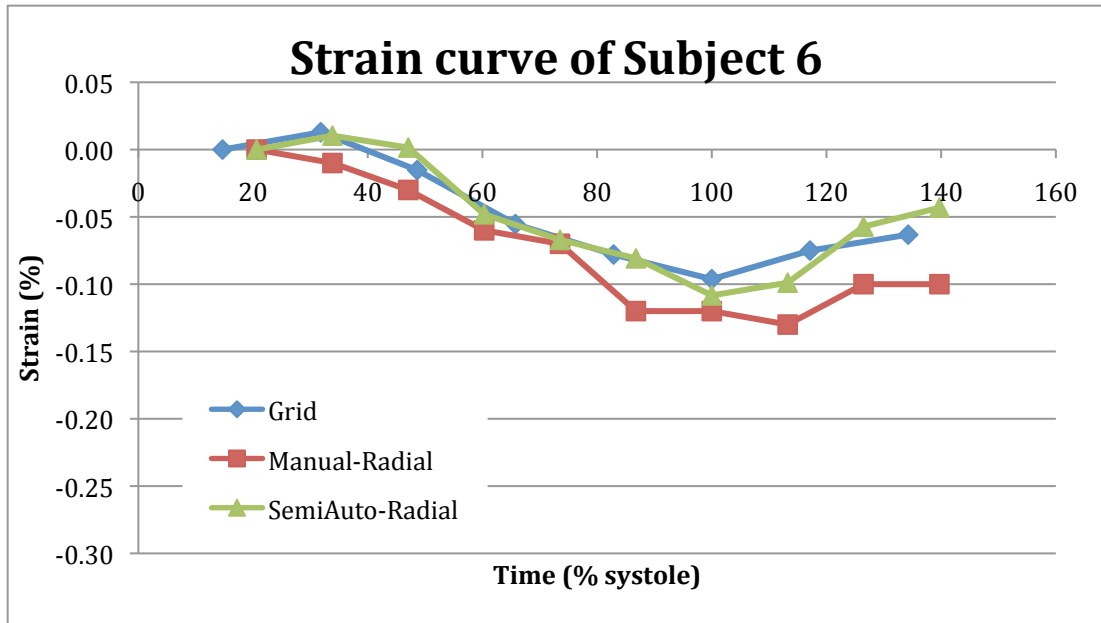


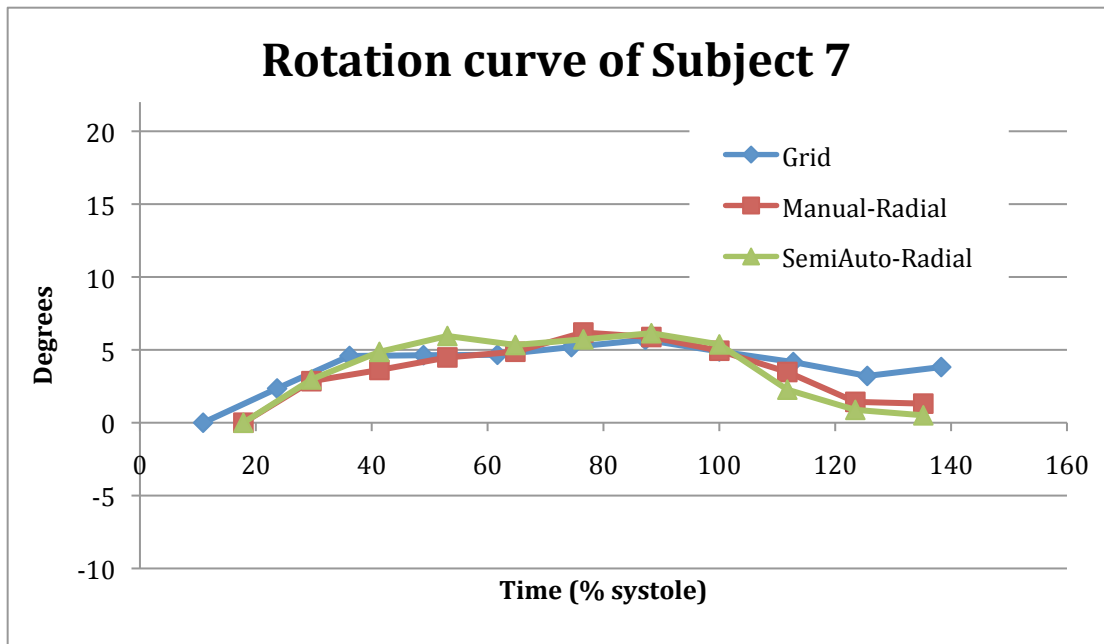
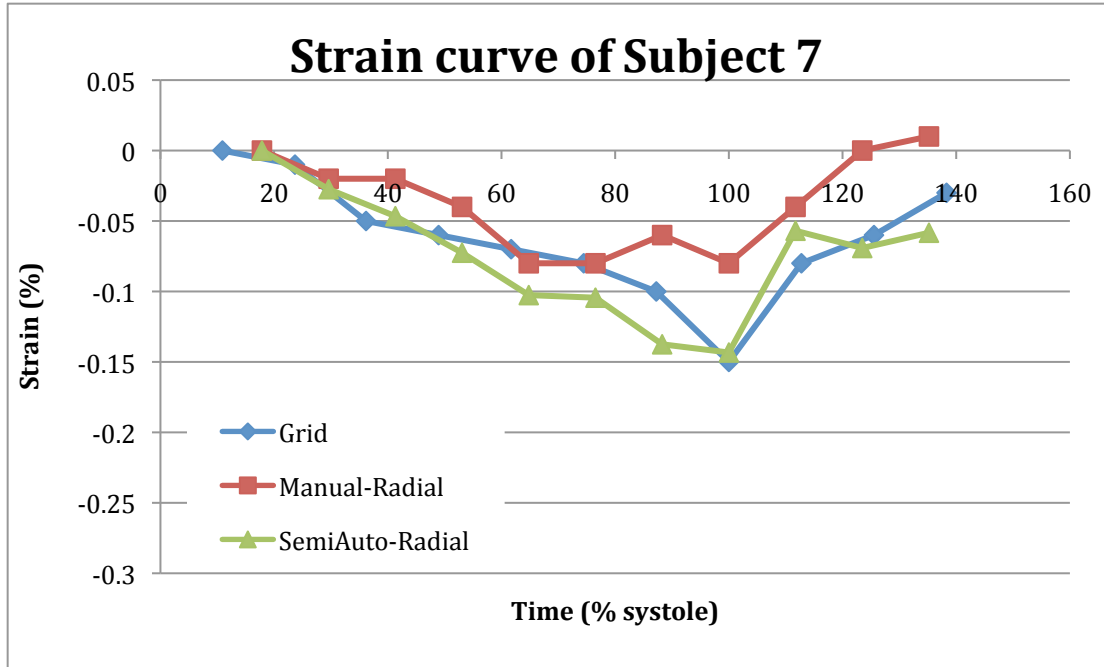


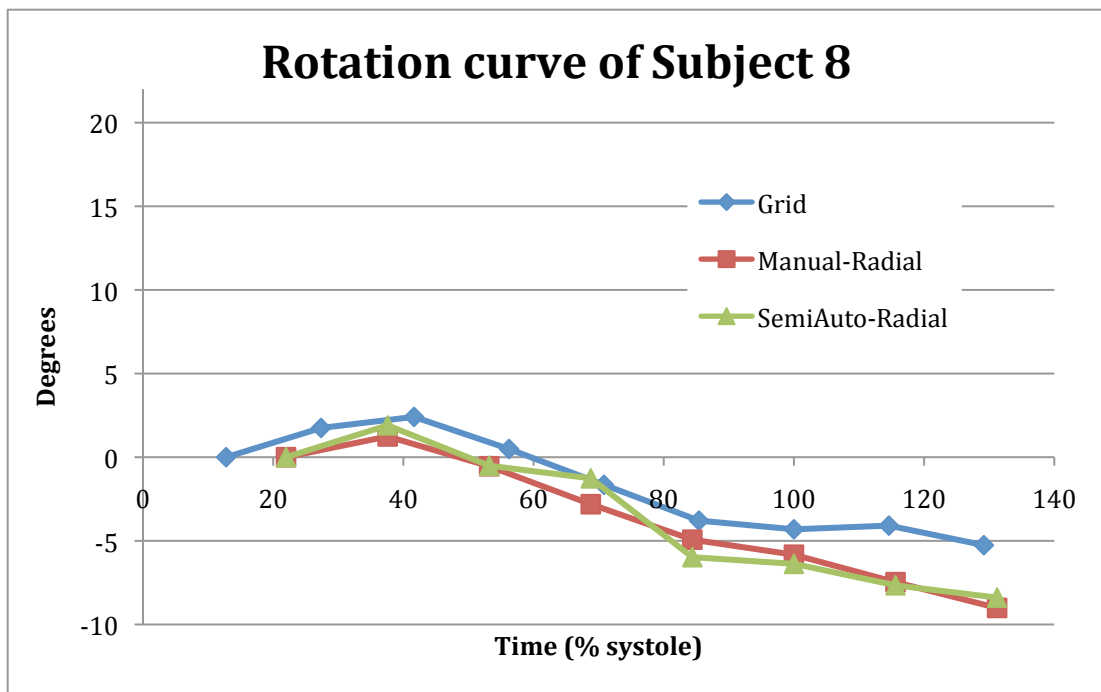
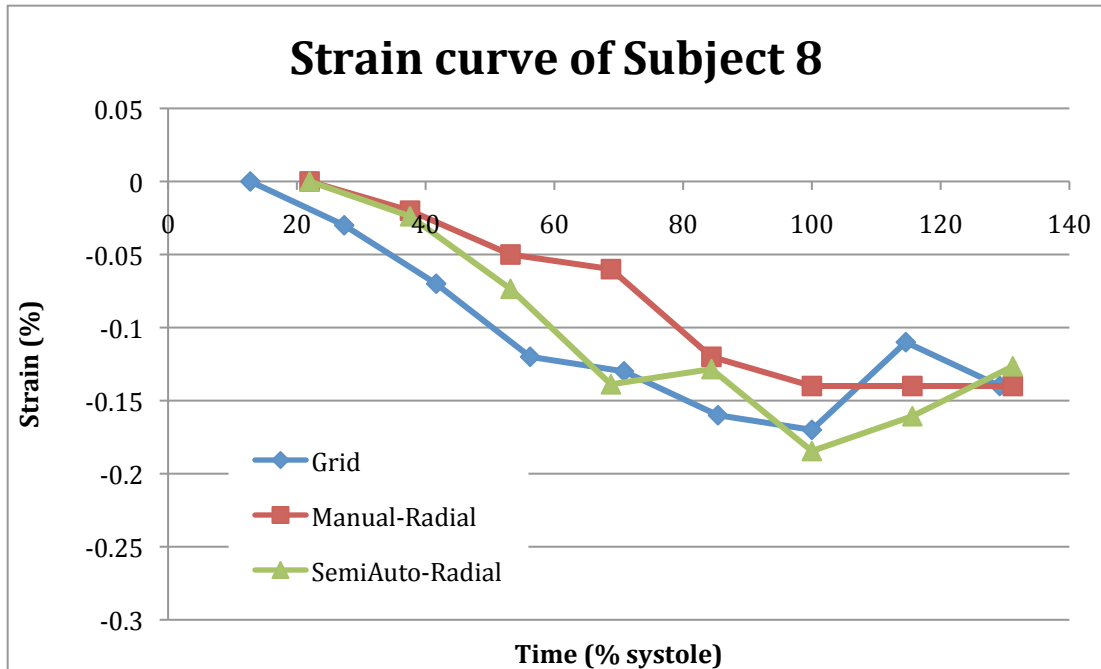


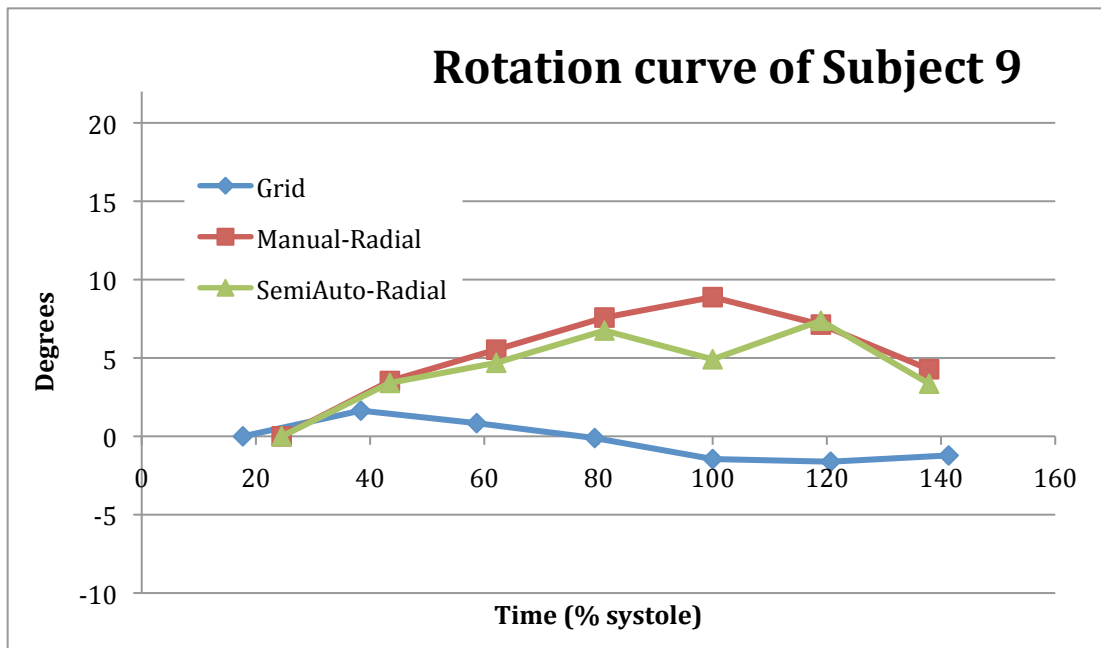
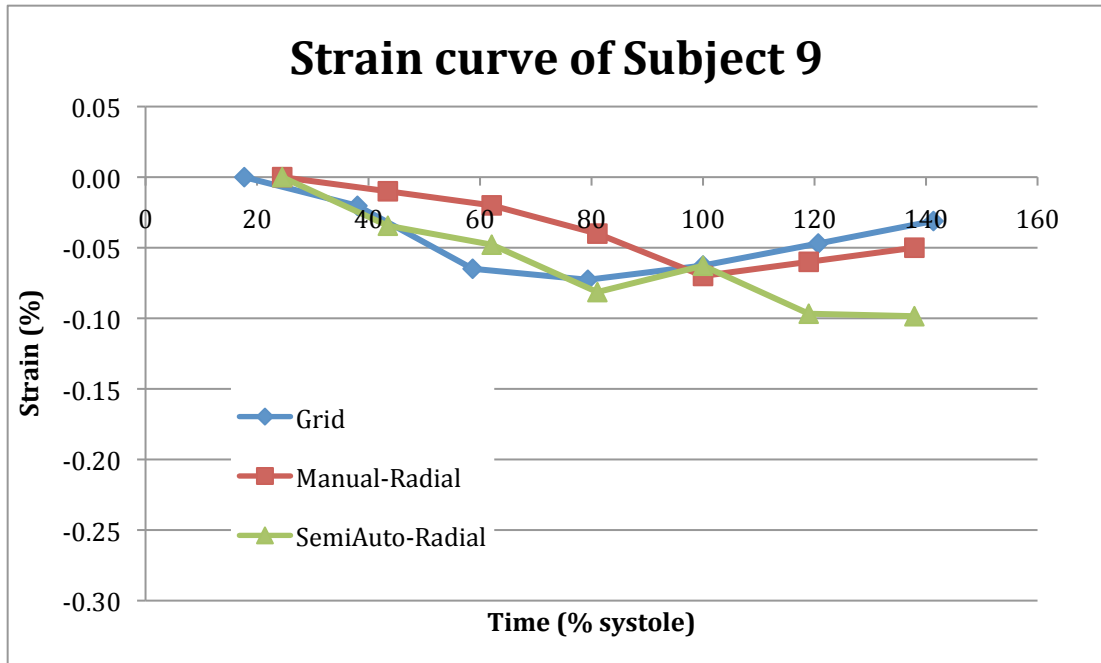


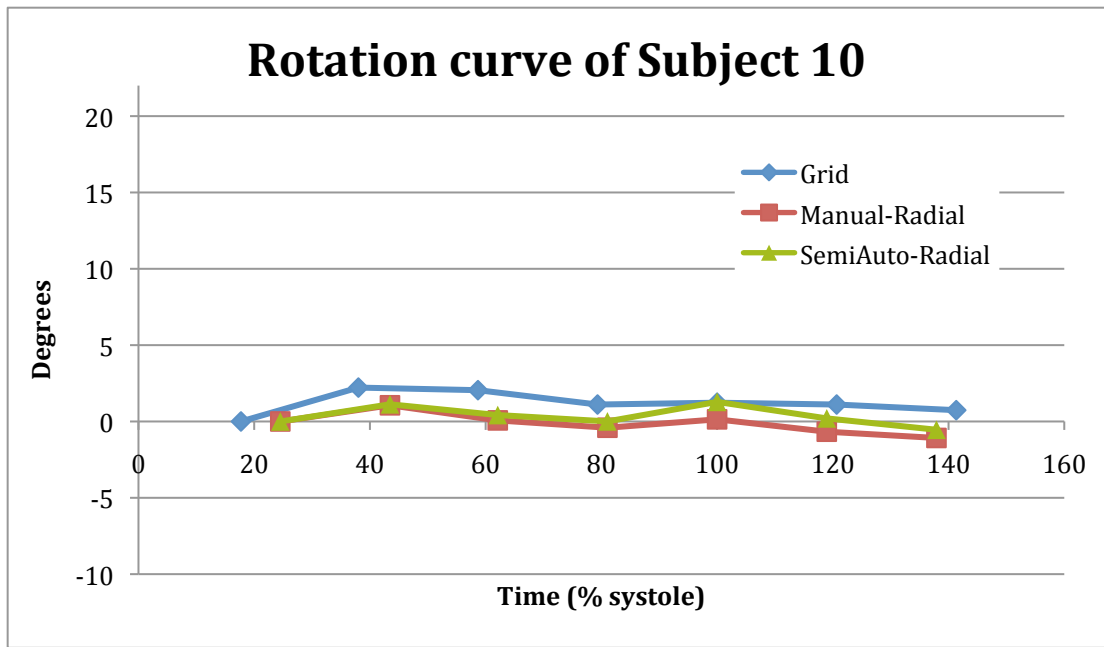
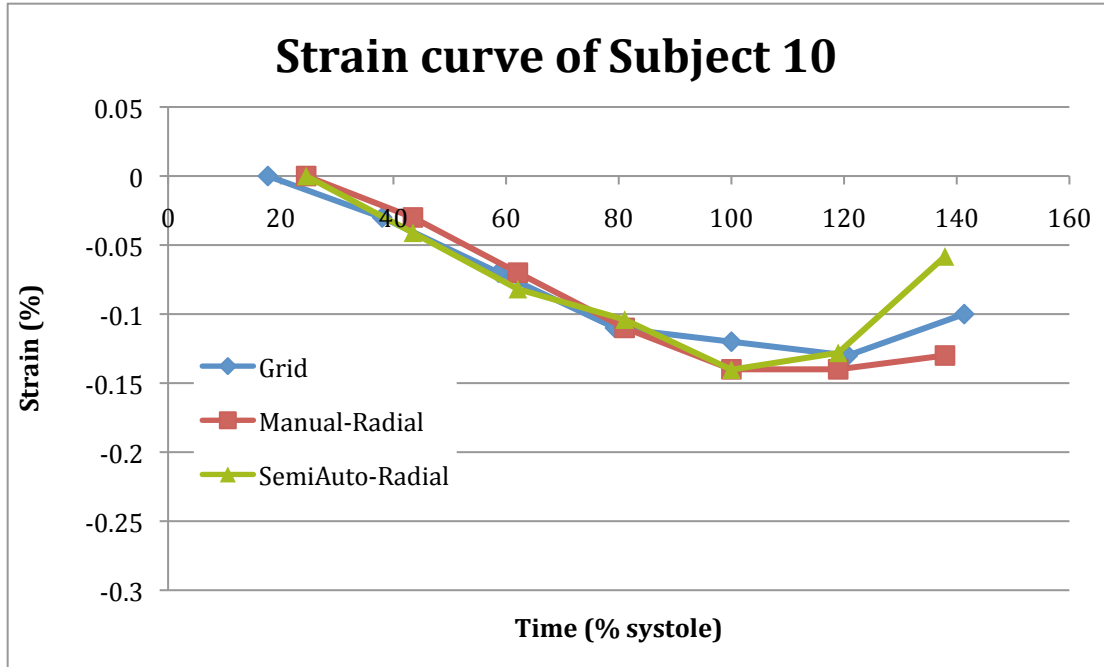


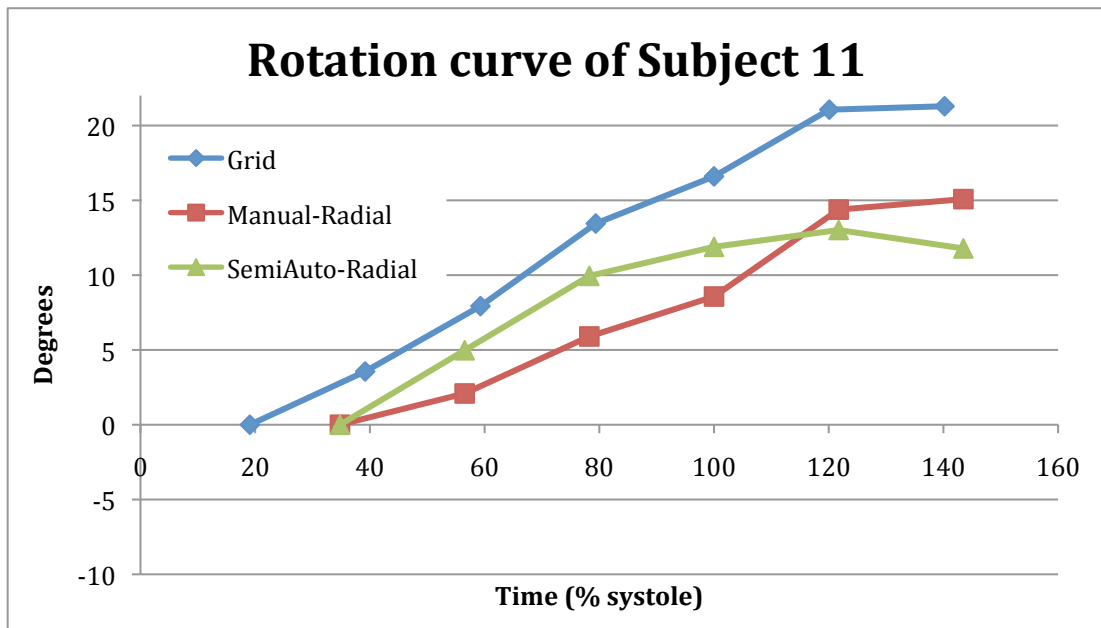
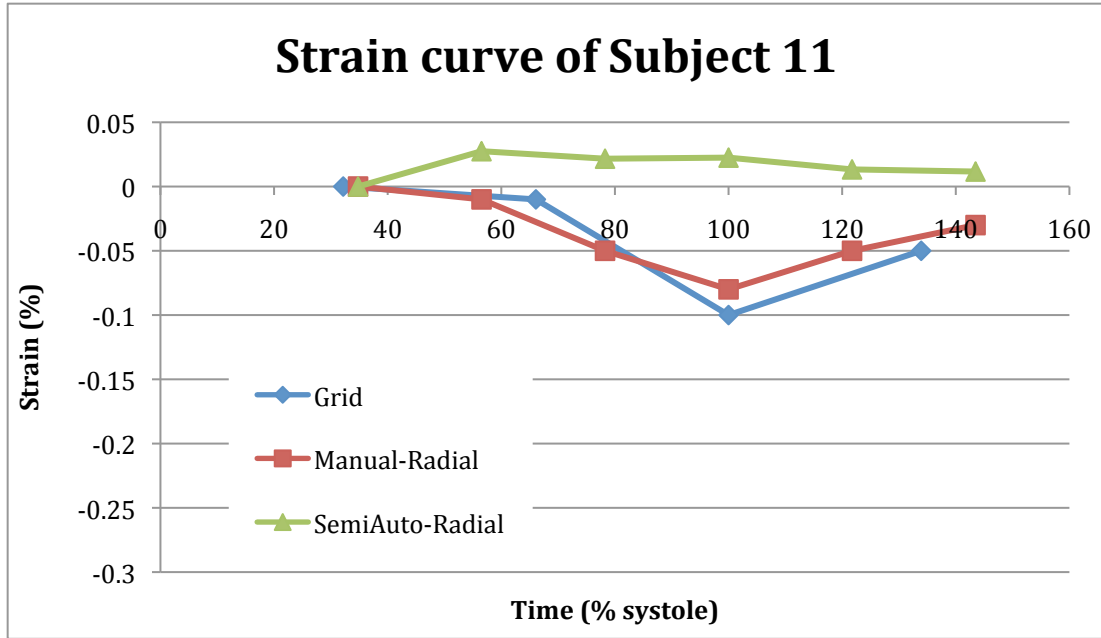


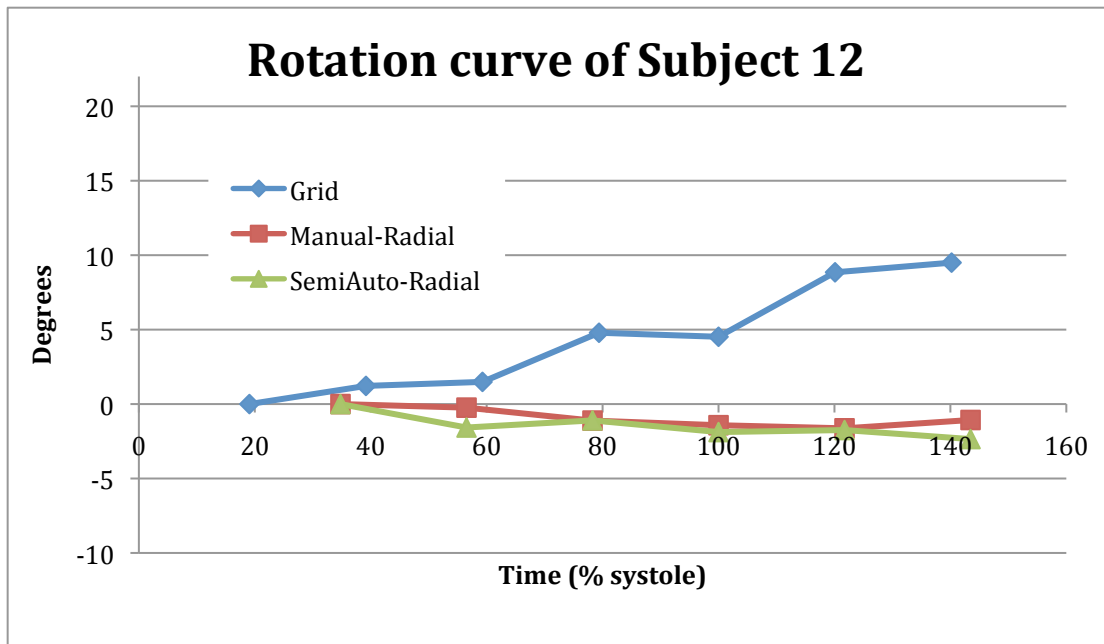
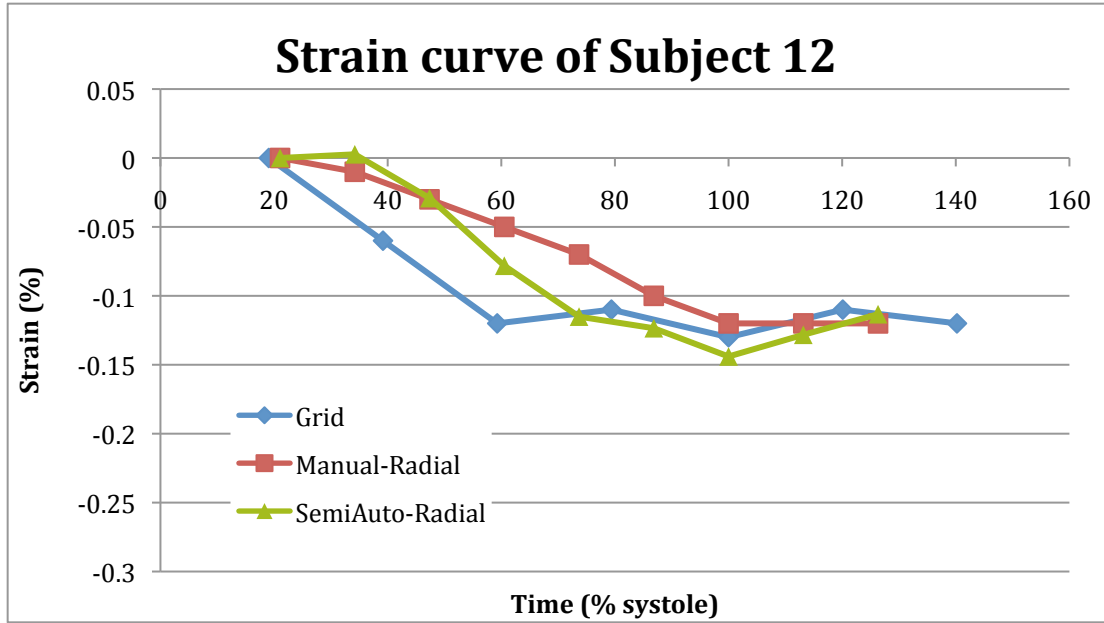


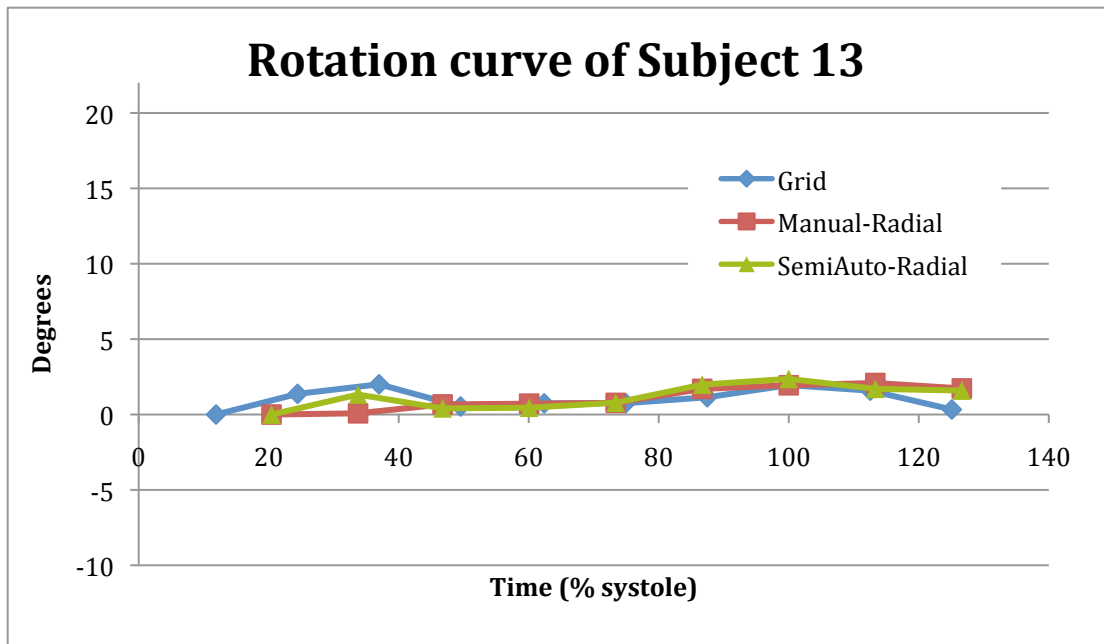
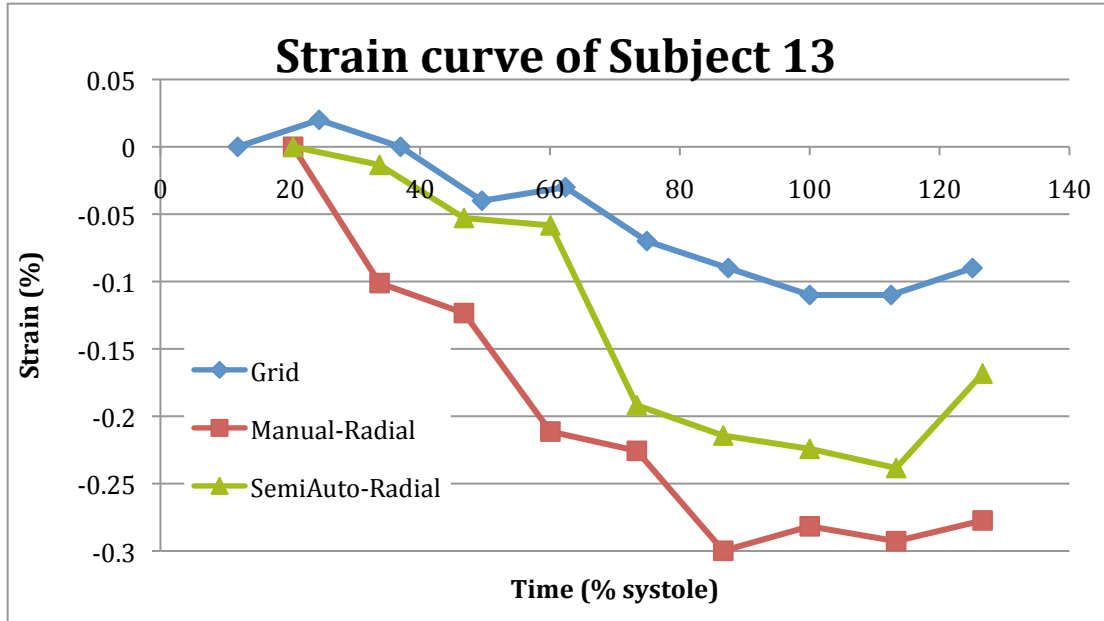


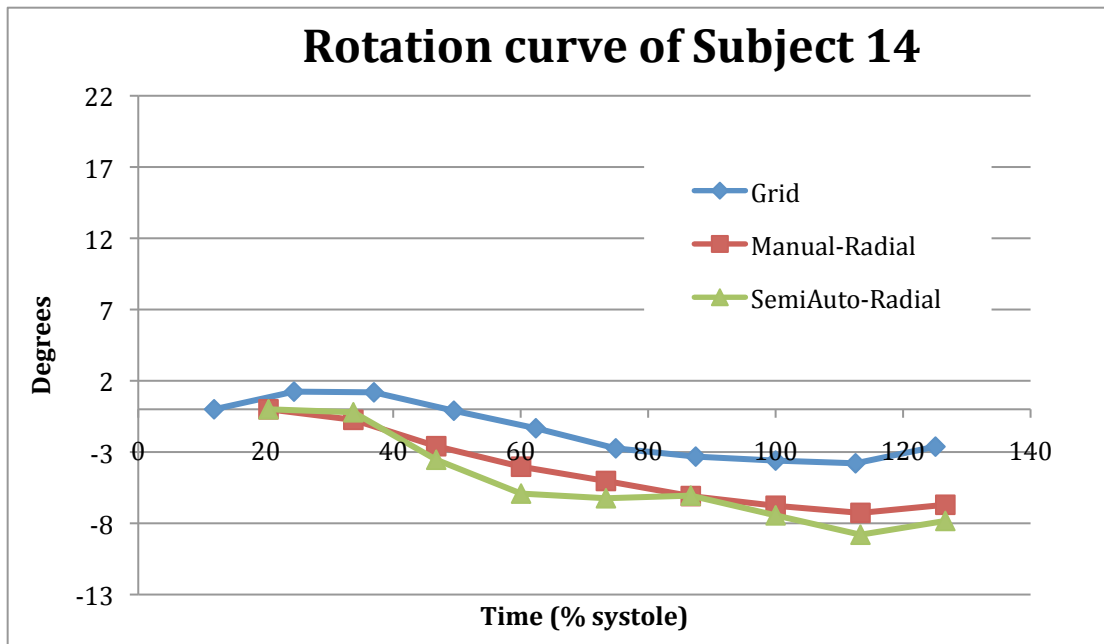
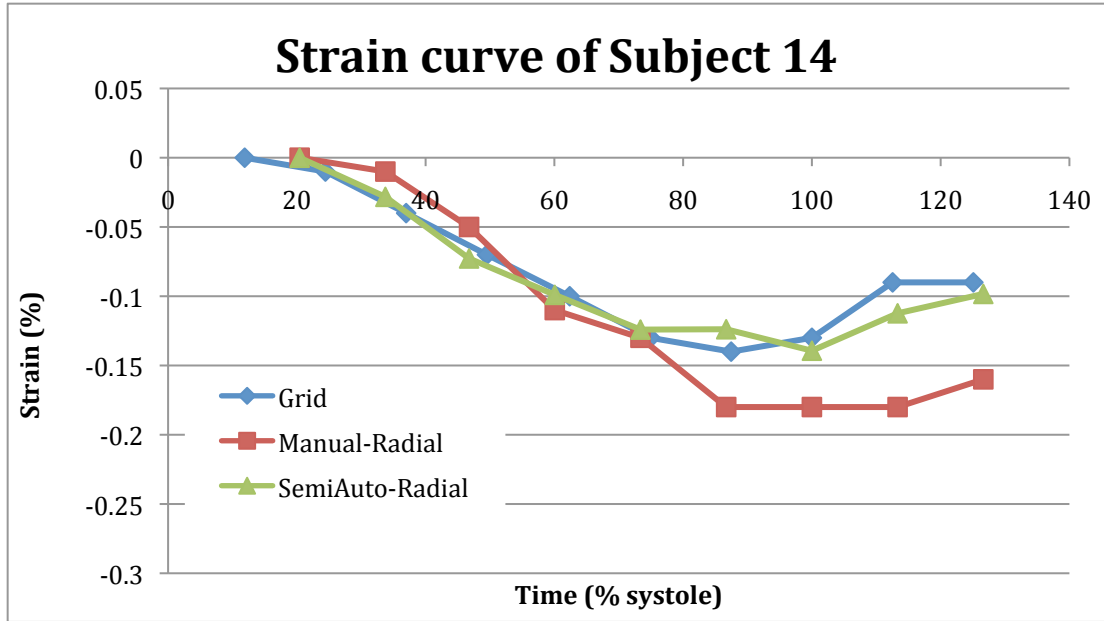












C. Copyright Permission

Fig. 1 used with permission from Patrick J. Lynch

<http://www.interactive-biology.com/75/show-me-a-diagram-of-the-human-heart-here-are-a-bunch/-!prettyPhoto>

YuJaung,

You are welcome to use my illustrations. Good luck with your thesis project!

Pat Lynch

Patrick J. Lynch
Senior Digital Officer
Office of Public Affairs & Communications
Yale University
2 Whitney Avenue, 353
New Haven, CT 06510-1220
203.436.2643

patrick.lynch@yale.edu
@patrylnch
<http://news.yale.edu>
<http://facebook.com/YaleUniversity>
<http://twitter.com/Yale>

=====

From: Yujaung Kim <y.kim16@csuohio.edu>
Date: Wed, 15 Feb 2012 21:19:22 -0500
To: Patrick Lynch <patrick.lynch@yale.edu>
Subject: Request permission for educational use

Dear Patrick Lynch,

My name is YuJaung Kim.
I'm an Master's student of Biomedical Engineering at Cleveland State University.
And now I'm attending the PhD program of BME at University of Iowa.

I am writing this e-mail to ask you for permission to re-use your copyrighted materials.
I'd like to add your figures to support my thesis background.

This thesis is not any purpose to publish journal or make profit.
It is only for my research report during the Masters'.

Attached the figures I would like to use and I added my thesis abstract.

I shall greatly appreciate it.
I look forward to hearing from you.

YuJaung Kim

Fig. 3 used with permission [3]

[3] Iris K. Russel, Marco J. W. Gotte, Jean G. Bronzwaer, Paul Knnapen, Walter J. Paulus, Albert C. van Rossum. Left Ventricular Torsion: An Expanding Role in the Analysis of Myocardial Dysfunction. JACC: Cardiovascular Imaging 2009;2:648-55.

License Details

This is a License Agreement between YuJaung Kim ("You") and Elsevier ("Elsevier"). The license consists of your order details, the terms and conditions provided by Elsevier, and the [payment terms and conditions](#).

[Get the printable license.](#)

License Number	2843500612003
License date	Feb 07, 2012
Licensed content publisher	Elsevier
Licensed content publication	JACC: Cardiovascular Imaging
Licensed content title	Left Ventricular Torsion: An Expanding Role in the Analysis of Myocardial Dysfunction
Licensed content author	Iris K. Russel, Marco J.W. Götte, Jean G. Bronzwaer, Paul Knaapen, Walter J. Paulus, Albert C. van Rossum
Licensed content date	May 2009
Licensed content volume number	2
Licensed content issue number	5
Number of pages	8
Type of Use	reuse in a thesis/dissertation
Portion	figures/tables/illustrations
Number of figures/tables/illustrations	1
Format	both print and electronic
Are you the author of this Elsevier article?	No
Will you be translating?	No
Order reference number	None
Title of your thesis/dissertation	Assessment of circumferential myocardial function using radial tagged MRI
Expected completion date	Feb 2012
Estimated size (number of pages)	80
Elsevier VAT number	GB 494 6272 12
Permissions price	0.00 USD
VAT/Local Sales Tax	0.0 USD / 0.0 GBP
Total	0.00 USD

Fig.4 used with permission [6]

[6] C. Matter, E. Nagel, M. Stuber, P. Boesiger, O. M. Hess. Assessment of systolic and diastolic LV function by MR myocardial tagging. Basic Res Cardiol 1996;91:2:23-28.

**SPRINGER LICENSE
TERMS AND CONDITIONS**

Feb 14, 2012

This is a License Agreement between YuJaung Kim ("You") and Springer ("Springer") provided by Copyright Clearance Center ("CCC"). The license consists of your order details, the terms and conditions provided by Springer, and the payment terms and conditions.

All payments must be made in full to CCC. For payment instructions, please see information listed at the bottom of this form.

License Number	2847900848755
License date	Feb 14, 2012
Licensed content publisher	Springer
Licensed content publication	Basic Research in Cardiology
Licensed content title	Assessment of systolic and diastolic LV function by MR myocardial tagging
Licensed content author	C. Matter
Licensed content date	Jan 1, 1996
Volume number	91
Issue number	0
Type of Use	Thesis/Dissertation
Portion	Figures
Author of this Springer article	No
Order reference number	2165484855
Title of your thesis / dissertation	Assessment of circumferential myocardial function using radial tagged MRI
Expected completion date	Feb 2012
Estimated size(pages)	80

Fig.5 used with permission [8]

[8] Castillo E, Lima J A.C., Bluernke D A. Regional myocardial function: advances in MR imaging and analysis. *Radiographics* 2003;23:S127-S140.



820 Jorie Blvd
Oak Brook, IL 60521
Tel: 1-630-571-2670
Fax: 1-630-571-7837
RSNA.org

February 7, 2012

Dear YuJaung Kim:

The Radiological Society of North America (RSNA[®]) is pleased to grant you permission to reproduce the following figure in print format for use in your Master's thesis intended for Cleveland State University, provided you obtain author permission* and give full credit to the authors and the original publication.

Figure 3

Castillo E, Lima J A.C., Bluernke D A. Regional myocardial function: advances in MR imaging and analysis. *Radiographics* 2003;23:S127-S140.

*Author e-mail: ecastillo@jhmi.edu

This permission is a one-time, non-exclusive grant for English language use and is exclusively limited to the usage stated and underlined above. The requestor guarantees to reproduce the material as originally published. Permission is granted under the condition that a full credit line is prominently placed (i.e. author name(s), journal name, copyright year, volume #, inclusive pages and copyright holder).

This permission becomes effective upon receipt of this signed contract. Please sign a copy of this agreement and return a signed copy to me and retain a copy for your files. Thank you for your interest in our publication.

[Print Name]: YuJaung Kim
SIGNATURE: [Signature] Date: 02/07/2012

Sincerely,

Ashley Day

Ashley Day
Manager, Intellectual Property
Publications and Communications

Phone: 630-590-7771
Fax: 630-590-7724
E-mail: permissions@rsna.org

Fig.7 used with permission [19]

[19] Andrew Webb. Introduction to Biomedical Imaging. New Jersey: John Wiley & Sons, Inc. 2003

License Details

This is a License Agreement between YuJaung Kim ("You") and John Wiley and Sons ("John Wiley and Sons"). The license consists of your order details, the conditions provided by John Wiley and Sons, and the [payment terms and conditions](#).

[Get the printable license.](#)

License Number	2843440286899
License date	Feb 07, 2012
Licensed content publisher	John Wiley and Sons
Licensed content publication	Wiley Books
Licensed content title	Introduction to Biomedical Imaging
Licensed content author	Andrew G. Webb (University of Illinois, Urbana)
Licensed content date	Dec 1, 2002
Type of use	Dissertation/Thesis
Requestor type	University/Academic
Format	Print and electronic
Portion	Figure/table
Number of figures/tables	1
Original Wiley figure/table number(s)	Figure 4.22
Will you be translating?	No
Order reference number	None
Total	0.00 USD

Fig. 8, 9, 12, and 13 used with permission [15]

[15] Setser RM, Chatzimavroudis GP. "Magnetic Resonance Imaging Physical Principles and Instrumentation." Noninvasive Cardiovascular Imaging: A Multimodality Approach. Ed. Mario Garcia. Lippincott Williams & Wilkins, 2009.

Dear Requestor:

We are pleased to grant permission to you for the reproduction of the following:

GARCIA, CARDIOVASCULAR IMAGING
Assmnt Crcmfrntl Mycrdl Fnctn.
F6.5, F6.6, p78, F6.10, p79, F6.12, p80.
Material must be orig to our book.

This permission is subject to the following conditions:

The fee for this request is 0.00. Permission is granted for print and electronic usage (CD-ROM and/or Internet Usage). This permission is a one-time, non-exclusive grant for English language use as described in your request. Permission is granted under the condition that a credit line is prominently placed. Internet permission is granted under the condition that a link is created to the Lippincott Williams & Wilkins home page (<http://lww.com>). Requestor agrees to secure permission from the author (for book material only).

Please sign and date this agreement and return with payment (if applicable) in the enclosed envelope. Please retain a copy for your files.

Payment can be made via credit card (Amex, VISA, Discover and MC) or by check.

If you opt not to use the material requested above, please notify LWW within 90 days of the original invoice date. Please note after 90 days, LWW will not cancel/credit your request which will result into a collection issue.

Card # _____ Exp Date: _____

Requestor Accepts: _____ Date: 02/27/2012

Fig.11 used with permission [19]

[19] Andrew Webb. Introduction to Biomedical Imaging. New Jersey: John Wiley & Sons, Inc. 2003

JOHN WILEY AND SONS LICENSE
TERMS AND CONDITIONS

Feb 07, 2012

This is a License Agreement between YuJaung Kim ("You") and John Wiley and Sons ("John Wiley and Sons") provided by Copyright Clearance Center ("CCC"). The license consists of your order details, the terms and conditions provided by John Wiley and Sons, and the payment terms and conditions.

All payments must be made in full to CCC. For payment instructions, please see information listed at the bottom of this form.

License Number	2843400373525
License date	Feb 06, 2012
Licensed content publisher	John Wiley and Sons
Licensed content publication	Wiley Books
Licensed content title	Introduction to Biomedical Imaging
Licensed content author	Andrew G. Webb (University of Illinois, Urbana)
Licensed content date	Dec 1, 2002
Type of use	Dissertation/Thesis
Requestor type	University/Academic
Format	Print and electronic
Portion	Figure/table
Number of figures/tables	1
Number of extracts	None
Original Wiley figure/table number(s)	Figure 4.16
Will you be translating?	No
Order reference number	None
Total	0.00 USD
Terms and Conditions	
TERMS AND CONDITIONS	

Fig.14 used with permission [9]

[9] Christopher C. Moore, Elliot R. McVeigh, Elias A. Zerhouni. Quantitative Tagged Magnetic Resonance Imaging of the Normal Human Left Ventricle. Topics in Magnetic Resonance Imaging. 2000;11(6):359-371.

License Details

This is a License Agreement between YuJaung Kim ("You") and Wolters Kluwer Health ("Wolters Kluwer Health"). The license consists conditions provided by Wolters Kluwer Health, and the [payment terms and conditions](#).

[Get the printable license.](#)

License Number	2843480068547
License date	Feb 07, 2012
Licensed content publisher	Wolters Kluwer Health
Licensed content publication	Topics in Magnetic Resonance Imaging
Licensed content title	Quantitative Tagged Magnetic Resonance Imaging of the Normal Human Left Ventricle
Licensed content author	Christopher Moore, Elliot McVeigh, and Elias Zerhouni
Licensed content date	Jan 1, 2000
Volume number	11
Issue Number	6
Type of Use	Dissertation/Thesis
Requestor type	Individual Account
Title of your thesis / dissertation	Assessment of circumferential myocardial function using radial tagged MRI
Expected completion date	Feb 2012
Estimated size(pages)	80
Total	0.00 USD

Fig.15 used with permission [17]

[17] Maurice B. Buchalter, MB, MRCPI, James L. Weiss, MD, Walter J. Rogers, BS, Elias A. Zerhouni, MD, Myron L. Weisfeldt, MD, Rafael Beyar, MD, DSc, and Edward P. Shapiro, MD. Noninvasive Quantification of Left Ventricular Rotational Deformation in Normal Humans Using Magnetic Resonance Imaging Myocardial Tagging. Circulation 1990;81:1236-1244.

License Details

This is a License Agreement between YuJaung Kim ("You") and Wolters Kluwer Health ("Wolters Kluwer Health"). The license consists of your order details, the terms & conditions provided by Wolters Kluwer Health, and the [payment terms and conditions](#).

[Get the printable license.](#)

License Number	2843341317640
License date	Feb 06, 2012
Licensed content publisher	Wolters Kluwer Health
Licensed content publication	Circulation
Licensed content title	Noninvasive quantification of left ventricular rotational deformation in normal humans using magnetic resonance imaging myocardial tagging
Licensed content author	MB Buchalter, JL Weiss, WJ Rogers, EA Zerhouni, ML Weisfeldt, R Beyar, EP Shapiro
Licensed content date	Apr 1, 1990
Volume number	81
Issue Number	4
Type of Use	Dissertation/Thesis
Requestor type	Individual Account
Title of your thesis / dissertation	Assessment of circumferential myocardial function using radial tagged MRI
Expected completion date	Feb 2012
Estimated size(pages)	80
Total	0.00 USD

Fig.16 used with permission [5]

[5] Marco J.W. Gotte, Tjeerd Germans, Iris K. Russel, Jaco J. M. Zwanenburg, J. Tim Marcus, Albert C. van Rossum, Dirk J. van Beldhuisen, FACC. Myocardial Strain and Torsion Quantified by Cardiovascular Magnetic Resonance Tissue Tagging. Journal of the Americal College of Cardiology 2006;48:2002-11.

License Details

This is a License Agreement between YuJaung Kim ("You") and Elsevier ("Elsevier"). The license consists of your order details, the terms and conditions provided by Elsevier, and the [payment terms and conditions](#).

[Get the printable license.](#)

License Number	2843350606557
License date	Feb 06, 2012
Licensed content publisher	Elsevier
Licensed content publication	Journal of the American College of Cardiology
Licensed content title	Myocardial Strain and Torsion Quantified by Cardiovascular Magnetic Resonance Tissue Tagging: Studies in Normal and Impaired Left Ventricular Function
Licensed content author	Marco J.W. Götte,Tjeerd Germans,Iris K. Russel,Jaco J.M. Zwanenburg,J. Tim Marcus,Albert C. van Rossum,Dirk J. van Veldhuisen
Licensed content date	21 November 2006
Licensed content volume number	48
Licensed content issue number	10
Number of pages	10
Type of Use	reuse in a thesis/dissertation
Portion	figures/tables/illustrations
Number of figures/tables/illustrations	1
Format	both print and electronic
Are you the author of this Elsevier article?	No
Will you be translating?	No
Order reference number	None
Title of your thesis/dissertation	Assessment of circumferential myocardial function using radial tagged MRI
Expected completion date	Feb 2012
Estimated size (number of pages)	80
Elsevier VAT number	GB 494 6272 12
Permissions price	0.00 USD
VAT/Local Sales Tax	0.0 USD / 0.0 GBP
Total	0.00 USD

Fig.17 used with permission [18]

[18] Marco J.W Gotte, Albert C van Rossum, Jos W. R Twisk, Joost P.A Kuijer, J. Tim Marcus, Cees A Visser. Quantification of regional contractile function after infarction: strain analysis superior to wall thickening analysis in discriminating infarct from remote myocardium. Journal of the American College of Cardiology 2001;37(3):808-817.

License Details

This is a License Agreement between YuJaung Kim ("You") and Elsevier ("Elsevier"). The license consists of your order details, the terms and conditions provided by Elsevier and the [payment terms and conditions](#).

[Get the printable license.](#)

License Number	2843360555426
License date	Feb 06, 2012
Licensed content publisher	Elsevier
Licensed content publication	Journal of the American College of Cardiology
Licensed content title	Quantification of regional contractile function after infarction: strain analysis superior to wall thickening analysis in discriminating infarct from remote myocardium
Licensed content author	Marco J.W Götte, Albert C van Rossum, Jos W.R Twisk, Joost P.A Kuijer, J. Tim Marcus, Cees A Visser
Licensed content date	March 2001
Licensed content volume number	37
Licensed content issue number	3
Number of pages	10
Type of Use	reuse in a thesis/dissertation
Portion	figures/tables/illustrations
Number of figures/tables/illustrations	1
Format	both print and electronic
Are you the author of this Elsevier article?	No
Will you be translating?	No
Order reference number	None
Title of your thesis/dissertation	Assessment of circumferential myocardial function using radial tagged MRI
Expected completion date	Feb 2012
Estimated size (number of pages)	80
Elsevier VAT number	GB 494 6272 12
Permissions price	0.00 USD
VAT/Local Sales Tax	0.0 USD / 0.0 GBP
Total	0.00 USD